Exact numerical simulations of strongly interacting atoms in 1D trap potentials and optical lattices

Dissertation

Bernd Schmidt

Vom Fachbereich Physik der Technischen Universität Kaiserslautern zur Verleihung des akademischen Grades „Doktor der Naturwissenschaften“ genehmigte Dissertation

Betreuer: Prof. Dr. Michael Fleischhauer
Zweitgutachter: Prof. Sebastian Eggert, Ph. D.

Datum der wissenschaftlichen Aussprache: 25.02.2009

D 386

Contents

Kurzfassung

Ultra-kalte Quantengase haben sich in den letzten Jahren zu einem sehr interessanten Experimentierfeld für die Vielteilchenphysik stark korrelierter Systeme entwickelt. Dies ist im Wesentlichen darauf zurückzuführen, dass es diese Systeme erlauben, wichtige Modell-Hamiltonoperatoren von Vielteilchensystemen quasi in Reinkultur mit variierbaren Parametern zu realisieren. Trotz der Entwicklung effizienter und kraftvoller Verfahren wie Quanten Monte Carlo und numerischer Renormierungsmethoden stellt die numerische Simulation von stark korrelierten Quantensystemen bis heute eine große Herausforderung für die theoretische Physik dar. Die vorliegende Arbeit „Exact numerical simulations of strongly interacting atoms in 1D trap potentials and optical lattices“ befasst sich mit verschiedenen solcher Verfahren angepasst an die besonderen Gegebenheiten für ultra-kalte Quantengase. Dabei wird vor allem auf die Entwicklung und Untersuchung neuer numerischer Methoden Wert gelegt, beziehungsweise auf die Erweiterung und Anwendung von bekannten numerischen Methoden auf physikalische Systeme, für die diese Methoden wenig oder noch nicht genutzt wurden. Die physikalischen Systeme die hierbei im Mittelpunkt des Interesses stehen sind quasi ein-dimensionale Bose- (und Fermi-) Gase in periodischen Gittersystemen bzw. in Fallen-Potentialen bei niedrigen Temperaturen. Gerade für solche inhomogenen Systeme mit starker Wechselwirkung sind noch nicht ausreichend numerisch exakte Methoden bekannt.

Ein Teil dieser Arbeit beschäftigt sich mit einer neuen stochastischen Methode. Diese Methode basiert auf einer Faktorisierung der kinetischen Energie durch Einführung zusätzlicher stochastischer Variablen, die den Hamiltonoperator des Systems quasi-lokal macht. Die Nicht-Lokalität des Hamiltonoperators wird erst durch die am Ende durchzuführende Mittelung von Erwartungswerten über die stochastische Variablen wieder hergestellt. Mit dieser Methode werden insbesondere Dichteverteilungen und Korrelationen erster Ordnung betrachtet und die Methode wird auf ihre praktische Anwendbarkeit überprüft.

Ein weiterer Teil dieser Arbeit beschäftigt sich mit der Erweiterung einer bereits bekannteren Methode auf inhomogene Systeme, der sogenannten Dichte-Matrix-

Renormierungs-Gruppe (DMRG). Diese ursprünglich für Gittersysteme entwickelte Methode wird auf inhomogene kontinuierliche Systeme erweitert. Es werden unter anderem Dichteprofile und Korrelationen im Grundzustand und bei sehr niedrigen Temperaturen berechnet. Sowohl bei der oben genannten stochastischen Methode als auch bei der DMRG werden die Ergebnisse mit den besten verfügbaren analytischen Näherungen verglichen. Diskutiert wird auch der Fall eines zweikomponentigen Gases mit Punktwechselwirkung, wobei das exakte Ergebnis des einkomponentigen Falles mit einer mean-field artigen inter-Spezies Wechselwirkung kombiniert wird.

Des Weiteren werden die Untersuchungen eines bosonischen Gases mit s-Wellenstreuung mittels einer Äquivalenz-Abbildung auf wechselwirkende spinpolarisierte Fermionen mit p-Wellenstreuung erweitert.

Ein weiterer Teil der Arbeit beschäftigt sich mit meta-stabilen angeregten Zuständen des Bose-Hubbard Modells, welches bosonische Teilchen in einem tiefen periodischen Gitterpotential beschreibt. Dieses System erlaubt die Existenz gebundener Teilchenpaare trotz abstoßender Teilchen-Teilchen Wechselwirkung. Es wird zunächst gezeigt, dass sich das Bose-Hubbard-Modell exakt auf einen zwei-Spezies Hamiltonoperator abbilden lässt, bei dem die eine Spezies repulsiv gebundene Teilchenpaare repräsentiert und die andere nicht gepaarte einzelne Teilchen. Es wird ein approximativer, effektiver Vielteilchen-Hamiltonoperator der Teilchenpaare abgeleitet und seine Gültigkeit mit numerischen Rechnungen überprüft. Anschließend wird der Fall attraktiv gebundener Teilchenpaare untersucht. Für diesen werden DMRG- Rechnungen sowohl mit harmonischem als auch mit Kastenpotential durchgeführt. Es wird eine Näherung vorgestellt die es erlaubt die Teilchenverteilung und Teilchen-Korrelation in bestimmten Fällen näherungsweise analytisch zu bestimmen. Die verschiedenen Phasenübergänge der Teilchenpaare sowohl im attraktiven als auch im repulsiven Fall werden diskutiert.

Ein weiterer Abschnitt der Arbeit beschäftigt sich mit einer Molekularfeldtheorie von Atom-Molekül-Gemischen und deren Phasendiagrammen. Die Rechnungen hier benutzen einen Gutzwiller Ansatz. Es wird versucht einen groben Überblick über die sehr strukturreichen Phasendiagramme zu gewinnen.

Da das Bose-Hubbard-System für diese Arbeit grundlegend ist werden darin auch die Abhängigkeit der Parameter des Modells von physikalischen Größen wie der Streulänge und der Gittertiefe noch einmal im Detail betrachtet. Es wird die Wannierfunktion des zweiten Bandes berechnet sowie Tunnel- und Wechselwirkungskonstanten innerhalb und zwischen den Bändern abgeleitet. Schließlich wird untersucht für welche Parameter die Ein-Band-Näherung gerechtfertigt ist.

Abstract

Ultra-cold quantum gases recently became a very interesting testing ground for multi-particle physics of strongly correlated systems. The main reason for this is, that such systems allow the realisation of important model Hamiltonians of multi-particle systems in their purest form with variable parameters. Despite the development of efficient and powerful techniques, like quantum Monte Carlo and numerical renormalization methods, the numerical simulation of strongly correlated quantum systems poses a big challenge to theoretical physics until today. The present work "Exact numerical simulations of strongly interacting atoms in 1D trap potentials and optical lattices" deals with various techniques of this kind adapted to the special features of ultra-cold quantum gases. Therefore, the main focus of this work is the exploration and development of new numerical methods and the extension of known methods to physical systems, where those methods have not much been applied to or have not been applied at all. Of interest are in particular the quasi-one-dimensional Bose- (and Fermi-) gases in periodic lattice systems and in trap potentials at low temperature. Especially for inhomogeneous systems with strong interaction appropriate numerical methods are not well developed.

A major part of this thesis therefore deals with a new stochastic method. This method is based on a factorisation of the kinetic energy by introducing stochastic variables, which transforms the Hamiltonian of the system into a quasi-local one. At the end of the procedure, non-locality is restored by averaging the expectation values over the stochastic variables. With this method, density distributions and first order correlations are examined and the method is tested for its practical applicability.

Another part of the thesis deals with an extension of a well developed method to inhomogeneous continuous systems, the so called density-matrix-renormalization-group (DMRG). This method, which was invented for lattice systems, is extended to inhomogeneous continuous systems. Among other things, density profiles and correlations are calculated for zero and very low temperature. Both the results of the stochastic method mentioned above and of the DMRG are compared to

the best available analytic approximations. Also the case of a two component Bose-gas with point interaction is discussed by combining the exact solution of the one-component case with a mean-field-like inter-species interaction.

Making use of a general mapping between bosons and fermions in 1D, the investigations of a bosonic gas with s-wave scattering is extended to interacting spin-polarised Fermions with p-wave scattering.

A further part of the thesis deals with meta-stable excited states of the Bose-Hubbard model, which describes bosonic particles in deep periodic lattice potentials. This system permits the existence of bound particle pairs, despite repulsive particle-particle interaction. Firstly it is shown, that the Bose-Hubbard model can be mapped exactly onto a two-species Hamiltonian, where one species represents the repulsively bound pairs and the other one unpaired single particles. An approximative, effective multi-particle Hamiltonian of particle pairs is derived and its validity checked by numerical calculations. After that the case of attractively bound pairs is examined. For that case DMRG calculations for both the harmonic and box potential are performed. An approximation is presented, which allows to determine the particle distribution and particle correlation in certain cases analytically. The various phase transitions of the particle pairs are discussed both for the attractive and repulsive case.

A further section of the thesis deals with a molecular-field theory of atom-molecule mixtures and its phase diagrams. A Gutzwiller mean-field ansatz is used here. An attempt is made to get an overview of the rich structure of the phase diagrams.

Since the Bose-Hubbard-Model is quite fundamental for this thesis the dependency of the parameters of the model on physical entities like the scattering length and the lattice depth are discussed in detail. The Wannier function of the second band is calculated and tunnelling and interaction constants in the bands and in-between the bands. Finally it is investigated for which parameters the one-band approximation is justified.

Chapter 1

Introduction

The subject of the present thesis is the theory and numerical simulation of one-dimensional (1D) multi-particle quantum systems. The detailed understanding of the quantum properties of many body systems represents still one of the major challenges in theoretical physics. Despite the fact that the basic interactions are often well known and can be formulated in terms of simple model Hamiltonians, it is very difficult to determine the unitary time evolution of a given initial state or even just the ground and thermal state of the system. The latter is related to the fact that the dimension of the Hilbert space of a many-body system increases exponentially with the system size, which has lead to the idea of a quantum computer by Richard Feynman. One-dimensional systems with finite-range interactions play a special role, since on one hand quantum effects are most important in lower dimensions and on another hand 1D systems offer some avenues for analytical and numerical approaches. Furthermore due to the recent advances in atomic physics and quantum optics 1D systems became accessible from the experimental side. Gas-atoms can be handled very efficiently in experiments. They can be cooled down to very low temperatures at which quantum mechanicle effects can be observed and studied. In the famous and Nobel-prize winning experiments by W. Ketterle [1], C. Wieman and E. Cornell [2] bosonic atoms have been cooled down to such a low temperature, that the so-called Bose-Einstein condensation occurred, a purely quantum mechanicle effect, where particles form a highly coherent state. By now this technique has become a standard tool in many labs.

Cold gases have a high level of controllability. The atoms can be put into potentials by which it is not only possible to control their position and movement, but also to control parameters like the interaction between the particles and many other properties.

An important class of experiments deals with atoms which are put into a lattice

potential. Such a lattice can be created by standing laser waves. Again, the high controllability of the laser allows for a very precise manipulation of the system. It was experimentally demonstrated [3] that bosonic atoms in an optical lattice show a Mott-insulator (MI) to superfluid (SF) phase transition, by which the particles are either in a state of fixed particle-number per lattice site (MI) or in a coherent state of fixed phase (SF), depending on the depth of the lattice-potential. An arrangement of atoms in lattices is also interesting for building quantum memories and quantum computers.

An important point, which should be emphasized, is that quantum mechanical multi-particle or multi-mode problems do not fall into the same category of difficulty than problems of classical physics. The number of parameters required to describe an arbitrary state of M quantum systems grows exponentially with M, a fact that renders the simulation of generic quantum many-body dynamics intractable. That is the reason why "brute force" methods like numerical diagonalization of the Hamiltonian are often not applicable.

Instead new numerical methods must be invented who cleverly avoid the problem of exponential growth. There are basically two main branches today. The first branch are stochastic methods, in particular quantum Monte Carlo (QMC) calculations, which only take some random sample of the Hilbert space into account and make use of the fact that a small sample often contains the essential information of the system. The second branch are real space renormalization methods for one dimensional lattice systems such as the density matrix renormalization group (DMRG). Typically the ground state of 1D lattice systems with finite range interactions turns out to be only slightly entangled in a local basis. It can be shown that the states of such slightly entangled systems occupy only a manifold of remarkably small dimension within the Hilbert space (see [4]). That makes it possible to simulate those systems with a computational cost which grows only linearly in the system size. One dimensional systems have the further advantage that in the case of translational invariance some exact solutions exists which can be obtained with the help of a Bethe ansatz. Also in the limit of low-energy excitations 1D systems can often successfully treated using bosonization techniques. For these reasons this work will be restricted to quantum systems in one spatial dimension.

From the numerical point of view, the 1D models studied here can be divided into two categories. In one category are those, which can be implemented numerically. E.g. the Bose-Hubbard-model (see Section 2.3), the hard-core-boson-model with nearest neighbour interaction which is equivalent to the spin-1/2 XXZ model (see Section 2.4) and Bose-Hubbard-like models for two particle species. In the

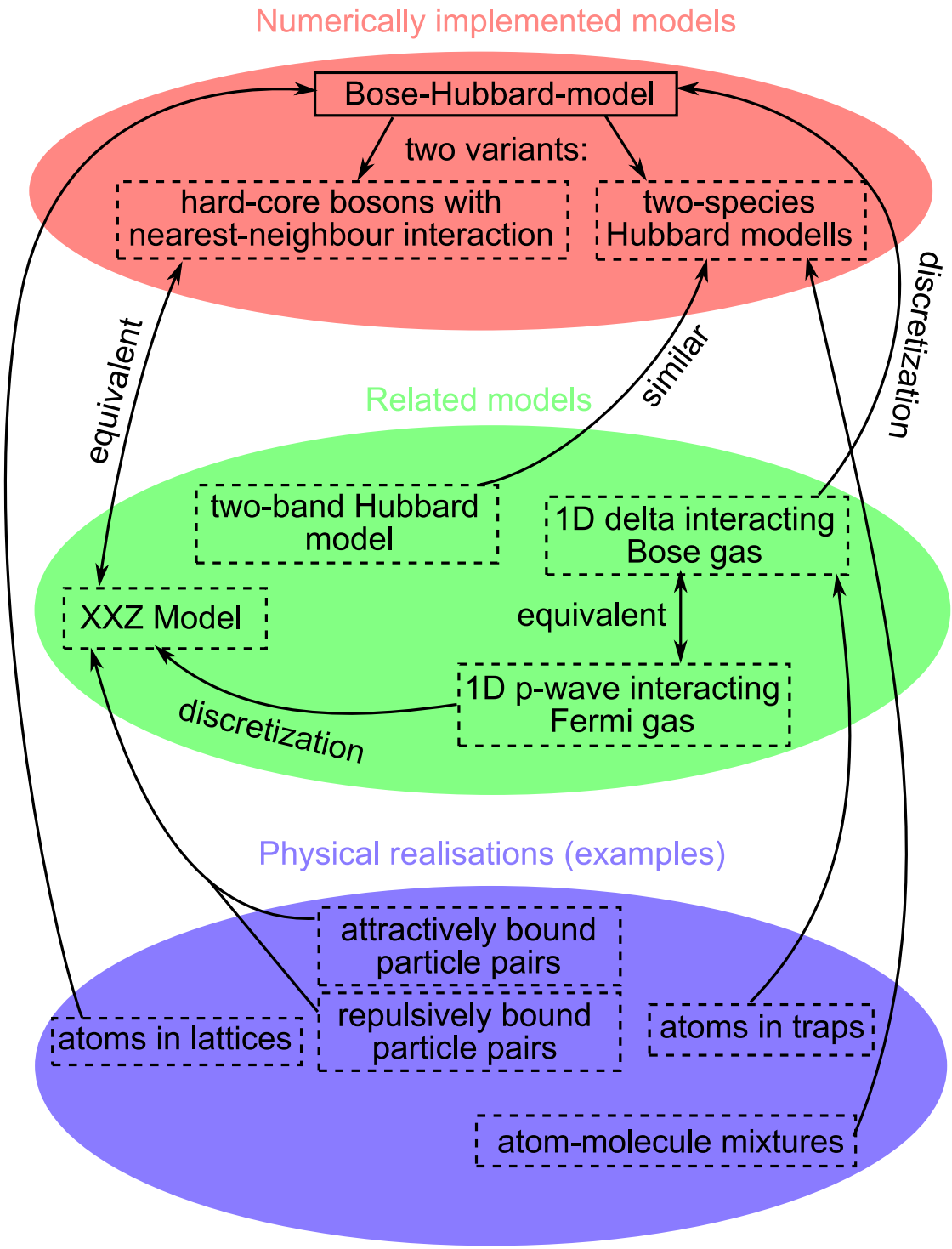

Figure 1.1: The diagram shows the models important for this thesis and their relations from a numerical point of view. The red models are those which are actually numerically implemented. The green models are those which can be mapped by some relation onto those of the red category and are thus also indirectly accessible to numerical treatment. The blue category contains some examples of physical systems which realize the models. There are of course many other realisations. Here are only those shown which are relevant to the present thesis.

other category are models, which first need to be mapped by discretization or other approximations to the models of the first category, like the 1D-delta-interacting Bose-gas (see Section 2.1) and the 1D spin-polarized Fermi-gas with local p-wave interaction (see Chapter 6). An overview of all the relationships between the models used in this thesis is given in Fig. 1.1 .

By using numerical methods to study multi-particle systems in the quantum regime, guides to interesting experiments can be provided, explanations for experiments given, the outcome of experiments checked, and in general much learned about such quantum mechanical systems.

The present thesis consists of four major parts. In Part I the main theoretical foundations of the work are outlined beginning with a detailed discussion of models for one-dimensional, homogeneous quantum gases in Chapter 2, the discussion of stochastic and DMRG numerical methods in Chapter 3 and some considerations about lattice models and their limitations in Chapter 4. Part II of the thesis is devoted to one-dimensional quantum gases in a confining trap potential. In Chapter 5 the 1D Bose gas with s-wave interaction is studied, in Chapter 6 the spin-polarised Fermi gas in 1D with p-wave interactions. Part III discusses novel meta-stable excited states of the Bose-Hubbard model, in particular the many-body dynamics of repulsively bound pairs of particles is studied in Chapter 7, that of attractively bound pairs in Chapter 8. Finally Part IV contains some thoughts about other multi-particle systems in lattices such as atom-molecular mixtures (Chapter 9) and two-component Bose gases (Chapter 10).

1.1 Units

In order to shorten the notation of mathematical expressions and to make the annotations of graphs easier to read, a set of units is introduced at the beginning of this thesis, which is always used when no particular unit is mentioned. This is possible because almost all formulas and graphs in this thesis deal with quantum multi-particle systems. Mathematical expressions dealing with such systems contain the Planck-constant $\hbar = 1.0545726\ldots \cdot 10^{-34} Js$ and the mass m of a single particle. This can be avoided by choosing $\hbar$ and m as the natural units. Together with a time-scale, $\hbar$ and m form a complete set of units. For a system in a harmonic trap potential this time-scale is given by the trap frequency ω. In systems which have no special time-scale it is tacitly assumed that some arbitrary time unit has been chosen. In this case the frequency ω is only to be understood as a formal unit. Unless otherwise stated everything in this thesis is written in units of m, $\hbar$

and ω. An exception is Chapter 4 where a different set of units is used which are explained at the beginning of that chapter. At some places m, $\hbar$ and ω still appear explicitly when they have an important meaning. From m, $\hbar$, and ω a length unit, the so-called oscillator length

$$l = \sqrt{\frac{\hbar}{m\omega}} \tag{1.1}$$

can be defined which is used whenever a variable appears which is a length or a position. Similarly energies are measured in units of $\hbar\omega$. Temperatures will be measured in units of $\hbar\omega/k_B$, where $k_B = 1.380658 \cdot 10^{-23} J/K$ is the Boltzmann constant.

Part I

Theoretical foundations

Chapter 2

Models of one-dimensional quantum gases

The purpose of this chapter is to give a brief introduction on various models which are used to describe many-particle systems in the quantum regime. The first section deals with the description of a one-dimensional (1D) interacting Bose-gas, where the interaction is modelled by a contact interaction. In the homogeneous case, i.e. when there is no spatially varying potential present, the solutions of the appropriate Hamiltonian can be found analytically by a Bethe ansatz. Since it is still difficult to obtain certain physical properties from the Bethe ansatz the second section introduces the Luttinger liquid theory from which one can more easily obtain information about first-order correlations of the system. The third section shows a way, how a mean field approximation can be obtained from a phase-space approach. The result is the Gross-Pitaevskii equation (GP), which is also called non-linear Schrödinger equation. Finally, the remaining two sections deal with models describing particles in optical lattices. The first one is the 1D-Bose-Hubbard-model, describing bosons in a lattice with an on-site interaction. The insulator to superfluid transition is discussed and the phase diagram shown. The second lattice model describes so-called hard-core bosons in a lattice with a nearest neighbour interaction. This model has many different and interesting phases. Furthermore the model is equivalent to a spin chain and the different interpretations of the phases in the spin- and particle picture are explored. This model is also solvable by a Bethe ansatz in 1D, thus the phase diagram is known. In the later chapters of this thesis it will become clear that all this models have a close relationship.

2.1 The one-dimensional interacting Bose gas

2.1.1 Realization and general properties

The investigation of quasi one-dimensional (1D) cold Bose gases has become of particular interest from the theoretical as well as from the experimental point of view. For the theorist it provides on the one hand insight into many purely quantum-mechanical effects like coherence, correlations, density-fluctuations, long-range-order effects and phase transitions. On the other hand, it is still simple enough that a mathematical and numerical analysis is not completely hopeless. Exact solutions are known for the homogeneous interacting gas [5, 6], and predictions for the correlation properties can be derived by Bogoliubov approximations [7, 8, 9] in the weak interaction limit and within the Luttinger-liquid theory [10, 11] for small energy excitations. It must be stressed here, that the 1D case cannot be regarded as a representative model for higher dimensions. Most of the properties of the 1D case cannot be translated into higher dimensions. The 1D Bose-gas has its own unique properties not found in higher dimensions and some of the properties of higher dimensions are not found in the 1D case. One of the remarkable differences to higher dimensions is that there is no true long range order in the 1D case, thus there is no proper Bose- Einstein-condensation at low temperature. The 1D case shows however something which is called quasi-long-range order, which manifests in an algebraic (rather than exponential) decay of first order correlations.

For the experimentalist the 1D Bose gas is interesting because it is a quantum system where quantum correlations are important but yet it is easy to realize with neutral ultra-cold atoms and its parameters can easily be manipulated.

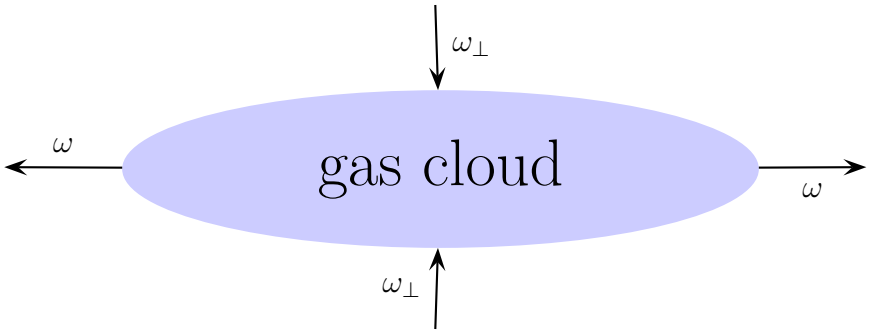

$$\hbar\omega_\perp \gg k_\mathrm{B}T, \mu, \hbar\omega$$

Figure 2.1: Creating a quasi one-dimensional gas

Furthermore it has many important applications like atom-lasers and quantum computers. For the latter it is necessary to know how single cold atoms can be positioned and their state changed and controlled. Therefore it seems clear that a detailed knowledge of properties of cold Bose-gases in 1D is necessary. To realize the one-dimensionality one has to confine the gas by a highly anisotropic trap. The confinement has important consequences as the interaction between atoms depends on the confinement strength. See [12] and Eq. (2.3).

It can be realized for example with a cylindrical trap where the radial trap frequency $\omega_\perp$ is much larger than the axial frequency ω. In the radial direction the motion is frozen to zero-point oscillations. This requires that any characteristic energy like $k_\mathrm{B}T$, where k_B is the Boltzmann constant and T is the temperature, or the chemical potential μ has to be much smaller than $\hbar\omega_\perp$. An upper limit for $\omega_\perp$ is given by the condition, that the radial oscillator length $l_\perp = \sqrt{\frac{\hbar}{m\omega_\perp}}$ has to be larger than the three-dimensional (3D) scattering length a_3D or at least larger than the effective range of the inter-particle potential.

Interaction between the particles at low energies can be modelled by so called pseudo-potentials. Pseudo-potentials replace the true inter-particle potential and usually contain a Dirac-Delta function $\delta(\vec{r}_2 - \vec{r}_1)$, where $\vec{r}_1, \vec{r}_2$ are the positions of two particles. This simplifies the theoretical treatment of interactions significantly, because interactions only come into play when particles occupy the same position. For a hard-sphere interaction exact pseudopotentials can be found [13, 14]. In 3D the pseudopotential for the hard sphere is

$$U(\vec{r}) = 4\pi a_\mathrm{3D}\delta(\vec{r})\frac{\partial}{\partial r}(r\cdot) \tag{2.1}$$

where $\vec{r} = \vec{r}_1 - \vec{r}_2$, $r = |\vec{r}|$ and a_3D is the diameter of the sphere and equal to the 3D scattering length. The dot in Eq. (2.1) is a placeholder for the wavefunction the pseudopotential is acting on. In one dimension the result is quite different. Here one finds

$$U(\vec{r}) = -\frac{2}{a_\mathrm{1D}}\delta(\vec{r}). \tag{2.2}$$

It can be shown that this pseudopotential is also a good approximation for general inter-atomic potentials, where a_1D and a_3D are the 1D and 3D scattering length. However, if a 1D system is created by confining a 3D system, then the effective 1D scattering length is different from the 3D scattering length. The 1D scattering length will depend on the confinement. In [12] the relation between a_1D and a_3D

was derived to be

$$a_{1\mathrm{D}} = -\frac{l_\perp^2}{a_{3\mathrm{D}}}\left(1 - 1.0326\frac{a_{3\mathrm{D}}}{l_\perp}\right). \tag{2.3}$$

Using the δ-like pseudo-potential (2.2), the Hamiltonian which describes a quantum mechanical gas of particles in one dimension has in second quantization the form

$$\hat{H} = -\frac{1}{2}\int dx\ \hat{\Psi}^\dagger(x)\partial_x^2\hat{\Psi}(x) + \int dx\ \hat{\Psi}^\dagger(x)V(x)\hat{\Psi}(x) + \\ + \frac{g_{1\mathrm{D}}}{2}\int dx\int dx'\,\hat{\Psi}^\dagger(x)\,\hat{\Psi}^\dagger(x')\delta(x-x')\,\hat{\Psi}(x')\,\hat{\Psi}(x), \tag{2.4}$$

where $g_{1\mathrm{D}} = -2/a_{1\mathrm{D}}$ is the coupling constant. The bosonic field operators have the properties

$$[\hat{\Psi}(x), \hat{\Psi}^\dagger(y)] = \delta(x-y), \tag{2.5}$$

$$[\hat{\Psi}(x), \hat{\Psi}(y)] = 0. \tag{2.6}$$

The first term of (2.4) describes the kinetic energy of the particles, the second term the potential energy of the particles and the third term the interaction between particles. From [5, 6] it is known that this system can be described by a universal parameter $\gamma = g_{1\mathrm{D}}/\rho$ in the homogeneous case, i.e. for $V(x) = 0$, where ρ is the density. This will be discussed in more detail in Section 2.1.2. If $\gamma \ll 1$ the system is in the weakly interacting regime where the energy and density are given by the Gross-Pitaevskii (GP) equation [15, 16, 17] (See also Section 2.2). In the opposite limit, $\gamma \gg 1$, the system enters the Tonks-Girardeau (TG) regime of a gas of impenetrable (hard-core) bosons [18, 19]. In the TG regime, the system behaves in many aspects like a gas of fermions.

2.1.2 The Bethe-ansatz solution

In this section the solutions for the Hamiltonian (2.1.2) with $V(x) = 0$, which have been derived by E. H. Lieb and W. Liniger [5] and C. N. Yang and C. P. Yang [6] are discussed. The formulation of the problem usually starts with the N-particle Schrödinger equation in first quantizations

$$\left[-\sum_{j=1}^{N}\frac{\partial_{x_j}^2}{2} + g_{1\mathrm{D}}\sum_{i<j}\delta(x_j - x_i)\right]\phi(x_1,\ldots,x_N) = E\phi(x_1,\ldots,x_N), \tag{2.7}$$

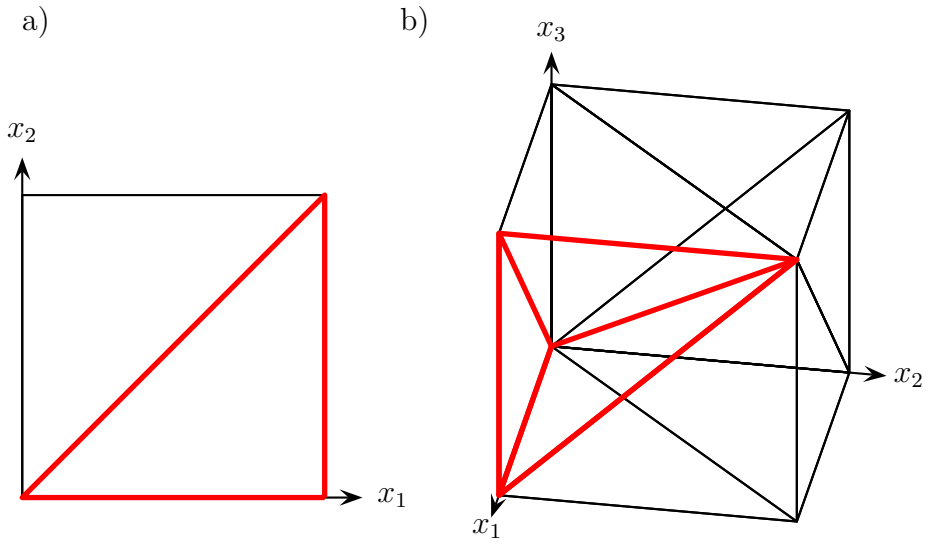

Figure 2.2: Simplex structure of the configuration space of 2 (a) and 3 (b) δ-interacting particles. The red marked simplexes correspond to $x_2 < x_1$ and $x_2 < x_3 < x_1$ respectively.

where ϕ is the multi-particle wave function. The Hamiltonian used in the Schrödinger equation (2.7) is equivalent with (2.4) for $V(x) \equiv 0$. An analytic solution of this equation is possible, because of two reasons. Firstly, due to the δ-interaction the gas is a free gas as long as the particles do not occupy the same position and secondly in one-dimension there is no way for the particles to pass each other without colliding. To make this more clear consider N particles with positions $x_1, x_2, \ldots, x_N$ in a one-dimensional box of size L. Since the particles move only in one dimension, the positions can be ordered $0 < x_{P(1)} < x_{P(2)} < \ldots < x_{P(N)} < L$ where P is some Permutation of the numbers $\{1, 2, 3, \ldots, N\}$. The set of all possible values x_i that does not destroy the ordering, defines a region in configuration space where no collision between particles happens. Thus, for this region the gas is a free gas. The same holds for all possible permutations P. In this way the configuration space splits into $N!$ regions R_i, $i = 1, 2, 3, \ldots, N!$. Geometrically this regions are N-simplexes, i.e. they are the convex hull of $N+1$ points in an N-dimensional space. Fig. 2.2 shows the simplexes for two and three particles. The simplex structure allows for a simple ansatz for the solution in terms of plane waves. On the simplex R_1 defined by $0 < x_1 < x_2 < \ldots < x_N < L$ the wavefunction can be written as

$$\phi(x_1, \ldots, x_N) = \sum_P a(P) \exp\left(i \sum_{j=1}^{N} k_{P(j)} x_j \right) . \tag{2.8}$$

The definition of the wavefunction on the other simplexes follows from the requirement of total symmetry under all particle permutations. This ansatz already solves the Schrödinger equation in the inner part of the simplexes, because plane waves solve the Schrödinger equation for non-interacting particles. The amplitudes $a(P)$ and the quasi-momenta k_j must be adjusted that the ansatz (2.8) also solves the Schrödinger equation at the simplex-boundaries. In fact it can be shown that the Schrödinger equation is fulfilled at the simplex-boundaries if the wave function on R_1 fulfils the contact condition

$$\left(\frac{\partial}{\partial x_{j+1}} - \frac{\partial}{\partial x_j}\right)\phi|_{x_{j+1}=x_j+} = g_{1\mathrm{D}}\phi|_{x_{j+1}=x_j+}. \tag{2.9}$$

Eq. (2.9) demands, that the derivative of the wavefunction is discontinuous at the boundary of the simplex. This can be seen by going to the simplex where x_j and x_{j+1} are ordered in the opposite way for a fixed j. Then the left side of Eq. (2.9) changes its sign, while ϕ itself is continuous and cannot change the sign due to the bosonic particle symmetry. Thus, when the second derivative of the kinetic energy part is applied to the wavefunction it results in a delta function which can absorb the delta interaction term. Furthermore, one has to take into account the physical boundary conditions. For periodic boundary conditions this leads to the conditions

$$\phi(0, x_2, \ldots, x_N) = \phi(x_2, \ldots, x_N, L), \tag{2.10a}$$

$$\frac{\partial}{\partial x}\phi(x, x_2, \ldots, x_N)|_{x=0} = \frac{\partial}{\partial x}\phi(x_2, \ldots, x_N, x)|_{x=L}. \tag{2.10b}$$

As is shown in the following all three boundary conditions (2.9),(2.10a) and (2.10b) determine the k_j and the $a(P)$ completely. The amplitudes $a(P)$ are of course only determined up to a phase factor. To derive an equation for the k_j it is sufficient to have a look at permutations P and Q which differ only by an exchange of two adjacent indices i.e.

$$Q^{-1}P = p_{j,j+1}, \tag{2.11}$$

where $p_{j,j+1}$ is a permutation with the properties

$$p_{j,j+1}(j) = j + 1, \tag{2.12}$$

$$p_{j,j+1}(j + 1) = j, \tag{2.13}$$

$$p_{j,j+1}(k) = k \text{ for } k \neq j, k \neq j + 1. \tag{2.14}$$

If (2.8) is inserted into (2.9) and those permutations are compared, which differ by $p_{j,j+1}$ the so called Bethe equation

$$a(Pp_{j,j+1}) = -a(P)\frac{g_{1D} - i(k_{P(i)} - k_{P(i+1)})}{g_{1D} + i(k_{P(i)} - k_{P(i+1)})} = -a(P)\exp(i\theta_{P(i+1)P(i)}) \tag{2.15}$$

is found, where

$$\theta_{ij} = \theta(k_i - k_j). \tag{2.16}$$

and

$$\theta(r) = -2\tan^{-1}(r/g_{1D}) \tag{2.17}$$

Since every permutation can be decomposed into $p_{j,j+1}$ permutations the amplitudes $a(P)$ can be calculated . If (2.8) is inserted into (2.10b) the relation

$$a(P) = a(PS)\exp(ik_{P(1)})L \tag{2.18}$$

is found, where S is a permutation defined by $S(j) = j + 1, j \neq N$, $S(N) = 1$. If S is factored into exchanges of adjacent indices the result is

$$S = p_{1,2}p_{2,3}\ldots p_{N-2,N-1}p_{N-1,N}. \tag{2.19}$$

Using (2.15) results in

$$a(PS) = (-1)^{N-1}a(P)\exp\left(i\sum_{j=0}^{N-1}\theta_{P(N-j),P(1)}\right) \tag{2.20}$$

$$= (-1)^{N-1}a(P)\exp\left(i\sum_{j=1}^{N}\theta_{j,P(1)}\right). \tag{2.21}$$

Together with (2.18) the final equation of the k_j is

$$(-1)^{N-1}e^{-ik_mL} = \exp\left(i\sum_{j=1}^{N}\theta_{j,m}\right). \tag{2.22}$$

Thus, the problem of solving the Schrödinger equation is reduced to finding a solution of (2.22). The whole structure of the procedure however shows that such a kind of solution is only possible in one dimension. In higher dimension not even the simplex structure of the configuration space exists. Only in one dimension the surfaces corresponding to colliding particles in configuration space are exactly

one dimension less than the configuration space itself. In higher dimensions the configurations space does not fall into pieces.

It should be noted that the knowledge of the N-particle wavefunction does not mean that one has easy access to all interesting physical quantities as this requires in general to integrate out all but a few degrees of freedom. The latter can be done in general only numerically using Monte-Carlo techniques. One is however able to gain access to all expectation values which are simple functions of the k_j. For example the energy which is proportional to $\sum_j k_j^2$. On the other hand, expectation values which are not simple functions of the k_j, for example non-local correlations of the system, are difficult if not impossible to obtain. In the thermodynamic limit it is possible to determine the density $\rho(k)$ of the k_j so that the number of k_j lying in an interval dk is $L\rho(k)dk$. Then the density of the gas is

$$\rho = \int_{-\infty}^{\infty} \rho(k)dk. \tag{2.23}$$

In [6] an equation for $\rho(k)$ in the thermodynamic limit was derived

$$2\pi\rho(k)\left[1 + \exp(E(k)/T\right] = 1 + 2g_{1\mathrm{D}} \int_{-\infty}^{\infty} \frac{\rho(q)dq}{c^2 + (k-q)^2} \tag{2.24}$$

where $E(k)$ must fulfil the equation

$$E(k) = -\mu + \frac{k^2}{2} - \frac{Tc}{\pi} \int_{-\infty}^{\infty} \frac{dq}{g_{1\mathrm{D}}^2 + (k-q)^2} \ln[1 + \exp(-E(q)/T)], \tag{2.25}$$

μ is the chemical potential and T is the temperature. Eq. (2.24) and (2.25) make it now possible to look for universal parameters of the delta interacting Bose gas. Universal parameters are variables that fully characterise the properties of the system. They define equivalence classes of the system-parameters for which the system has basically the same properties. From the three system-parameters $g_{1\mathrm{D}}$, T, μ at least one should be possible to eliminate. One successful possibility is to define the parameters

$$\chi = \frac{\mu}{g_{1\mathrm{D}}^2}, \tag{2.26}$$

$$\tau = \frac{T}{g_{1\mathrm{D}}^2}, \tag{2.27}$$

and to introduce the rescaled functions

$$\sigma(k) = \rho(g_{1\mathrm{D}}k), \tag{2.28}$$

$$\xi(k) = E(g_{1\mathrm{D}}k)/g_{1\mathrm{D}}^2. \tag{2.29}$$

With these equations (2.24) and (2.25) can be rewritten as

$$2\pi\sigma(k)(1+\exp(\xi(k)/\tau) = 1 + 2\int_{-\infty}^{\infty} \frac{\sigma(q)dq}{1+(k-q)^2}, \tag{2.30}$$

$$\xi(k) = -\chi + \frac{k^2}{2} - \frac{\tau}{\pi}\int_{-\infty}^{\infty} \frac{dq}{1+(k-q)^2}\ln(1+\exp(-\xi(q)/\tau)). \tag{2.31}$$

This shows that the basic properties of the system depend only on χ and τ.

The parameter χ is not directly related to physical properties. It will be replaced in the following by a parameter which is as close as possible related to the density of the gas but is still universal in the sense that it is itself a function only of χ and τ. This parameter is the so called Tonks-Giradeau parameter

$$\gamma = \frac{g_{1\mathrm{D}}}{\rho}. \tag{2.32}$$

The parameter is universal, since

$$\gamma\int_{-\infty}^{\infty}\sigma(k)dk = 1 \tag{2.33}$$

and the integral over $\sigma(k)$ is only a function of χ and τ. In the same way one can define universal functions

$$\epsilon_m(\gamma,\tau) = \gamma^{m+1}\int_{-\infty}^{\infty} k^m\sigma(k) \tag{2.34}$$

which are useful for calculating expectation values that are simple functions of k.

An important special case is the zero temperature limit $\tau \to 0$. In this limit the logarithm in (2.31) will go to zero when $E(q) > 0$ and go to $-E(q)$ if $E(q) < 0$. In [6] it is shown, that $E(k)$ is a monotonically increasing function of k^2. Thus, $E(q)$ has zeros only at some value $q = \lambda$ and $q = -\lambda$. Eq. (2.30) and (2.31) then become

$$2\pi\sigma(k) = 1 + 2\int_{-\lambda}^{\lambda}\frac{\sigma(q)dq}{1+(k-q)^2} \tag{2.35}$$

$$\xi(k) = -\chi + \frac{k^2}{2} + \frac{1}{\pi}\int_{-\lambda}^{\lambda} \frac{\xi(q)dq}{1+(k-q)^2} \tag{2.36}$$

As stated above all these quantities are related only two the knowledge of the k_j. From those only local properties can be calculated. For long-distance-correlations the best approximative analytic calculations known to the author are predictions from Luttinger liquid theory which will be discussed in the next section. Short-distance-correlations can still be calculated exactly from the Lieb-Liniger solution making use of the fact that they correspond to large momentum and large momentum corresponds to wave-length much smaller than the simplex-size.

For the inhomogeneous case γ is not well defined, because its definition contains the density, which in the inhomogeneous case depends on position . One could use χ instead, because the chemical potential is a well defined number also for inhomogeneous systems. On the other hand χ and the chemical potential are – as already mentioned – only indirectly related to physical properties. However, the relation in the homogeneous case

$$\chi = \frac{3\epsilon_2(\gamma) - \gamma\epsilon_2'(\gamma)}{2\gamma^2} := f(\gamma) \tag{2.37}$$

between χ and γ can be used to define some local gamma. This local gamma is implicitly defined by replacing χ in Eq. (2.37) by

$$\chi_{\text{eff}} = \chi - \frac{V(x)}{g_{1\text{D}}^2} \tag{2.38}$$

Using the Lieb-Liniger solution for the homogeneous gas with the replacement (2.38) is called a local density approximation (LDA), because the density is now calculated from the homogeneous solution by replacing the chemical potential by the effective chemical potential $\mu - V(x)$. One important implication of the Lieb-Liniger-solution is, that the Gross-Pitaevskii (GP) solution in one dimension is only valid for very small interaction and large density. This means that apart from the TG-limit there is a large regime of intermediate interaction strength, where a one-dimensional Bose-gas has properties not well described by simple approximations. E.g. one finds for the relative error between the GP-density ρ_{GP} and the Lieb-Liniger (LL) density ρ_{LL}

$$\frac{\rho_{\text{GP}}}{\rho_{\text{LL}}} - 1 = f(\gamma)\gamma - 1, \tag{2.39}$$

and for the relative error between the TG-density ρ_{TG} and the Lieb-Liniger den-

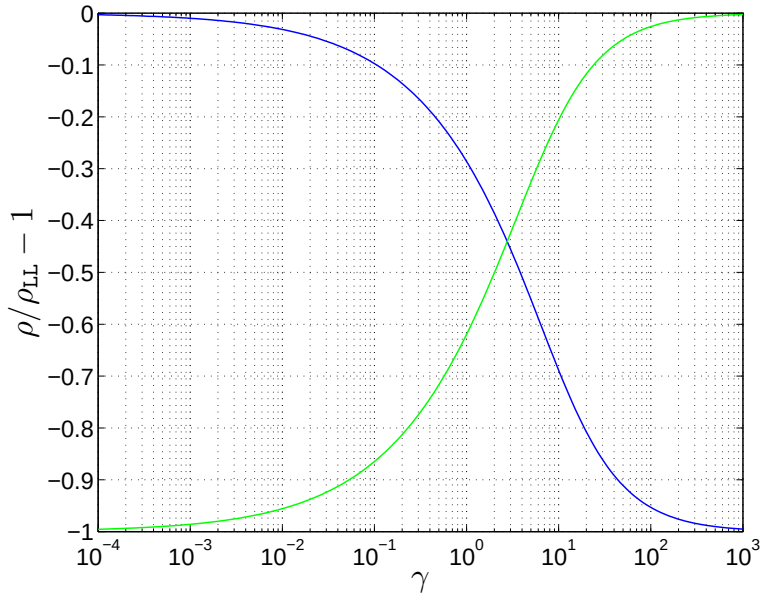

Figure 2.3: Relative error of the density predicted by the Gross-Pitaevskii (blue) and the Tonks-Giradeau approximation (green).

sity ρ_{LL}

$$\frac{\rho_{\mathrm{TG}}}{\rho_{\mathrm{LL}}} - 1 = \frac{\sqrt{2f(\gamma)}}{\pi}\gamma - 1. \tag{2.40}$$

Fig. 2.3 shows how much the densities predicted by the GP-approximation and the TG gas differ from the Lieb-Liniger density. One finds that the GP prediction differs more than 1% for $\gamma > 10^{-3}$, thus only for quite large densities the GP approximation is good. On the other hand the TG gas differs more than 1% for $\gamma < 270$. Thus, in between those two gamma values none of the two approximations is valid. Fig. 2.3 suggests that the centre of intermediate interactions is somewhere around $\gamma = 2.8$.

2.1.3 1D bosons as Luttinger liquid

In the previous section it became clear that the Bethe ansatz solution of the interacting Bose-gas does not provide an easy access to correlations. For many gap-less 1D-quantum mechanical systems it is however known that they can be approximated as a Luttinger liquid, for which the long range correlation properties can be obtained. The Hamiltonian of such a Luttinger liquid is given by

$$\hat{H} = \frac{1}{2\pi}\int dx \left[uK(\partial_x\hat{\phi}(x))^2 + \frac{u}{K}(\pi\hat{\Pi}(x))^2\right], \tag{2.41}$$

where K is the Luttinger parameter and u is the phase velocity. The operator $\hat{\Pi}(x)$ is related to the density operator by

$$\hat{\Psi}^\dagger(x)\,\hat{\Psi}(x) \approx \rho_0 + \hat{\Pi}(x). \tag{2.42}$$

$\hat{\phi}(x)$ can be identified as a phase operator, such that the field operator can be approximately thought of as

$$\hat{\Psi}(x) \approx e^{i\hat{\phi}(x)}\sqrt{\hat{\Psi}^\dagger(x)\,\hat{\Psi}(x)}. \tag{2.43}$$

$\hat{\phi}(x)$ and $\hat{\Pi}(x)$ are canonically conjugated fields, i.e.

$$[\hat{\Pi}(x), \hat{\phi}(x')] = i\delta(x - x'). \tag{2.44}$$

That shows that they can always be represented as linear-combinations of bosonic operators. For fermionic Hamiltonians like the Fermi-Hubbard Hamiltonian or spin-models this approximation is known under the term bosonization, because the excitations around the Fermi-energy have bosonic properties. Thus for bosonic Hamiltonians one could call this approximation bosonization of bosons, which might be confusing, since the bosons which are used to represent $\hat{\phi}(x)$ and $\hat{\Pi}(x)$ must be distinguished from the actual particles.

An important result of the bosonization is that the parameters u, K can be obtained relatively easy from the Bethe ansatz solution of the exact Hamiltonian. For that it is sufficient to know how the Energy E of the ground state depends on the particle number and how it depends on a twist $\hat{\Psi}(L) = e^{i\hat{\phi}}\,\hat{\Psi}(0)$ in the boundary conditions. The relations defining K and u finally are

$$uK = \pi L \partial_\phi^2 E(\phi), \tag{2.45}$$

$$\frac{u}{K} = \frac{1}{\pi} L \partial_N^2 E(N). \tag{2.46}$$

From these equations it is now possible to determine the first order correlation properties of the interacting Bose-gas. Let the first order correlation function be defined as

$$g_1(x_1, x_2) = \frac{\langle\, \hat{\Psi}^\dagger(x_1)\,\hat{\Psi}(x_2)\rangle}{\sqrt{\langle\, \hat{\Psi}^\dagger(x_1)\,\hat{\Psi}(x_1)\rangle}\sqrt{\langle\, \hat{\Psi}^\dagger(x_2)\,\hat{\Psi}(x_2)\rangle}}. \tag{2.47}$$

The Luttinger-Liquid theory [11] predicts an algebraic decay

$$g_1(x,0) \propto x^{-\frac{1}{2K}} \tag{2.48}$$

at $T = 0$ and an exponential decay

$$g_1(x,0) \propto e^{-|x|/L_c(T)} \tag{2.49}$$

for $T > 0$. The thermal length L_c is not so easily obtained from the exact solution. But for $T = 0$ the exponent is a simple function of K. Furthermore, for a Galilean invariant system one has

$$uK = \pi \frac{N}{L}. \tag{2.50}$$

The energy of the interacting Bose-gas is given by the Lieb-Liniger solution

$$E(N) = \frac{N^3}{2L^2} \epsilon_2 \left(\frac{g_{1\mathrm{D}} L}{N} \right). \tag{2.51}$$

With that one finds

$$K = \sqrt{\frac{\pi^2}{-\gamma^3 f'(\gamma)}} \tag{2.52}$$

with the Tonks-Girardeau parameter $\gamma = \frac{g_{1\mathrm{D}} L}{N}$ and $f'(\gamma) = \partial_\gamma f(\gamma) < 0$. It turns out that the Luttinger parameter is only a function of the Tonks-Gireadeau parameter and thus displays its universal nature.

2.2 Phase-space representation for bosons and Gross-Pitaevskii equation for weakly interacting bosons

Phase-space methods provide a way to map the dynamics of quantum systems onto stochastic differential equations of classical c-numbers. They help to understand to what extend quantum systems can be seen as classical systems with probabilistic or stochastic behaviour, and also where this analogy breaks down. The aim of this section is to introduce an important approximation for weakly interacting Bose gases, the Gross-Pitaevskii (GP) equation, with the help of the phase space

approach. A simple one-mode problem, the Kerr oscillator with the Hamiltonian

$$\hat{H} = \omega \hat{a}^\dagger \hat{a} + \frac{\kappa}{2} \hat{a}^{\dagger 2} \hat{a}^2 \tag{2.53}$$

will be used to explain the method. $\hat{a}^\dagger$ and $\hat{a}$ are bosonic creation- and annihilation operators (see Section 2.3). The generalization to multi-mode problems is then accomplished easily. A phase space representation of the problem is obtained expanding the statistical operator $\hat{\rho}$ in the overcomplete set of Glauber-coherent states

$$|\alpha\rangle = e^{-\frac{|\alpha|^2}{2}} \sum_{n=0}^{\infty} \frac{\alpha^n}{\sqrt{n!}} |n\rangle, \quad \alpha \in \mathbb{C}. \tag{2.54}$$

The statistical operator can then be written in the form

$$\hat{\rho}(t) = \int d^2\alpha P(\alpha, t) |\alpha\rangle\langle\alpha|. \tag{2.55}$$

The function P is real-valued because $\rho(t)$ is self-adjoint and has the property

$$\int d^2\alpha P(\alpha, t) = 1 \tag{2.56}$$

since $\operatorname{Tr} \hat{\rho}(t) = 1$. P could naively be interpreted as a probability distribution, however it is not positive in general. In that respect P is not in all cases a classical probability distribution. For mapping the dynamics of $\hat{\rho}$ to P one can use the following identities [20]

$$\hat{a}|\alpha\rangle = \alpha|\alpha\rangle, \tag{2.57}$$

$$\hat{a}^\dagger|\alpha\rangle = \left(\frac{\alpha^*}{2} + \partial_\alpha\right)|\alpha\rangle, \tag{2.58}$$

from which one can derive the following mapping:

$$\hat{a}\hat{\rho} \longrightarrow \alpha P(\alpha), \tag{2.59}$$

$$\hat{a}^\dagger\hat{\rho} \longrightarrow (\alpha^* - \partial_\alpha) P(\alpha). \tag{2.60}$$

The von Neumann equation

$$\partial_t \hat{\rho}(t) = -i[\hat{H}, \hat{\rho}(t)] \tag{2.61}$$

can then be written as a generalized Fokker-Planck equation for P

$$\partial_t P(\alpha,t) = \Big[\partial_\alpha(i\omega + i\kappa|\alpha|^2)\alpha - \partial_{\alpha^*}(i\omega + i\kappa|\alpha|^2)\alpha^* - i\frac{\kappa}{2}(\partial_\alpha^2\alpha^2 - \partial_{\alpha^*}^2\alpha^{*2})\Big]P(\alpha,t). \quad (2.62)$$

The resulting differential equation is non-linear because of the $\kappa|\alpha|^2$ term. With the solution of the Fokker-Planck equation normal ordered, equal-time quantum averages can be calculated

$$\langle \hat{a}^{\dagger n}\hat{a}^m\rangle = \int d^2\alpha P(\alpha,t)\alpha^{*n}\alpha^m, \quad (2.63)$$

which establishes the correspondence between quantum and classical variables. It can be shown that the dynamics of P is equivalent to the stochastic differential equations [20, 21]

$$i\partial_t\alpha(t) = [\omega + \kappa|\alpha|^2]\alpha + i\sqrt{i\kappa/2}[\xi_1(t) + \xi_2(t)]\alpha(t), \quad (2.64)$$

$$i\partial_t\alpha^*(t) = -[\omega + \kappa|\alpha|^2]\alpha^* + \sqrt{i\kappa/2}[\xi_2(t) - \xi_1(t)]\alpha^*(t), \quad (2.65)$$

where the stochastic variables ξ_1 and ξ_2 fulfil

$$\overline{\xi_1(t)\xi_1(t')} = \overline{\xi_2(t)\xi_2(t')} = \delta(t-t') \quad (2.66)$$

$$\overline{\xi_1(t)\xi_2(t')} = 0. \quad (2.67)$$

The line denotes stochastic averaging. It holds

$$\langle \hat{a}_{(t)}^{\dagger n}\hat{a}_{(t)}^m\rangle = \int d^2\alpha P(\alpha,t)\alpha^{*n}\alpha^m = \overline{\alpha^{*n}(t)\alpha^m(t)}. \quad (2.68)$$

When κ is small one can neglect the terms in Eq. (2.64) and (2.65) containing the stochastic variables. Then those equations become classical differential equations.

Generalizing this procedure for the Hamiltonian (2.4) of an interacting Bose gas is now easy because it has the same structure as the simple example (2.53) which was discussed here. ω plays the role of the kinetic energy and κ corresponds to $g_{1\mathrm{D}}^B$. Neglecting the stochastic variables then leads to the Gross-Pitaevskii equation

$$i\partial_t\psi(x,t) = \left[-\frac{\partial_x^2}{2} + g_{1\mathrm{D}}^B|\psi(x,t)|^2 + V(x)\right]\psi(x,t) \quad (2.69)$$

where $\psi(x,t)$ is a complex function corresponding to α. The Gross-Pitaevskii equation can be used to describe a weakly interacting Bose gas.

2.3 The one-dimensional Bose-Hubbard model

In many experiments interacting bosonic particles are manipulated with the help of periodic lattice potentials. These lattice potentials are usually created by standing-wave laser beams and thus allow both a high controllability of the distance between two lattice sites and of the lattice depth. In this way particles can be easily brought into array structures and their properties examined. For lattice potentials it is well known that their energy spectrum consists of bands. In the regime of low temperature, where quantum properties of the particles can be observed, one can assume that all particles are in the lowest energy band. In that case the particles can only move through the lattice via quantum mechanical tunnelling. The speed of the tunnelling depends on the lattice depth. On the other hand the particles interact usually repulsively when they are sitting on the same lattice site, thus particle tunnelling to a site is suppressed when this site is already occupied by other particles and the interaction is sufficiently strong. As a result there is an interplay between the two processes of tunnelling and interaction. The energy penalty of particles which sit on the same site is in a good approximation proportional to the square of the number of the particles. A model Hamilton should therefore contain a part which describes the hopping of the particles between sites and a part which describes the interaction. This Hamiltonian can be most easily formulated in terms of bosonic creation and annihilation operators $\hat{a}_j^\dagger$ and $\hat{a}_j$, which either create or annihilate a particle at lattice site j. Application of the creation and annihilation operators to the number states yield

$$\hat{a}_j^\dagger|n_j\rangle = \sqrt{n_j+1}|n_j+1\rangle, \tag{2.70}$$

$$\hat{a}_j|n_j\rangle = \sqrt{n_j}|n_j-1\rangle. \tag{2.71}$$

They obey the commutation relations

$$[\hat{a}_i, \hat{a}_j^\dagger] = \hat{a}_i\hat{a}_j^\dagger - \hat{a}_j^\dagger\hat{a}_i = \delta_{ij} \tag{2.72}$$

$$[\hat{a}_i, \hat{a}_j] = \hat{a}_i\hat{a}_j - \hat{a}_j\hat{a}_i = 0 \tag{2.73}$$

An important property is, that operators of different sites always commute. This simplifies for example much the numerical representations of these operators in

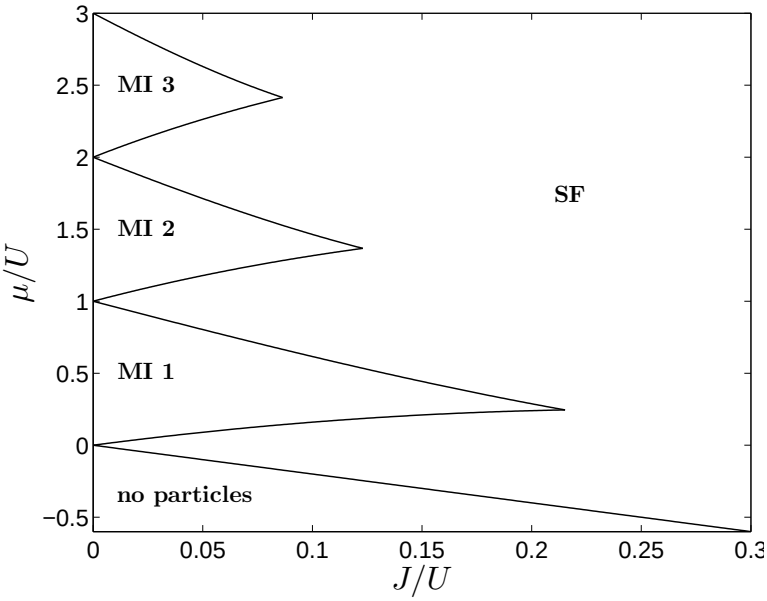

Figure 2.4: Phase diagram of the one-dimensional Bose-Hubbard model at zero temperature. μ is the chemical potential, i.e. the energy which is necessary to add one particle. Shown are the boundaries of the Mott insulator (MI) phases for 0, 1, 2 and 3 particles per site as obtained from a third order perturbation calculation [22]. Beyond the tips of the MI phases (whose values are listed in Tab. 2.1) only a superfluid (SF) phase exists.

terms of tensor products. With the help of $\hat{a}_j^\dagger$ and $\hat{a}_j$ it is now possible to write down a Hamiltonian which describes the interacting particles in a lattice. This Hamiltonian is called the Bose-Hubbard-Hamiltonian and reads

$$\hat{H} = -J \sum_j (\hat{a}_j^\dagger \hat{a}_{j+1} + \hat{a}_{j+1}^\dagger \hat{a}_j) + \frac{U}{2} \sum_j \hat{a}_j^{\dagger 2} \hat{a}_j^2 + \sum_j D_j \hat{a}_j^\dagger \hat{a}_j. \tag{2.74}$$

The parameter J governs the tunnelling rate of the particles between adjacent sites and U is a measure of how strong the particles interact. The variables D_j model an additional weak potential which is superposed to the lattice but varies spatially much slower than the lattice potential.

The Bose-Hubbard model is interesting because it can describe the quantum phase transition of particles in a lattice from a Mott insulator to a superfluid phase. The Mott insulator phase arises when the lattice is very deep and the number of particles is an integer multiple of the number of lattice sites. Then the particle number fluctuations per site go to zero, the compressibility

$$\frac{\partial \langle \hat{n} \rangle}{\partial \mu} \tag{2.75}$$

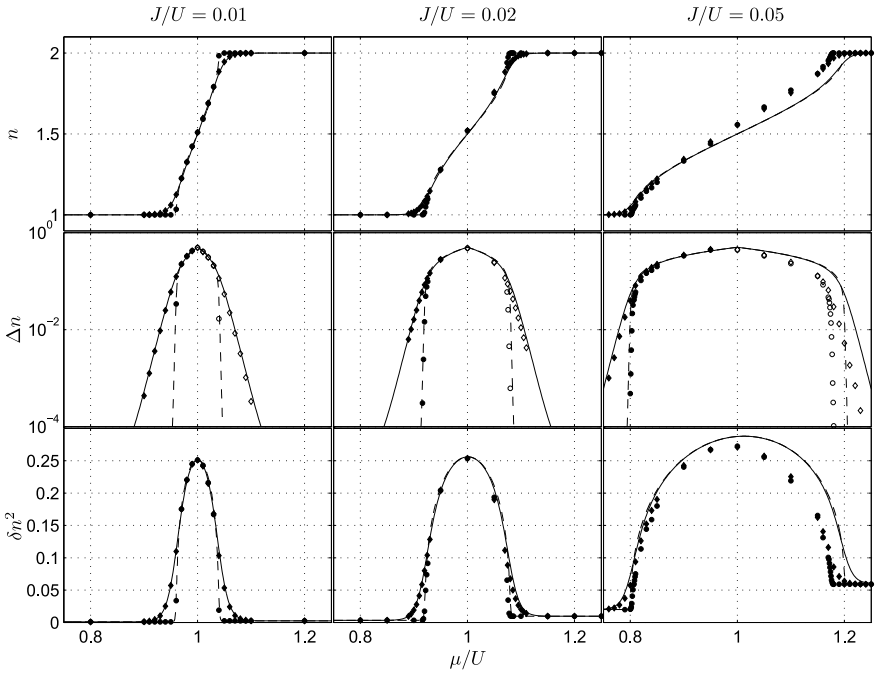

Figure 2.5: Average number and number fluctuation versus the chemical potential μ for two temperatures ($T = 0.01U, 0.001U$) and three values of the hopping parameter ($J = 0.01U, 0.02U, 0.05U$). Top row, on-site population, $n = \langle \hat{a}_k^\dagger \hat{a}_k \rangle$; middle row, difference Δn between n and the nearest integer; bottom row, on-site number fluctuations $\delta n^2 = \langle (\hat{a}_k^\dagger \hat{a}_k)^2 \rangle - \langle \hat{a}_k^\dagger \hat{a}_k \rangle^2$. The lines show perturbative results ($T = 0.001U$, solid line; $T = 0.01U$, dashed line); the markers show results of DMRG calculations ($T = 0.001U$, diamonds; $T = 0.01U$, circles. Open markers are used for $\Delta n < 0$. Source of data and graphs: [23].

vanishes, and the particles do not move anymore. Here $\langle \hat{n} \rangle$ is the average number per site (compare Fig. 2.5). When the lattice depth is lowered the tunnelling of the particles at a certain point dominates again and the quantum mechanical wavefunction of each particle spreads across the whole lattice. The particles go into a coherent state with a fixed phase relation between distant sites and the gas becomes superfluid. The analytic predictions of the boundaries of the Mott insulator phases is only possible approximatively. A third order perturbation calculation in J/U [22] of the upper and lower boundaries of the Mott-insulator phases yields

$$\frac{\mu_{\text{upper}}}{U} = n - 2(n+1)\frac{J}{U} + n^2 \left(\frac{J}{U}\right)^2 + n(n+1)(n+2)\left(\frac{J}{U}\right)^3, \tag{2.76}$$

$$\frac{\mu_{\text{lower}}}{U} = n - 1 + 2n\frac{J}{U} - (n+1)^2 \left(\frac{J}{U}\right)^2 + n(n+1)(n-1)\left(\frac{J}{U}\right)^3. \tag{2.77}$$

In Fig. 2.4 the boundaries are shown. The critical values for J/U beyond which

n	Critical J/U
1	0.215
2	0.123
3	0.0864
4	0.0667

Table 2.1: Table of values for critical J/U of the one-dimensional Bose-Hubbard model obtained by third order perturbation theory. For J/U larger than the critical value no insulating phase can appear for a filling of n particles per site.

no insulating phases can occur are listed in Tab. 2.1 for a filling of $n = 1, 2, 3$ and 4 particles per lattice site.

Fig. 2.5 shows the behaviour in the superfluid region between $n = 1$ and $n = 2$.

2.3.1 Mean field approximation

A mean field theory for the Bose-Hubbard model is obtained by replacing the influence of adjacent lattice sites on their neighbouring sites by a mean field (See [24]). The hopping term in (2.74) is replaced by

$$-2J\alpha(\hat{a}_i^\dagger + \hat{a}_i), \tag{2.78}$$

where $\alpha = \langle \hat{a}_i \rangle$ is the mean field. This is equivalent to the assumption that the state of the system factorizes into a product of local states. Such a state is also known as Gutzwiller state. In general α depends on the lattice site, but for the translational invariant Bose-Hubbard-model it can be assumed equal for every lattice site. The results is a quasi-local Hamiltonian. The locality of the mean field Hamiltonian makes it easy to calculate expectation values of the system. Regarding the local Hamiltonian as functional of α, the expectation value $h(\alpha) = \langle \hat{a} \rangle$ becomes a function of α. In general there are more than one solution of the consistency equation $h(\alpha) = \alpha$, with $\alpha = 0$ being always a solution. If this solution is stable the system is in the Mott-insulator-phase. The stability of the $\alpha = 0$ solution can be determined by calculating the first derivative of h at $\alpha = 0$. If $\frac{\partial h}{\partial \alpha}|_{\alpha=0} < 1$ then the zero-solution is stable. The boundaries of the Mott-insulator phases within this mean field approach can be calculated analytically. The result is

$$\frac{\mu}{U} = \frac{1}{2}\left[2n - 1 - \frac{2J}{U}\right] \pm \frac{1}{2}\sqrt{1 - 4\frac{J}{U}(2n+1) + \left(\frac{2J}{U}\right)^2}. \tag{2.79}$$

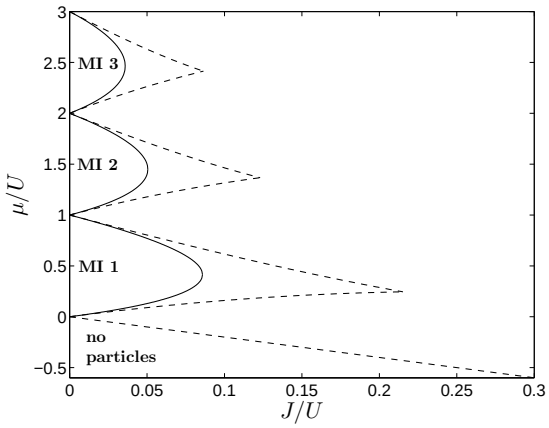

Figure 2.6: Boundaries of the Mott-insulator phases in 1D as obtained from mean field theory (solid lines). For comparison the result of the third order perturbation theory is shown (dashed lines).

Furthermore the critical J in mean field approximation is given by

$$\frac{J_c}{U} = \left(2n + 1 + \sqrt{(2n+1)^2 - 1}\right)^{-1} /2 \tag{2.80}$$

which is much smaller than the critical values found from the third order perturbation theory as can be seen in Fig. 2.6.

2.4 Hard-core bosons with nearest neighbour interaction

This section discusses a Hamiltonian similar to the Bose-Hubbard-Hamiltonian (see previous chapter) which is used to model bosonic particles in a lattice potential, that are not allowed to occupy the same lattice site. This so-called hard-core boson model can be adequate for bosons if for some reason a high energy gain or loss would be necessary for two particles to hop onto the same site. Due to virtual hopping processes to occupied sites there is still some effective interaction which happens between particles which sit on neighbouring sites. This interaction can be either attractive or repulsive, so that it is either favourable for the particles to sit next to each other or not. To model such hard-core bosons one can introduce creation and annihilation operators $\hat{b}_j^\dagger$ and $\hat{b}_j$ which can create or annihilate a particle at lattice site j. Unlike the usual boson operators they can however not create more than one particle per site. If these operators act onto a state $|1_j\rangle$, i.e.

where one particle is sitting at site j the results are

$$\hat{b}_j^\dagger|1_j\rangle = 0 \tag{2.81}$$
$$\hat{b}_j|1_j\rangle = |0_j\rangle. \tag{2.82}$$

If there is no particle sitting at site j one gets

$$\hat{b}_j^\dagger|0_j\rangle = |1_j\rangle \tag{2.83}$$
$$\hat{b}_j|0_j\rangle = 0. \tag{2.84}$$

The creation and annihilation operators have the commutation relations

$$\hat{b}_j\hat{b}_j^\dagger + \hat{b}_j^\dagger\hat{b}_j = 1 \tag{2.85}$$
$$\hat{b}_i\hat{b}_j^\dagger - \hat{b}_j^\dagger\hat{b}_i = 0 \text{ for } i \neq j \tag{2.86}$$
$$\hat{b}_i\hat{b}_j - \hat{b}_j\hat{b}_i = 0 \tag{2.87}$$

and the important property

$$\hat{b}_j^{\dagger 2} = \hat{b}_j^2 = 0. \tag{2.88}$$

With the $\hat{b}_j$ and $\hat{b}_j^\dagger$ it is now possible to write down a Hamiltonian which contains a part which describes the tunnelling of particles between neighbouring sites and a part which describes the effective interaction of particles sitting on neighbouring sites. It reads

$$\hat{H} = -J\sum_j(\hat{b}_j^\dagger\hat{b}_{j+1} + \hat{b}_{j+1}^\dagger\hat{b}_j) + V\sum_j \hat{b}_j^\dagger\hat{b}_j\hat{b}_{j+1}^\dagger\hat{b}_{j+1} + \sum_j D_j\hat{b}_j^\dagger\hat{b}_j. \tag{2.89}$$

J is the tunnelling rate of the hard-core bosons and V is the strength of the repulsion (if $V > 0$) or attraction (if $V < 0$). In Fig. 2.7 the phase diagram of Hamiltonian (2.89) is shown.

The Hamiltonian (2.89) is of particular interest because it is equivalent to two other important model Hamiltonians. It is equivalent to a Hamiltonian describing fermions with nearest neighbour interaction and equivalent to the spin-1/2 XXZ model which describes a chain of coupled spins. The fermionic Hamiltonian can be obtained by the Jordan-Wigner transformation. The fermionic creation and

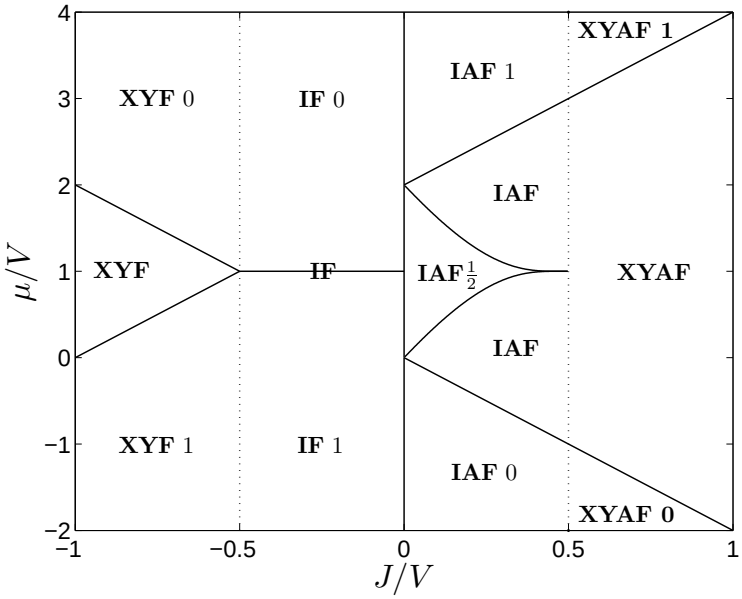

Figure 2.7: Phase diagram of the one-dimensional hard-core boson Hamiltonian (2.89) with nearest neighbour interaction and positive J . The phase borders which are shown are taken from the exact solution of the model in the thermodynamic limit (See [25, 26]). The phases are named after the phases of the equivalent spin model. XY-ferromagnet (XYF): The interaction of the particles is attractive but the hopping dominates. Ising-ferromagnet (IF): The interaction of the particles is attractive and the interaction dominates. Ising-anti-ferromagnet (IAF): The interaction of the particles is repulsive and the interaction dominates. XY-anti-ferromagnet (XYAF): The interaction of the particles is repulsive but the hopping dominates. The numbers behind the abbreviations denote particle-filling. Where there is no number given, all fillings between 0 and 1 are possible. In the IAF$\frac{1}{2}$-phase empty and filled lattice sites alternate. The critical point, beyond which no IAF$\frac{1}{2}$ exists is $J/V = 1/2$. In the IF regime fillings different from 0 and 1 appear only on the line $\frac{\mu}{V} = 1$. This degeneracy shows that here is a regime of phase separation. The particles form quasi-stable clusters in the IF-phase.

annihilation operators $\hat{c}_j^\dagger$ and $\hat{c}_j$ can be defined by the relation

$$\hat{c}_j = \prod_{k<j} \exp(i\pi \hat{b}_k^\dagger \hat{b}_k)\hat{b}_j \tag{2.90}$$

They fulfil similar equations like (2.81),(2.82),(2.83),(2.84) except that another sign of the resulting state is produced depending on where the other particles in the lattice are located. Altogether they fulfil the usual commutation relations for fermionic operators

$$\hat{c}_i\hat{c}_j^\dagger + \hat{c}_j^\dagger\hat{c}_i = \delta_{ij}, \tag{2.91}$$

$$\hat{c}_i\hat{c}_j + \hat{c}_j\hat{c}_i = 0. \tag{2.92}$$

It is easily verified, that when (2.90) is inserted into Hamiltonian (2.89), the form of the Hamiltonian is not changed. This means that the fermionic Hamiltonian can be obtained by replacing the $\hat{b}_j$ by the $\hat{c}_j$.

A mapping to the XXZ model

$$\hat{H} = \frac{J}{2}\sum_j (\hat{\sigma}_j^x\hat{\sigma}_{j+1}^x + \hat{\sigma}_j^y\hat{\sigma}_{j+1}^y + \Delta\hat{\sigma}_j^z\hat{\sigma}_{j+1}^z) + \frac{h}{2}\sum_j \hat{\sigma}_j^z \tag{2.93}$$

in a magnetic field h is obtained by setting

$$\hat{\sigma}_j^x = (-1)^j\left(\hat{b}_j + \hat{b}_j^\dagger\right), \tag{2.94}$$

$$\hat{\sigma}_j^y = i(-1)^j\left(\hat{b}_j - \hat{b}_j^\dagger\right), \tag{2.95}$$

$$\hat{\sigma}_j^z = 2\hat{b}_j^\dagger\hat{b}_j - 1. \tag{2.96}$$

The $\hat{\sigma}_j^x$, $\hat{\sigma}_j^y$, $\hat{\sigma}_j^z$ are the Pauli matrices with the property $\hat{\sigma}_j^{x2} = \hat{\sigma}_j^{y2} = \hat{\sigma}_j^{z2} = 1$. The Hamiltonian (2.93) becomes equivalent to (2.89) for

$$\Delta = \frac{V}{2J} \tag{2.97}$$

The chemical potential μ of (2.89) is related to the magnetic field by

$$\mu = 2J\Delta - h \tag{2.98}$$

or alternatively

$$h = V - \mu. \tag{2.99}$$

2.5 Summary

The present chapter discussed several models of one-dimensional quantum gases. It was shown how the one-dimensional Bose-gas with s-wave interaction can be solved by Bethe ansatz. From this the universal parameters of the model could be extracted. The homogeneous solution was used to obtain a local density approximation for the inhomogeneous case. Furthermore it was discussed how the Luttinger parameter of the system can be obtained from the exact solution. Moreover it was demonstrated how a mean-field approximation can be derived in a consistent way by a phase space approach. The result was the Gross-Pitaevskii equation. After that two important models for particles in periodic potentials have been discussed. The first one is the one-dimensional Bose-Hubbard model. Its phase diagram was investigated and results which are known from pertubative treatments and mean-field approximations recapitulated. The second one is the hard-core boson model with nearest neighbour interaction. The mapping of this model to fermions and the XXZ model was investigated. Since the one-dimensional XXZ model is solvable by a Bethe ansatz, the phase diagram for the hard-core bosons could be obtained exactly.

Chapter 3

Numerical Methods for simulating one-dimensional quantum gases

In the present thesis various numerical methods have been developed or implemented and optimized for the description of ultra-cold bosonic or fermionic atoms in 1D trapping potentials or lattice potentials. One of the special properties of trapped ultra-cold atoms is the intrinsic inhomogeneity of these systems due to the confining potentials, which needs to be accounted for in the numerical algorithms. These methods will be introduced and discussed in the following. For obtaining the numerical results in Chapter 5, 6, 7 and 8 the described algorithms have been implemented in MATLAB®[1].

3.1 Stochastic simulations

The first method developed in this thesis is a stochastic simulation technique for bosons. This was motivated by the success of stochastic phase space techniques used in quantum optics to simulate quantum properties of non-linear optical processes.

3.1.1 Stochastic factorization

Assume the Hilbert space $\mathcal{H}$ of a many particle systems is given as a tensor product of smaller spaces $\mathcal{H}_j$

$$\mathcal{H} = \mathcal{H}_1 \otimes \mathcal{H}_2 \otimes \ldots \otimes \mathcal{H}_n. \tag{3.1}$$

Operators $\hat{A}_j : \mathcal{H}_j \to \mathcal{H}_j$, which are restricted to a certain subspace, will be denoted with the appropriate index and as usual they are extended to the whole

[1] MATLAB®, The MathWorks, Natick, MA

Hilbert space by

$$\hat{A}_j(\phi_1 \otimes \phi_2 \otimes \ldots \otimes \phi_n) = \phi_1 \otimes \phi_2 \otimes \ldots \phi_{j-1} \otimes \hat{A}_j(\phi_j) \otimes \phi_{j+1} \otimes \ldots \otimes \phi_n \quad (3.2)$$

if $\phi_i \in \mathcal{H}_i$. Furthermore, assume that the Hamilton operator is of the form $\hat{H} = \hat{B} + \hat{L}$ with

$$\hat{B} = \sum_j \hat{B}_j, \quad \hat{L} = \sum_{ij} C_{ij} \hat{L}_i^\dagger \hat{L}_j. \quad (3.3)$$

The operators $\hat{B}_j$ and $\hat{L}_j$ are restricted to the subspace $\mathcal{H}_j$. The $\hat{B}_j$ will be called the blocks and $\hat{L}_i\hat{L}_j$ the links between those blocks. To calculate thermodynamic properties of the system one needs to evaluate the statistical sum containing the operator $e^{-\beta\hat{H}}$. The Trotter expansion

$$e^{-\beta\hat{H}} \approx \left(e^{-\frac{\beta}{A}\hat{L}} e^{-\frac{\beta}{A}\hat{B}}\right)^A, \quad (3.4)$$

allows to split off blocks from links. To this end a discretization in β is introduced. Let $d\beta = \beta/A$. The block part already factorizes with respect to the block-subspaces. The blocks themselves should be sufficiently small to handle them numerically. In the calculations presented in Section 5.3 the blocks consist of three to nine adjacent sites and the links are the remaining hopping terms between the edges of those blocks. To evaluate the action of $e^{-\beta\hat{H}}$ it would be desirable to factorize it into terms that act only on states within the Hilbert space of on block. This is prevented by the links in the Hamiltonian $\hat{H}$. The factorization is however possible by introducing stochastic variables similar to the stochastic Hubbard-Stratonovich transformation [27]

$$\exp(-d\beta\hat{L}) \approx 1 - d\beta\hat{L} \approx \overline{\prod_i \left[1 - \sqrt{d\beta}\eta_i \hat{L}_i^\dagger\right]\left[1 + \sqrt{d\beta}\eta_i^* \hat{L}_i\right]}. \quad (3.5)$$

If the stochastic variables $\eta_i \in \mathbb{C}$ fulfil the conditions

$$\overline{\eta_i} = \overline{\eta_i\eta_j} = 0 \quad (3.6)$$

$$\overline{\eta_i\eta_j^*} = C_{ij} \quad (3.7)$$

then the right side of (3.5) equals the left site up to order $d\beta$. This is sufficient for the Trotter-expansion to hold. The problem has now been completely factorized with respect to the block-subspaces. All calculations can now be done in the small subspaces (for example calculating the trace of the operator (3.4)). After that the

product of the resulting expressions is taken. This process must then be repeated and averaged over the stochastic variables.

3.1.2 Block factorization

So far the stochastic factorization described is quite general. In this section it will be discussed how specific Hamiltonians like the Bose-Hubbard Hamiltonian have to be divided into blocks and links. One important property of the Bose-Hubbard Hamiltonian is that it only has nearest-neighbour links. Let local terms like $\hat{a}_j^\dagger \hat{a}_j$ be denoted in a pictorial way by a bullet $\bullet$ and hopping terms like $\hat{a}_j^\dagger \hat{a}_{j+1}$ by an arc $\frown$. Then the structure of the Hamiltonian is

The important point here is that a division of such a Hamiltonian into blocks and links is not unique. Some parts of the Hamiltonian can either be shifted to the blocks or to the links. Cutting the Hamiltonian for example in blocks of three sites would result in

One sees that some hopping terms are now completely within blocks and some are completely outside. Those which are not in a block will form the links. However this is not the only possibility. The outermost $\bullet$ of the blocks can also be put to the links. This results in

In fact it is possible to put only a fraction of the bullet term into the links. By using blocks for the Bose-Hubbard Hamiltonian the matrix C becomes actually very simple. Usually the links consist only of the right-most and left-most creation and annihilation operators of the block $\hat{a}_j^r$,$\hat{a}_j^l$. In Hamiltonians which contain only nearest neighbour terms, only links of the form $(\hat{a}_j^r)^\dagger \hat{a}_{j+1}^l + \text{h. c.}$ or $(\hat{a}_j^r)^\dagger \hat{a}_j^r$ and $(\hat{a}_j^l)^\dagger \hat{a}_j^l$ will appear, but not $(\hat{a}_j^l)^\dagger \hat{a}_{j+1}^r + \text{h. c.}$ Thus, by ordering the links properly,

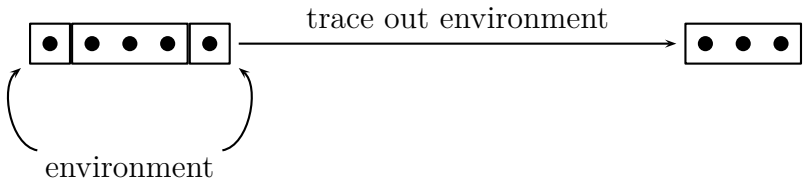

Figure 3.1: To improve the numerical representation of blocks, which are only small parts of the system, environment in the form of one additional site can be glued to each side of the block. The environment is traced out for the density matrix of this extended block and gives an reduced density matrix of the original block, which serves as a better approximation to the actual density matrix.

C can be transformed into a matrix of the structure

$$C = \begin{pmatrix} A & 0 & 0 & \dots & 0 \\ 0 & A & 0 & \dots & 0 \\ 0 & 0 & A & \dots & 0 \\ \vdots & \vdots & \vdots & \ddots & 0 \\ 0 & 0 & 0 & 0 & A \end{pmatrix}. \tag{3.8}$$

which consists of 2 by 2 matrices

$$A = \begin{pmatrix} d & -J \\ -J & d \end{pmatrix} \tag{3.9}$$

on the diagonal. The possibility that one is free to choose which part of the local terms goes into the links, means now that one is actually free to choose the value of d. This is equivalent to rewriting the local part of the Hamiltonian like

$$\hat{H} = \ldots + \sum_j D_j \hat{a}_j^\dagger \hat{a}_j + \ldots = \ldots + \sum_j (D_j - d)\hat{a}_j^\dagger \hat{a}_j + d\hat{a}_j^\dagger \hat{a}_j + \ldots \tag{3.10}$$

Ideally d is chosen such that one of the eigenvalues of the matrix (3.9) becomes zero. Since those eigenvalues are multiplied by the noise (see Section 3.1.4) in the stochastic simulation some of the noise is removed, which results in a better convergence of the stochastic simulation. One possible choice to make one eigenvalue zero is to take $d = J$ for the diagonal elements.

3.1.3 Environment

The starting point in the block representation is the number-state basis. The block Hamiltonians are constructed of creation and annihilation operators in number-

state representation. This representation is still quite inefficient for numerical calculations. It would be better if the representation could be reduced to those states which are physically important. The first idea is certainly to take the eigenstates of the block Hamiltonian. The block Hamiltonians can be diagonalized numerically and one could choose only the lowest eigenstates. This would surely result in a good representation of the block itself for low temperatures. However the ground state of the complete Hamiltonian does not factorize into the ground states of the blocks. In this sense the blocks are not a good representation of the whole system. The most relevant states must be found for a block which is still coupled to some environment. This can be realized by constructing an extended block, meaning that one additional site is added at each side to the block functioning as environment. After that, the density matrix of the extended block can be constructed and the reduced density matrix of the block can be calculated by tracing out the environment (see Fig. 3.1). The lowest eigenstates of the reduced density matrix of the remaining block serve as the representation of the block Hilbert-space.

3.1.4 Noise generation

In the section about stochastic factorization it is shown, that one needs stochastic variables η_i with the properties $\overline{\eta_i} = \overline{\eta_i \eta_j} = 0$ and especially $\overline{\eta_i \eta_j^* = C_{ij}}$. Note, that the Matrix C is usually self-adjoint and positive definite. In Matrix notation, where η is a column vector, the last property can be written as

$$\overline{\eta \eta^T} = C \tag{3.11}$$

where $(\cdot)^T$ denotes the matrix transpose. The required η can be generated by diagonalizing C in the usual way by

$$C = V D V^T \tag{3.12}$$

where D is diagonal and $V V^T = V^T V = \mathbb{1}$. In order to make everything symmetric the square root of D which is straight forward for a diagonal positive matrix can be taken and C can be written as

$$C = V \sqrt{D} \sqrt{D}^T V^T. \tag{3.13}$$

Introducing now a Gaussian variable ξ with the properties $\overline{\xi\xi^T} = \mathbb{1}$, for which many numerical generators are available, allows to write

$$C = \overline{V\sqrt{D}\xi(V\sqrt{D}\xi)^T} \tag{3.14}$$

and it is clear that η can be generated from the independent variables ξ by the transformation

$$\eta = V\sqrt{D}\xi. \tag{3.15}$$

3.2 Density matrix renormalization group method

The DMRG method is a method which is especially well suited for calculating ground state properties of one-dimensional lattice systems. The following discussion will mainly focus on the Bose-Hubbard-Hamiltonian (2.74). As mentioned in the introduction the exponentially growing Hilbert space of a lattice system poses a general problem for numerical methods. The idea of DMRG is to grow the described system site by site and to keep only a part of the Hilbert space of fixed dimension in every step (See Fig. 3.2). The method is thus a real-space renormalization approach. This reduction of the Hilbert space prevents the dimension of the computational state space from growing in an exponential manner. Instead the size of the part of the Hilbert space considered as important stays constant during the growing. The assumption is, that one needs only to know a few eigenstates of the reduced density matrix of the n-site system to find the most important eigenstates of the $n+1$ - site system. Since in 1D systems with finite-range interactions the entropy of a connected block of sites is independent of the block size for non-critical systems and only increases logarithmically with the size in the case of a critical system, this is a well justified assumption.

3.2.1 Initializing the DMRG

At the beginning of the DMRG a decision must be made what kind of representation is used to construct the operators. The natural choice is here to start with a number-state representation. Numerically only a finite number d of states per site can be treated. For the Bose-Hubbard model it means that one has a cut-off in the number of particles per site which one can take into account. Such a cut-off usually does not introduce a bad approximation to the full system, since for any

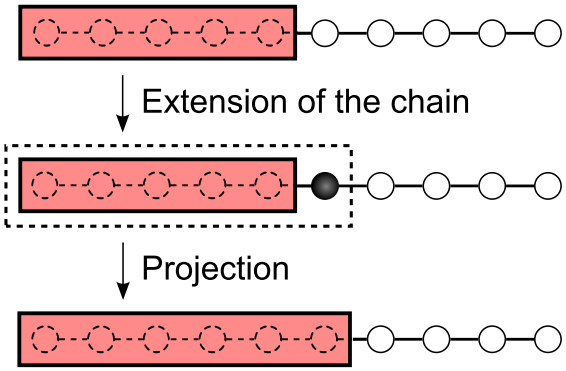

Figure 3.2: The general idea of DMRG is to grow the system site by site and to project down to some subspace after every step.

interacting system the number of particles per site is limited also physically by the energy. For the annihilation operator one can than simply use a finite matrix representation such as

$$\hat{a} = \begin{pmatrix} 0 & 1 & 0 & 0 & 0 \\ 0 & 0 & \sqrt{2} & 0 & 0 \\ 0 & 0 & 0 & \sqrt{3} & 0 \\ 0 & 0 & 0 & 0 & \sqrt{4} \\ 0 & 0 & 0 & 0 & 0. \end{pmatrix}. \tag{3.16}$$

This example is for $d = 5$. In the Bose-Hubbard-model also terms of the form $\hat{a}_j^\dagger \hat{a}_{j+1}$ appear. Such expressions which contain operators of distinct sites can be represented by tensor products. A tensor product of a $m \times m$ matrix $\hat{A}$ with a $k \times k$ matrix $\hat{B}$ which results in a $(mk) \times (mk)$ matrix can be defined by

$$(\hat{A} \otimes \hat{B})_{ij} = \hat{A}_{\frac{i}{k}\frac{j}{k}} \hat{B}_{i \bmod k, j \bmod k} \tag{3.17}$$

where the division in the indices is to be understood as an integer division. This is how for example the `kron` function in MATLAB® works.

Assume that for a part of the system consisting of n adjacent sites, a numerical representation of the Hamiltonian in form of a matrix $\hat{B}_n$ has been found. This can be achieved for example by exact numerical diagonalization if n is very small. Higher states would usually be cut off, because it is unlikely that they are important for the ground state properties of the entire system and only the m lowest states are kept. $\hat{B}_n$ is then a $m \times m$ matrix. For the Bose-Hubbard model $\hat{B}_n$ is some

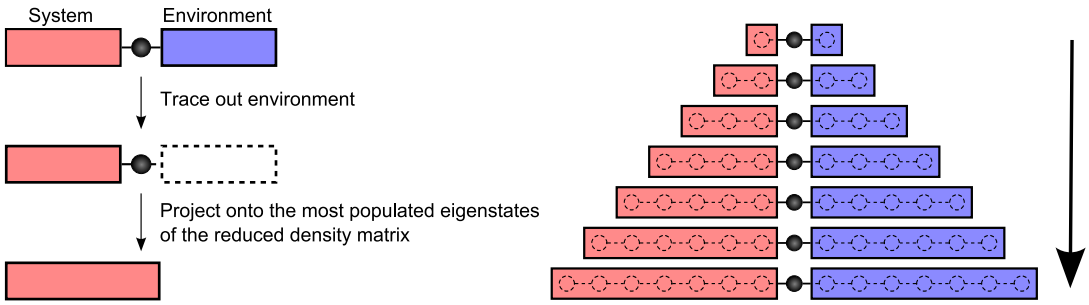

Figure 3.3: First growing of the system block using a mirror image of the system as environment (infinite size DMRG).

representation for

$$\hat{H} = -J \sum_{j=1}^{n-1} (\hat{a}_j^\dagger \hat{a}_{j+1} + \hat{a}_{j+1}^\dagger \hat{a}_j) + \sum_{j=1}^{n} \hat{h}_j \tag{3.18}$$

where the

$$\hat{h}_j = D_j \hat{n}_j + \frac{U}{2} \hat{a}_j^{\dagger 2} \hat{a}_j^2 \tag{3.19}$$

are the purely local parts of the Hamiltonian.

3.2.2 The growing step with environment (infinite size DMRG)

In the next step from n to $n+1$ sites one site must now be added to $\hat{B}_n$. The matrix where one site is added to $\hat{B}_n$ is called here $\hat{B}_{\text{lift}}$ since $\hat{B}_n$ is lifted into the $m \times d$ dimensional Hilbert space of $\hat{B}_n$ plus one site. The result is

$$\hat{B}_{\text{lift}} = \hat{B}_n \otimes \hat{\mathbb{1}}_d - J \left(\hat{a}_n^{r\dagger} \otimes \hat{a} + \hat{a}_n^r \otimes \hat{a}^\dagger \right) + \hat{\mathbb{1}}_m \otimes \hat{h}_{n+1}. \tag{3.20}$$

The important term is here the hopping term which connects the site $n+1$ to the block. It contains the rightmost annihilation operator $(\hat{a}^r)^\dagger$ of the block $\hat{B}_n$. The representation of $(\hat{a}^r)^\dagger$ must be in the same basis and subspace as that of $\hat{B}_n$. The dimension of the Hilbert space has now grown by a factor of d. However, it is not necessary to keep the full $m \times d$ Hilbert space representation, since only zero temperature or low temperature properties are of interest. The question now arises which subspace of this Hilbert-space should be kept. This question can be answered by the density matrix of the system. If the density matrix of the whole system would be known, those states would be kept which best describe

the reduced density matrix of the $n+1$-site subsystem. Since the density matrix of the whole system is not available an approximation must be made. This is accomplished by fitting in a replacement for those parts of the system where a representation has not been obtained for yet, i.e. everything beyond the site $n+1$. This replacement will be called an environment for the block $\hat{B}_n$ or $\hat{B}_{\text{lift}}$, since it simulates the surrounding of the block. This environment can be for example a mirror image of the block $\hat{B}_n$ itself. This is what is usually done (See Fig. 3.3). The addition of the environment $\hat{E}_n$ will lead to the so called extended block

$$\hat{B}_{\text{ext}} = \hat{B}_{\text{lift}} \otimes \hat{\mathbb{1}}_m - J\left(\hat{a}^{\dagger}_{\text{lift}} \otimes \hat{a}^{\text{env}}_n + \hat{a}_{\text{lift}} \otimes \hat{a}^{\text{env}\dagger}_n\right) + \hat{\mathbb{1}}_{\text{lift}} \otimes \hat{E}_n \tag{3.21}$$

For simplicity it is assumed here that the environment also has the dimension m. It is however not necessary to have the same dimension as the block. The extended block is then of dimension m^2k. A density matrix can now be build up either by taking the ground state of the extended block, if one is only interested in ground state properties, or a certain number of the lowest states, if one is interested in low temperature properties. From that density matrix the environment can be traced out and an approximation of the reduced density matrix of the $n+1$ site subsystem can be found. Diagonalizing the reduced density matrix yields a number of eigenstates from which m will be kept, namely those with the largest eigenvalues. Numerically this means that the final result is a set of m vectors v_j of dimension md. They span the subspace into which $\hat{B}_{\text{lift}}$ is to be projected. If one writes those vectors into an $md \times m$ matrix

$$\hat{V} = (v_1, v_2, \ldots, v_m) \tag{3.22}$$

then the representing matrix of the $n+1$ site system is

$$\hat{B}_{n+1} = \hat{V}^{\dagger}\hat{B}_{\text{lift}}\hat{V} \tag{3.23}$$

Since in the next step also the right annihilation operator is needed one has also to project $\hat{a}_{\text{lift}}$ to get

$$\hat{a}^{r}_{n+1} = \hat{V}^{\dagger}\hat{a}_{\text{lift}}\hat{V}. \tag{3.24}$$

3.2.3 Sweeping (finite size DMRG)

In the previous section a complete step from a block of n sites to a block of $n+1$ sites was described which can now be repeated until all sites are added. The

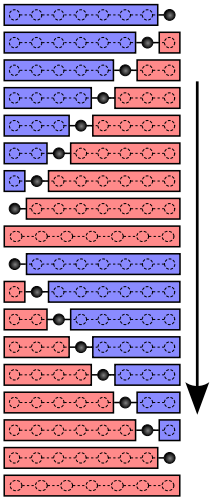

Figure 3.4: Sweeping after the first growing sweep (infinite size DMRG) is completed. Red is the growing system block now starting from right to left. Blue is the environment. After every full sweep the system block and the environment change roles.

result however will still not be very good because only a bad approximation was used for the environment. However, the first run (sweep) through all the sites provides a representation of all the blocks $\hat{B}_n$. Those blocks can now serve as a much better approximation for the true environment. It is now possible to start at the opposite end of the lattice with the DMRG-growing and have always a good approximation for the remaining part of the system (See Fig. 3.4). If the result of this second sweep is also not good enough than the sweeping can be repeated arbitrarily often until it converges. In every sweep the blocks are used which are produced in the previous sweep. However, one must note that not, as it may seem, the representation of the blocks is the variable which is iterated but merely it is the matrices $\hat{V}$ which are optimized by this procedure. Finally only the $\hat{V}$ are needed to calculate expectation values. The whole numerical algorithm for a sweep is visualized in Fig. 3.5.

3.2.4 Evaluating expectation values

As noted in the last section only the projections $\hat{V}_n$ contain the information how the lifted $n+1$ site Hilbert space is related to the projected $n+1$ site Hilbert space. It is thus very simple to calculate the expectation value of virtually any operator. In general almost any operator of interest can be decomposed into a sum of products of local operators. Without loss of generality it can therefore be assumed that an operator $\hat{A}$ of which the expectation value is to be calculated can be factored into a product of local operators.

$$\hat{A} = \prod_{j=1}^{M} \hat{A}_j \tag{3.25}$$

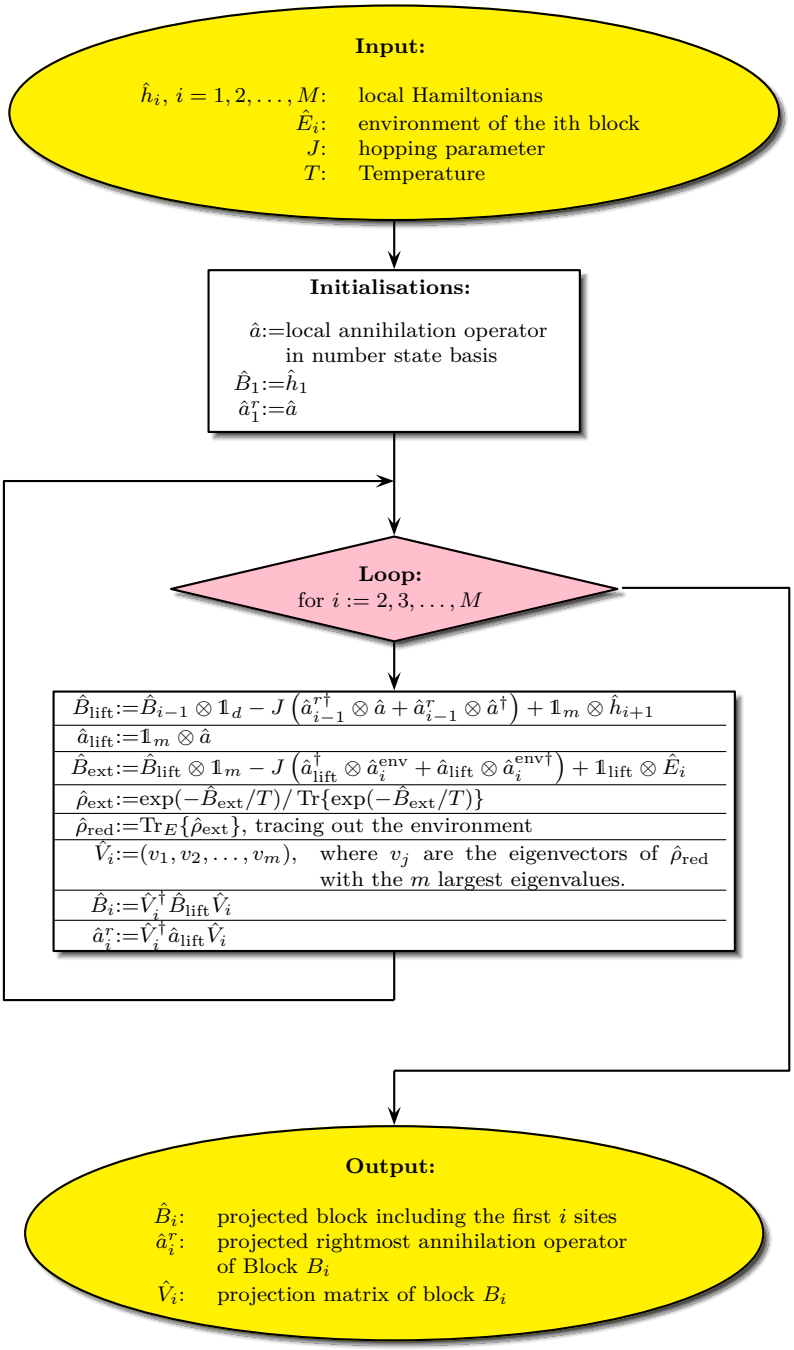

Figure 3.5: Scheme of the DMRG algorithm for one sweep.

The first operator $\hat{A}_1$ belongs to the small subspace the DMRG started with. It may have been just one site or a small number of sites, which e.g. was diagonalized exactly. A unitary matrix $\hat{V}_1$ of eigenvectors was obtained by this. Thus, the first step is to transform $\hat{A}_1$ into the representation of those eigenvectors.

$$\hat{A}_1^P = \hat{V}_1^\dagger \hat{A}_1 \hat{V}_1 \tag{3.26}$$

After that $\hat{A}_1^P$ has to be lifted

$$\hat{A}_1^{P\text{lift}} = \hat{A}_1^P \otimes \hat{A}_2 \tag{3.27}$$

and projected with $\hat{V}_2$

$$\hat{A}_2^P = \hat{V}_2^\dagger \hat{A}_1^{P\text{lift}} \hat{V}_2 \tag{3.28}$$

This is then iterated through all sites

$$\hat{A}_n^{P\text{lift}} = \hat{A}_n^P \otimes \hat{A}_{n+1} \tag{3.29}$$

$$\hat{A}_{n+1}^P = \hat{V}_{n+1}^\dagger \hat{A}_n^{P\text{lift}} \hat{V}_{n+1} \tag{3.30}$$

The last operator A_M^P is then a kind of projected version of the operator $\hat{A}$ and the expectation value can be directly obtained from it.

3.3 Summary

In the present chapter two numerical methods to simulate inhomogeneous multi-particle lattice systems were discussed. The first method is a new stochastic method which uses a factorization of the kinetic energy-term, which transforms the calculation into a local problem, where the non-locality is restored by stochastic averaging. The method was refined by dividing the system not only into single sites, but also into larger blocks. The numerical representation of the blocks was improved by introducing an environment. The method is expected to work best for non-zero temperatures.

The second method was a real-space renormalization approach using the density matrix renormalization group. The method was extended to inhomogeneous systems. The main difference to the homogeneous case is the treatment of the environment. This method is expected to work best at zero temperature, but can also be used for small temperatures.

Chapter 4

Theory of quantum particles in periodic potentials

In Section 2.3 the Bose-Hubbard model has been introduced only in a formal manner. It was stated that the Bose-Hubbard-model describes particles in periodic potentials. In this chapter it will be shown how the Bose-Hubbard-model can be derived from the general Schrödinger equation describing particles in periodic potentials. The main focus will be on the limits of the one-band Bose-Hubbard model and on the extension of the model to two energy bands. A detailed knowledge of the break-down of the one-band Bose-Hubbard model is necessary because of the physically interesting regime of strong interaction. In this regime it is possible that the particles leave the lowest energy-band even at zero temperature. The final aim of this chapter will therefore be the determination of the parameter regime where the one-band approximation remains valid even when the interaction is strong.

In this chapter a special set of units is used, to make the expressions shorter. A natural length scale is given by the period of the periodic potential. The length unit used here will be the wavenumber k related to this period. If for example a periodic potential is created by a standing laser wave, then the wavenumber of the lattice would be $k = \frac{\pi}{\lambda}$ if λ is the wavelength of the laser. The mass unit is as always the mass m of a single particle. In summary the following units are used for the physical parameters:

- all lengths (z,b,l) are given in units of the inverse wavenumber k^{-1}
- all Energies (η,J,U,Δ) are given in units of the recoil energy $E_R = \frac{\hbar^2 k^2}{2m}$
- the interaction constant g is given in units of $E_R k^{-1}$

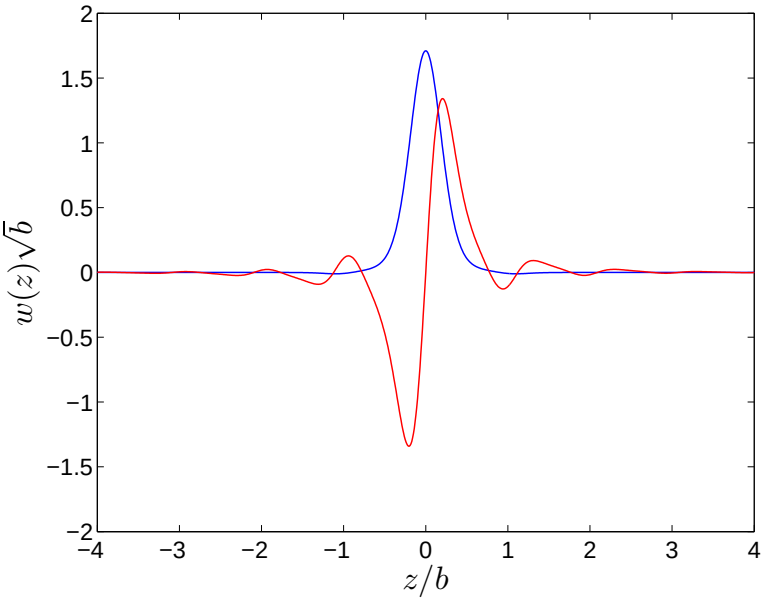

Figure 4.1: Wannier functions of the first (blue) and second band (red) at $\eta = 10$.

4.1 Bloch waves and Wannier functions

The motion of a single particle in a lattice is governed by a Schrödinger equation with a periodic potential. In one dimension and in the units mentioned at the beginning of this chapter its stationary version may be written as

$$[-\partial_z^2 + V(z)]\Psi(z) = E\Psi(z) \tag{4.1}$$

where

$$V(z+b) = V(z). \tag{4.2}$$

For the following calculations a potential

$$V(z) = \eta \sin^2(z), \tag{4.3}$$

is used, i.e. $b = \pi$. For the allowed ranges of E, (4.1) has solutions of the form

$$\varphi_{n,r}(z) = u_{n,r}(z)e^{irz} \tag{4.4}$$

where $u_{n,r}(z)$ has the same periodicy as $V(z)$. These are the well known Bloch waves [28]. The allowed ranges of E are energy bands. $n = 0, 1, 2, \ldots$ denotes the index of those bands and $-1 < r < 1$ parametrises the different solutions within

the band. From the Bloch waves the Wannier functions [29]

$$w_n(z) = \frac{1}{\sqrt{2}} \int_{-1}^{1} \varphi_{n,r}(z) dr \tag{4.5}$$

can be created which are in contrast to the Bloch waves localized on a lattice site (See Fig. 4.1). Note, that (4.5) alone does not define the Wannier functions uniquely, because there is still a freedom in the choice of the phases of the Bloch waves. The most general Bloch function can be written as

$$\Phi_{n,r}(z) = e^{i\theta(r)} \varphi_{n,r}(z). \tag{4.6}$$

The choice of the phase is made such, that the Wannier function has the properties: (i) It is real. (ii) It is symmetric or antisymmetric about $z = 0$. (iii) It falls off exponentially as

$$w_n(z) \sim \exp(-h_n z). \tag{4.7}$$

In [30] it was proven that there is exactly one Wannier function fulfilling those three conditions. There are two cases for the lattice potential (4.3) and fixed n:

1. $\varphi_{n,0}(0) \neq 0$ and $\varphi_{n,1}(0) \neq 0$
2. $\varphi_{n,0}(0) = 0$ and $\varphi_{n,1}(0) = 0$

In the first case the phase is fixed by demanding $\varphi_{n,r}(0) > 0$ and in the second by $\varphi'_{n,r}(0) > 0$. This results in a symmetric Wannier function in the first case and an anti-symmetric in the second case. For the lattice potential (4.3) it is easily shown that the Wannier functions are symmetric for the even bands and antisymmetric for the odd bands. A simple argument for that is, that in the case $\eta \to \infty$ the lattice sites are like harmonic potentials, so the Wannier functions look like the eigenstates of the harmonic oscillator.

4.2 Numerical calculation of the Wannier functions

The most feasible method to calculate the Wannier function numerically is to calculate its Fourier transform

$$\tilde{w}_n(k) = \frac{1}{\sqrt{2\pi}} \int dz w_n(z) e^{-ikz}. \tag{4.8}$$

From Eq. (4.4) for $u_{n,r}$ the equation

$$\left[(-i\partial_z + r)^2 + \eta \sin^2(z)\right] u_{n,r}(z) = E_{n,r} u_{n,r}(z) \tag{4.9}$$

is found. Since $u_{n,r}$ is periodic there exists a Fourier series expansion

$$u_{n,r}(z) = \sum_m a_m^{(n,r)} e^{i2mz}. \tag{4.10}$$

The Fourier components obey the equation

$$\left[(2m+r)^2 + \frac{\eta}{2}\right] a_m^{(n,r)} - \frac{\eta}{4}\left[a_{m-1}^{(n,r)} + a_{m+1}^{(n,r)}\right] = E_{n,r} a_m^{(n,r)}. \tag{4.11}$$

This equation can be solved numerically by standard methods. Then inserting (4.10) into (4.4) shows that the Fourier transform of the Wannier function is simply given by

$$\tilde{w}_n(k) = \frac{1}{\sqrt{2}} a_{\left[\frac{k}{2}\right]}^{\left(n,k-2\left[\frac{k}{2}\right]\right)} \tag{4.12}$$

where the brackets $[*]$ denote rounding to the nearest integer.

4.3 The two-band Hubbard-model

Since for strong repulsive interactions mediated for example by a Feshbach resonance and not too deep optical lattices the physics of lattice bosons may not entirely be described by the lowest Bloch band, the single-band analysis of Jaksch [31] is extended in the following and the two-band Hubbard model is discussed. For the two-band model the field operator is expanded in the following form

$$\hat{\Psi}(z) = \sum_j \hat{a}_j w_0(z - j\pi) + \sum_j \hat{A}_j w_1(z - j\pi) \tag{4.13}$$

where $\hat{a}_j$ and $\hat{A}_j$ are bosonic annihilation operators with the usual commutation rules in the first and second band respectively. If the ansatz (4.13) is inserted into the Hamiltonian for a delta-interacting Bose-gas in an optical lattice

$$\hat{H} = \int dz\, \hat{\Psi}^\dagger(z) \left[-\partial_z^2 + V(z) + \frac{g}{2}\hat{\Psi}^\dagger(z)\hat{\Psi}(z)\right] \hat{\Psi}(z) \tag{4.14}$$

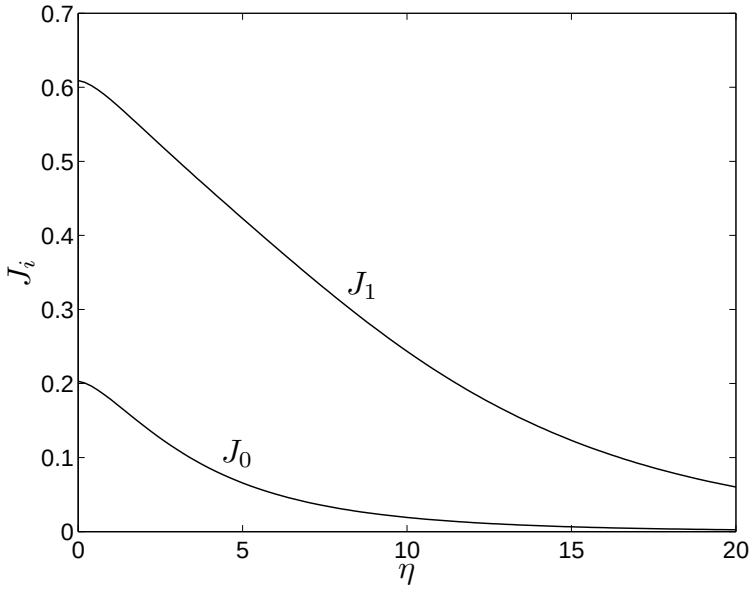

Figure 4.2: Numerical exact calculation of the hopping rate in the first and second band.

the result is a Hamiltonian of the form

$$\begin{aligned}\hat{H} = &\\ &\sum_{\langle i,j\rangle}\left[-J_{00}\hat{a}_i^\dagger\hat{a}_j - J_{11}\hat{A}_i^\dagger\hat{A}_j - J_{01}\left(\hat{a}_i^\dagger\hat{A}_j + \text{h.c.}\right)\right] + \sum_j\left[\Delta_0\hat{a}_j^\dagger\hat{a}_j + \Delta_1\hat{A}_j^\dagger\hat{A}_j\right]\\ &+\sum_j\left[U_{0001}\left(\hat{a}_j^\dagger\hat{a}_j^\dagger\hat{a}_j\hat{A}_j + \text{h.c.}\right) + U_{0111}\left(\hat{a}_j^\dagger\hat{A}_j^\dagger\hat{A}_j\hat{A}_j + \text{h.c.}\right)\right]\\ &+\sum_j\left[\frac{U_{0011}}{2}\left(\hat{a}_j^{\dagger 2}\hat{A}_j^2 + 2\hat{a}_j^\dagger\hat{A}_j^\dagger\hat{a}_j\hat{A}_j + \text{h.c.}\right) + \left(\frac{U_{0000}}{2}\hat{a}_j^{\dagger 2}\hat{a}_j^2 + \frac{U_{1111}}{2}\hat{A}_j^{\dagger 2}\hat{A}_j^2\right)\right]. \quad (4.15)\end{aligned}$$

All non-local terms arising from the interaction terms have already been neglected because the Wannier functions fall off exponentially. Furthermore only tunnelling due to the kinetic energy between neighbouring sites is taken into account. The constants are given by

$$J_{jk} = -\int dz w_j(z-\pi)[-\partial_z^2 + \eta\sin^2(z)]w_k(z), \quad (4.16)$$

$$\Delta_{jk} = \int dz w_j(z)[-\partial_z^2 + \eta\sin^2(z)]w_k(z), \quad (4.17)$$

$$U_{ijkl} = g\int dz w_i(z)w_j(z)w_k(z)w_l(z). \quad (4.18)$$

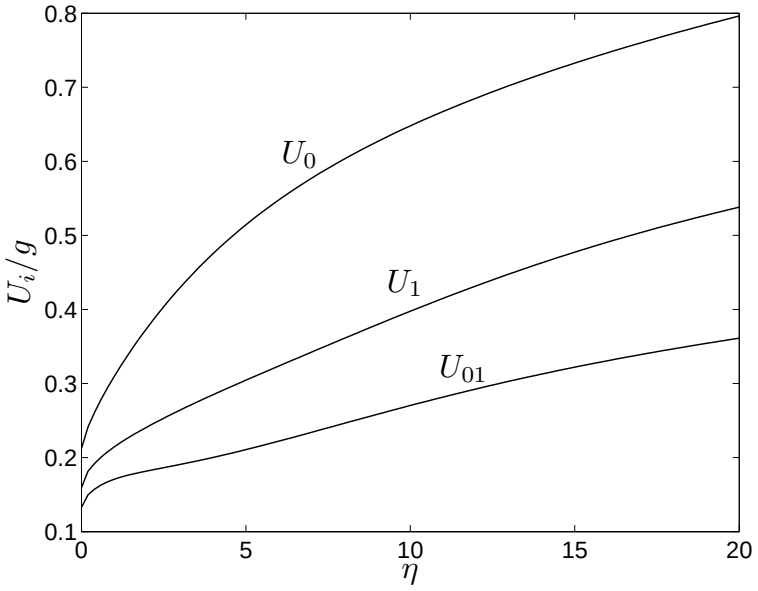

Figure 4.3: Numerically exact interaction constants of the two-band Bose-Hubbard

If one inserts Eq. (4.5) into (4.16) the result is

$$J_{jk} = -\frac{1}{2}\int_{-1}^{1} dr \int_{-1}^{1} dr' \int dz \varphi_{j,r'}(z) e^{-i\pi r} E_{k,r} \varphi_{k,r}(z) = -\delta_{jk} \frac{1}{2} \int_{-1}^{1} E_{j,r} e^{-i\pi r} dr, \tag{4.19}$$

$$\Delta_{jk} = \frac{1}{2}\int_{-1}^{1} dr \int_{-1}^{1} dr' \int dz \varphi_{j,r'}(z) E_{k,r} \varphi_{k,r}(z) = \delta_{jk} \frac{1}{2} \int_{-1}^{1} E_{j,r} dr, \tag{4.20}$$

where the Kronecker delta arises from the fact that the Bloch waves of different bands are orthogonal. In particular $J_{01} = 0$ and $\Delta_{01} = 0$ for this reason. This means that a single particle cannot tunnel from the first into the second band. However, also some of the two-particle processes are not allowed. It was mentioned earlier that the Wannier function is a symmetric function for the lowest band and antisymmetric for the next highest band. From this follows that the integrals in (4.18) become zero for U_{0001} and U_{0111}. Finally one finds a two-band Hamiltonian

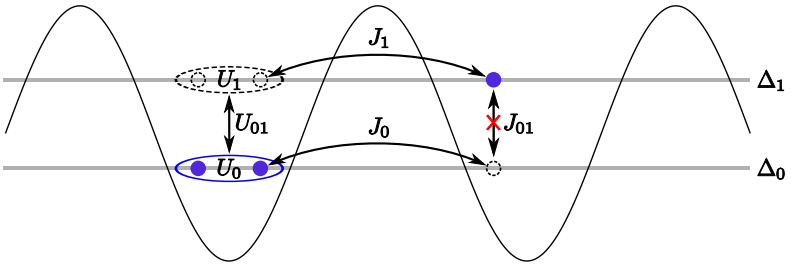

Figure 4.4: Two-band Bose-Hubbard model. Single particles can tunnel between lattice sites if they stay in the same band. Transition of particles from the first into the second band is only possible in pairs via the two-particle process U_{01}.

of the form

$$\hat{H} = -J_0 \sum_{\langle i,j \rangle} \hat{a}_i^\dagger \hat{a}_j + J_1 \sum_{\langle i,j \rangle} \hat{A}_i^\dagger \hat{A}_j + \Delta_0 \sum_j \hat{n}_j + \Delta_1 \sum_j \hat{N}_j + \sum_j \frac{U_{01}}{2} [\hat{a}_j^{\dagger 2} \hat{A}_j^2 + \hat{A}_j^{\dagger 2} \hat{a}_j^2 + 4 \hat{n}_j N_j] + \frac{U_0}{2} \sum_j \hat{a}_j^{\dagger 2} \hat{a}_j^2 + \frac{U_1}{2} \sum_j \hat{A}_j^{\dagger 2} \hat{A}_j^2 \quad (4.21)$$

where for a simpler notation $J_0 = J_{00}$, $J_1 = -J_{11}$, $\Delta_k = \Delta_{kk}$, $U_0 = U_{0000}$, $U_1 = U_{1111}$, $U_{01} = U_{0011}$, $\hat{n}_j = \hat{a}_j^\dagger a_j$, $\hat{N}_j = \hat{A}_j^\dagger \hat{A}_j$ was used . It can be seen that particles can only tunnel in pairs between the bands. The rate of this process is given by U_{01}. However, this process will be suppressed if U_{01} is small compared to $\Delta_1 - \Delta_0$. The case where the second band can also be neglected and the particles stay completely in the lowest band leads to the simple Bose-Hubbard-model with the Hamiltonian (2.74).

4.4 The deep lattice: harmonic oscillator approximation

In the literature very often an approximative calculation of J_0, which is called Gaussian approximation is used. It assumes, that the Wannier functions can be approximated by Gaussian functions

$$w_0(z) \approx \frac{e^{-\frac{z^2}{2l^2}}}{\pi^{\frac{1}{4}} l^{\frac{1}{2}}}, \quad (4.22)$$

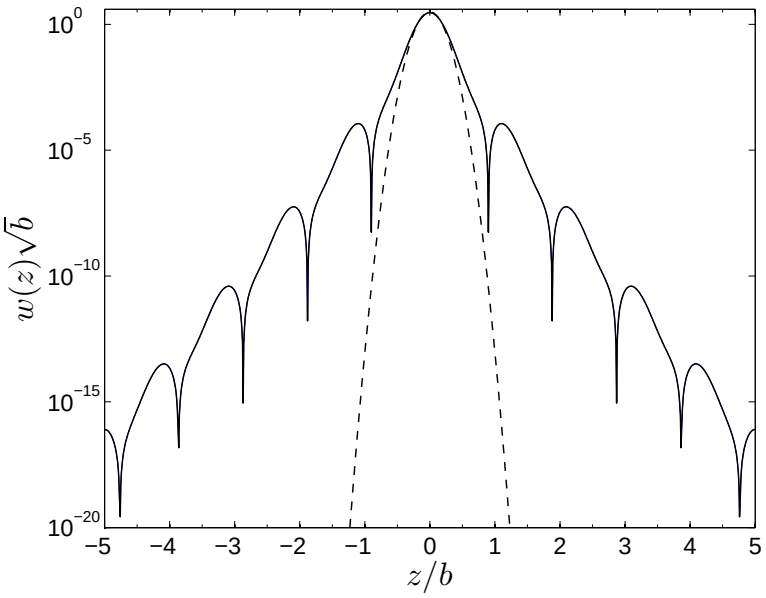

Figure 4.5: Wannier function of the lowest band (solid line) at $\eta = 10$ compared to the Gaussian approximation (dashed line). It is visible that the Gaussian approximation is only good at the centre of the Wannier function. On the neighbouring lattice site it is already much different.

where l is the characteristic length of a lattice site potential approximated as harmonic potential. In the present units $l = \eta^{-1/4}$. Since the second band is also considered here, the term Gaussian approximation is not quite appropriate anymore. In general the Wannier functions of the higher bands can be well approximated by the solutions of the harmonic oscillator if the lattice is deep enough. For the second band the Wannier function can thus be written as

$$w_1(z) \approx \frac{\sqrt{2} z e^{-\frac{z^2}{2l^2}}}{\pi^{\frac{1}{4}} l^{\frac{3}{2}}}. \tag{4.23}$$

However, such an approximation must be taken with care, if one considers nonlocal properties like hopping. The harmonic oscillator functions are only good approximations inside the lattice site where they are centred. On the neighbouring site they differ quite a lot from the proper Wannier function. In Fig. 4.5 the Wannier function of the lowest band is shown on a logarithmic scale together with the Gaussian approximation. The difference is quite obvious. For this reason the use of this approximation for the calculation of the hopping is questionable. The results one gets in the harmonic oscillator approximation are

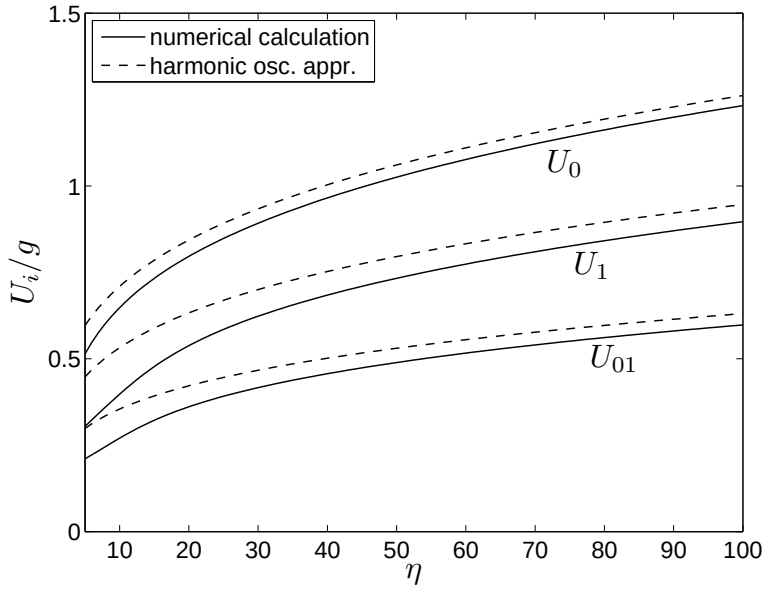

Figure 4.6: Comparison of the interaction in the first and second band as well as the interband interaction with the harmonic oscillator approximation.

$$J_0 = -\frac{1}{4}e^{-\frac{4+\eta\pi^2}{4\sqrt{\eta}}}[2\eta + e^{\frac{1}{\sqrt{\eta}}}(2\sqrt{\eta} - \eta(-2+\pi^2))] \tag{4.24}$$

$$J_1 = -\frac{1}{8}e^{-\frac{4+\eta\pi^2}{4\sqrt{\eta}}}\sqrt{\eta}[8 - 4\sqrt{\eta} + 2\eta\pi^2 - e^{\frac{1}{\sqrt{\eta}}}(12 + \sqrt{\eta}(4-12\pi^2) + \eta\pi^2(\pi^2-2))] \tag{4.25}$$

from which one can find the asymptotics for $\eta \to \infty$ [32],

$$J_0 = \eta e^{-\sqrt{\eta}\frac{\pi^2}{4}}\left(\frac{\pi^2}{4} - 1\right), \tag{4.26}$$

$$J_1 = \eta^{3/2}e^{-\sqrt{\eta}\frac{\pi^2}{4}}\frac{\pi^2}{2}\left(\frac{\pi^2}{4} - 1\right). \tag{4.27}$$

For local properties like U_0,U_1,U_{01},Δ_k the harmonic oscillator approximation should yield quite good results for deep lattices. One finds

$$U_0 = g\frac{1}{\sqrt{2\pi}}\eta^{1/4} \tag{4.28}$$

$$U_1 = g\frac{3}{4\sqrt{2\pi}}\eta^{1/4} \tag{4.29}$$

$$U_{01} = g\frac{1}{2\sqrt{2\pi}}\eta^{1/4}. \tag{4.30}$$

From this one recognizes that the interband hopping U_{01} is always of the same order of magnitude than the interactions U_0,U_1. Numerical calculations show that

this remains true for small η. See Fig. 4.3. For the energy offset one finds in harmonic oscillator approximation

$$\Delta_1 - \Delta_0 = \sqrt{\eta}(1 + e^{-\frac{1}{\sqrt{\eta}}}) \tag{4.31}$$

which is simply $2\sqrt{\eta}$ for deep lattices and is nothing else than the usual $\hbar\omega$ energy offset of a harmonic oscillator.

4.5 Determining the hopping via the bandwidth

Since the harmonic oscillator approximation is not well suited for obtaining analytic results for the hopping other ways must be found. In principle Eq. (4.1) can be solved analytically. The solutions are Mathieu functions. However it is still difficult to obtain analytic results for the hopping. It is not known to the author if the integrals which need to be calculated for the hopping have simple analytic solutions. Normally a simple trick is used here to circumvent this problem. The trick consists in the assumption that the energy-bands can be approximated by a cosine function. This leads also only to approximative results but they should be exact for deep lattices. The trick is justified by the following consideration. The hopping term in the BHM

$$\hat{H}_{\text{hop}} = -J \sum_j \left[\hat{a}_j^\dagger \hat{a}_{j+1} + \hat{a}_j^\dagger \hat{a}_{j-1}\right] \tag{4.32}$$

of a band can be diagonalized easily by using

$$\hat{a}_j = M^{-1/2} \sum_n^M \hat{d}_n e^{2\pi i n j/M} \tag{4.33}$$

where $\hat{d}_n$ are also bosonic annihilation operators and M is the number of sites. The result is

$$\hat{H}_{\text{hop}} = \sum_n^M \left(-2J\cos(2\pi n/M)\right) \hat{d}_n^\dagger d_n. \tag{4.34}$$

This suggests a cosine shaped energy-band and the width of this energy-band is $4J$. The analytically exact known width of the energy bands (which are relatively easily obtained) can now be taken and set equal to $4J$. The analytically exact width ΔE_n of the nth band is given by the so called Mathieu characteristic functions a_n and

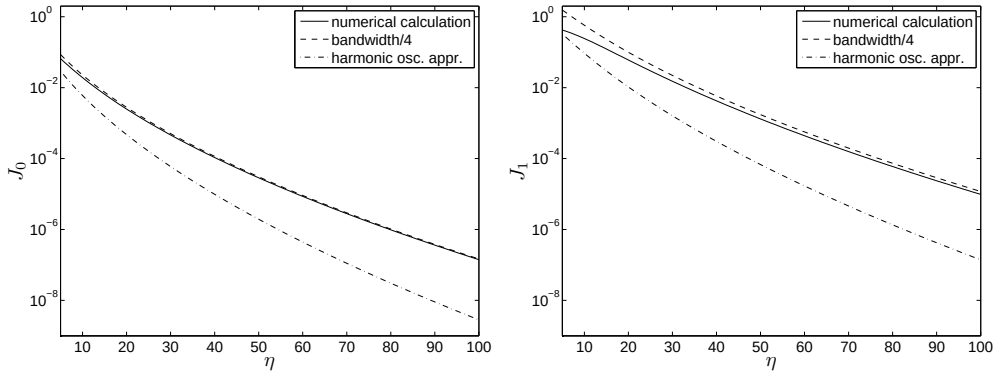

Figure 4.7: Comparison of the hopping in the first and second band with approximative results. One sees that the harmonic oscillator approximations is different by an order of magnitude. The bandwidth however gives a good estimate for the hopping.

b_n. The result is

$$\Delta E_n = b_{n+1}\left(\frac{\eta}{4}\right) - a_n\left(\frac{\eta}{4}\right) = 4J_n \tag{4.35}$$

$$J_n = 2^{4n+3}\sqrt{2/\pi}\left(\frac{\eta}{4}\right)^{\frac{1}{2}n+\frac{3}{4}} e^{-2\sqrt{\eta}}/n!. \tag{4.36}$$

See [33]. Note that this result is significantly different from the Gaussian (or harmonic oscillator) approximation (4.24), (4.25) even for arbitrary deep lattices. As was mentioned earlier it was to be expected that the harmonic oscillator approximation is very bad for non-local properties. For a comparison of the different deep lattice approximations see Fig. 4.7 and Fig. 4.6.

4.6 Regime of small hopping and one-band approximation

The investigation of the two-band Hubbard model rises the question in which parameter regime the second and higher bands can be neglected. This is especially interesting for the experimentally important regime of small hopping, i.e. $J_0/U_0 \ll 1$. This regime requires that U_0 is large. However, that means that U_{01} is also large since it is always of the same order of magnitude as U_0. The one-band approximation requires that U_{01} is small compared to $\Delta = \Delta_1 - \Delta_0$. U_0 and U_{01} depend on g, whereas J_0 and Δ are independent of g and depend only on the

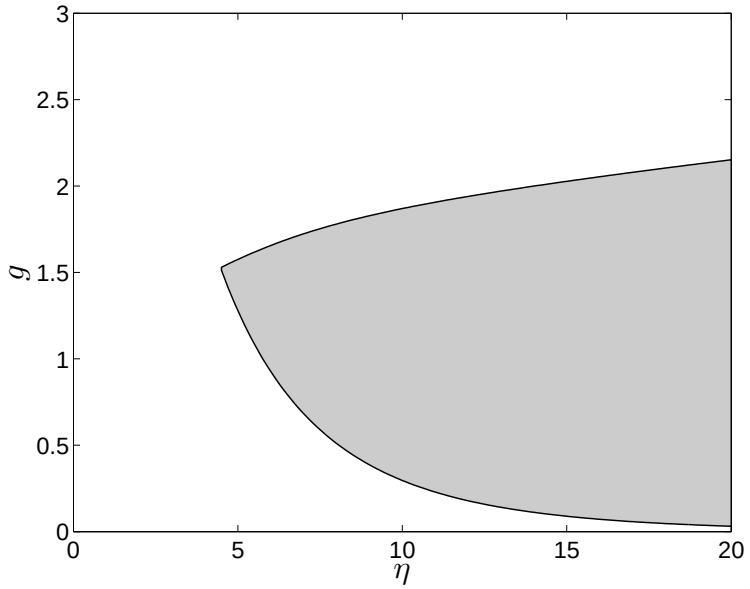

Figure 4.8: Regime of the one-band approximation for small hopping. The grey shaded area corresponds to all g for which $J_0/U_0 < 0.1$ and $U_{01}/\Delta < 0.1$.

lattice depth. Thus the question is: Can g be chosen such that J_0/U_0 and U_{01}/Δ become small at the same time? Fig. 4.8 shows that this is indeed possible. One also recognizes however, even for deep optical lattices, i.e. $\eta \approx 20$ there is an upper limit for the interaction strength at which the single band model is justified.

4.7 Summary

In the present chapter the validity of the lowest Bloch band approximation for particles in periodic potentials was analysed. It was studied under what conditions higher bands can be ignored and when the second band needs to be taken into account. To this end the two-band Hubbard model was derived. Hopping and interaction parameters in the first and second band have been calculated. It was shown that single particles can not tunnel between the bands. This is only possible for particle pairs. Finally, the two-band model allowed to determine the limitations of the single band model. The regime of the interaction strength was calculated, where the single band approximation is justified.

Part II

One-dimensional quantum gases in the trap

Chapter 5

1D Bose gas in the trap

5.1 From homogeneous to lattice models: discretization

A Hamiltonian like (2.4) is not numerical tractable until some additional constraints and approximations are introduced.

Firstly, the eigenvalue spectrum is not expected to be discrete. This is resolved by introducing boundary conditions. Loosely speaking, these boundary conditions should be designed to select a discrete set of eigenvectors of the Hamiltonian.

Secondly, even after introducing boundary conditions the spectrum as well as the Hilbert space, which the eigenvectors span, is still infinite. A preselection of eigenvectors i.e. eigenstates must be introduced which is suitable in a physical sense. In thermodynamic considerations, states of an energy much higher than the temperature can be neglected. However, in general the energies and eigenstates of the Hamiltonian are not known, since in this case everything important about the system would be known anyway. Instead it is assumed here that states with a momentum or kinetic energy larger than the temperature can be neglected. This is done in total analogy to the boundary condition in real space. As particles are restricted for example to a box in real space they are restricted as well to a box in momentum space. The following discussion may give some insight that this is exactly equivalent to introducing a spatial discretization.

In the following periodic boundary conditions for the Bose-field $\hat{\Psi}(x)$ in one dimension are assumed. This means $\hat{\Psi}$ has the property

$$\hat{\Psi}(x+L) = \hat{\Psi}(x), \quad L > 0. \tag{5.1}$$

Furthermore, as a Bose-field, $\hat{\Psi}$ has to fulfil the commutation relations

$$[\hat{\Psi}(x_1), \hat{\Psi}(x_2)] = 0, \quad [\hat{\Psi}(x_1), \hat{\Psi}^\dagger(x_2)] = \delta(x_1 - x_2). \tag{5.2}$$

It is easy to see that $\hat{\Psi}$ fulfils these conditions if one makes an ansatz

$$\hat{\Psi}(x) = \sum_{j\in\mathbb{Z}} \hat{d}_j \phi_j(x), \tag{5.3}$$

with creation and annihilation operators $\hat{d}_j^\dagger$, $\hat{d}_j$ and an orthonormal set of functions $\phi_j(x)$ with the properties

$$[\hat{d}_i, \hat{d}_j] = 0, \quad [\hat{d}_i, \hat{d}_j^\dagger] = \delta_{ij}, \tag{5.4}$$

$$\sum_{j\in\mathbb{Z}} \phi_j^*(x_1)\phi_j(x_2) = \delta(x_1 - x_2). \tag{5.5}$$

For the sake of convenience let

$$\phi_j(x) = \frac{1}{\sqrt{L}} e^{ik_j x}, \quad k_j = j\Delta k + k_0, \quad j \in \mathbb{Z}. \tag{5.6}$$

Note that the periodicity condition (5.1) already demands to select only certain k's. Furthermore Δk is fixed by the relation

$$\Delta k = \frac{2\pi}{L} \tag{5.7}$$

Relation (5.7) can be interpreted as that boundary conditions in x-space are equivalent to discretization in k-space. The aim now is to redefine $\hat{\Psi}$ in a way that the same relation holds for the conjugate variable, namely that restricting the k's leads to a discretization in x. Of course this must be done in a way, that physical considerations are not violated. The kinetic energy now reads

$$\hat{H}_{\text{kin}} = -\frac{\hbar^2}{2m} \int dx\, \hat{\Psi}^\dagger(x) \frac{\partial^2}{\partial x^2} \hat{\Psi}(x) = \frac{\hbar^2}{2m} \sum_j \hat{d}_j^\dagger k_j^2 \hat{d}_j \tag{5.8}$$

which implies, that a high kinetic energy corresponds to large k. It makes therefore sense to neglect large k's or rather keep the smallest k's. It is clear from the equidistant structure of the k's that this will be for example the M k_j closest to zero. This imposes also a condition on k_0. E.g. when $j = 1, 2, \ldots, M$ then

$$k_0 = -\frac{\pi}{L}(M + 1). \tag{5.9}$$

Let equidistant grids in position- and quasi-momentum spaces be introduced, with grid constants Δx and Δp, respectively: $\Delta x \Delta p = 2\pi\hbar/M$, M being the number of grid points. This is equivalent to putting the system into a box of size $L = M\Delta x$ with periodic boundary conditions and restricting the quasi-momentum to an interval of length $P = M\Delta p$. The grids are given by the points

$$x_j = j\Delta x + x_0, \tag{5.10}$$

$$p_j = j\Delta p + p_0, \tag{5.11}$$

$$j \in \{0, 1, 2, 3, \ldots, M-1\}. \tag{5.12}$$

The Bose field with discretized modes $\hat{d}_j$ corresponding to wave numbers $k_j = p_j/\hbar$ is related to local bosonic operators via the discrete Fourier transformation: $(j, l = 0, \cdots, M-1)$

$$\hat{a}_j = \frac{1}{\sqrt{M}} \sum_{l=0}^{M-1} \hat{d}_l e^{ik_l x_j}, \quad [\hat{a}_j, \hat{a}_l^\dagger] = \delta_{jl}. \tag{5.13}$$

If (5.13) is inserted into (5.8) it will result in hopping terms between any two sites. This is not desirable for many numerical methods. The hopping terms between distant sites are small and can be neglected. Technically this can be done by approximating in (5.8)

$$k_j^2 \approx \frac{4}{\Delta x^2} \sin^2\left(\frac{k_j \Delta x}{2}\right). \tag{5.14}$$

The result of that is a kinetic energy which contains only nearest neighbour hopping terms

$$\hat{H}_{\text{kin}} = \frac{\hbar^2}{2m\Delta x^2} \sum_j (2\hat{a}_j^\dagger \hat{a}_j - \hat{a}_j^\dagger \hat{a}_{j+1} - \hat{a}_j^\dagger \hat{a}_{j-1}) \tag{5.15}$$

which is the same as if the differential operator in the kinetic energy has been approximated by difference quotients. If the interaction energy

$$\hat{H}_{\text{int}} = \frac{g}{2} \int \hat{\Psi}^\dagger(x)\, \hat{\Psi}^\dagger(x)\, \hat{\Psi}(x)\, \hat{\Psi}(x) dx \tag{5.16}$$

is discretized the result is straightforwardly

$$\hat{H}_{\text{int}} = \frac{g}{2\Delta x} \sum_j \hat{a}_j^\dagger \hat{a}_j^\dagger \hat{a}_j \hat{a}_j \tag{5.17}$$

It seems remarkable, that the kinetic energy scales like Δx^{-2}, whereas the interaction—like Δx^{-1}. This does however not mean that the interaction can be neglected in the limit $\Delta x \to 0$. . The interaction term will only play a role if two particles are sitting at the same position. In that case the kinetic energy term will also produce a term scaling with Δx^{-1} because the wavefunction has a discontinuity in the first derivative. More details about this can be found in Chapter 6.

The final result is that the discretized grand canonical Hamiltonian is equivalent to a Bose-Hubbard model (BHM) with effective hopping

$$J = \hbar^2/2m\Delta x^2, \tag{5.18}$$

effective on-site interaction

$$U = g_{1\mathrm{D}}/\Delta x, \tag{5.19}$$

and effective chemical potential

$$\mu_{\mathrm{BH}} = \mu - 2J. \tag{5.20}$$

The scaled hopping can be expressed in terms of the Tonks parameter at the trap centre, $J/U = 2/\gamma n(0)\Delta x$. The Bose-Hubbard model is known to posses insulating phases, where the on-site particle number fluctuation is almost zero. For the discretized model those phases have no meaning. In fact those phases must lie outside the validity region of the discretization. The question, if this is truly the case is discussed in the next section. Finally it will turn out that, since a reasonable range of values for Δx is $\Delta x \ll n(0)^{-1}$, the 1D gas always corresponds to a superfluid phase of the BHM, close to the line $\mu_{\mathrm{BH}} = -2J$.

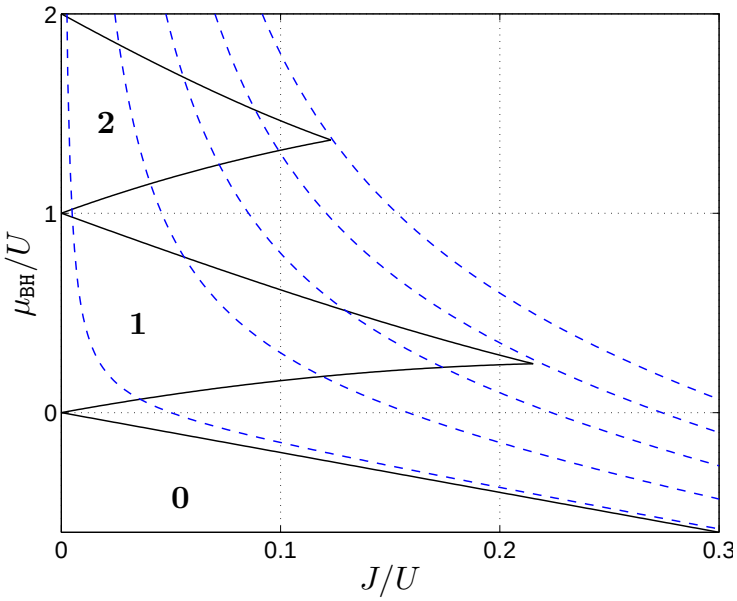

Figure 5.1: Eq. 5.24 (dashed lines) overlapped with the 1D Bose-Hubbard phase diagram (solid lines). From bottom to top: $\chi = 0.01,\ 0.1,\ 0.2,\ 0.3,\ 0.4$. The asymptotics of (5.24) coincides with (the perturbative approximation to) the upper boundary of the zero-filling lobe.

5.2 From 1D trapped bosons to a 1D Bose-Hubbard model

5.2.1 Location of the discretized system in the BH-phase diagram

In the previous chapter it was derived that discretising Hamiltonian (2.4) results in:

$$\mathcal{H} = \frac{\hbar^2}{2m\Delta x^2}\sum_k \Big(\hat{a}_k^\dagger - \hat{a}_{k+1}^\dagger\Big)\Big(\hat{a}_k - \hat{a}_{k+1}\Big) + \sum_k \Big(V_k - \mu\Big)\hat{a}_k^\dagger\hat{a}_k + \frac{g_{\rm 1D}}{2\Delta x}\sum_k \hat{a}_k^{\dagger 2}\hat{a}_k^2, \quad (5.21)$$

which is just the Bose Hubbard model with the parameters

$$J = \frac{\hbar^2}{2m\Delta x^2}\,, \quad \mu_{\rm BH} = \mu - 2J\,, \quad U = \frac{g_{\rm 1D}}{\Delta x}\,. \quad (5.22)$$

Here naturally the question arises, if the continuous system maps onto a lattice system, where is the continuous system found in the phase diagram of the lattice

system? Clearly the continuous system must stay away from the insulating phases characteristic for lattice systems. If Δx is chosen such that one is in an insulating phase the validity of the discretization obviously breaks down. Thus, there must be a strict upper bound for Δx. For the phase diagram of the Bose-Hubbard the dimensionless values

$$\frac{J}{U} = \frac{\hbar^2}{2mg_{1\mathrm{D}}\Delta x}, \tag{5.23}$$

$$\frac{\mu_{\mathrm{BH}}}{U} = \frac{\mu\Delta x}{g_{1\mathrm{D}}} - \frac{2J}{U} = \chi\frac{U}{2J} - \frac{2J}{U}. \tag{5.24}$$

are important. The continuous system however is fully characterized by the parameter,

$$\chi = \frac{\hbar^2\mu}{mg_{1\mathrm{D}}^2}\,, \tag{5.25}$$

which distinguishes between the Gross-Pitaevskii ($\chi \gg 1$) and Tonks ($\chi \lesssim 1$) regimes. The relation between Eq. (5.24) and the Bose-Hubbard phase diagram in 1D is illustrated in Fig. 5.1. It may also be worth noting that Eq. (5.24) can be written as:

$$\frac{\mu}{U} = \Delta x n_{\mathrm{TF}} - \frac{2J}{U}\,, \tag{5.26}$$

where $n_{\mathrm{TF}} = \mu/g_{1\mathrm{D}}$ is the Thomas-Fermi density.

Is it possible to be inside the insulator lobe of filling 1 for example? This only may happen if $\chi \ll 1$, i.e., in the Tonks regime, and requires

$$\chi\frac{U}{2J} - \frac{2J}{U} \geq \frac{2J}{U}, \tag{5.27}$$

or, equivalently,

$$\mu \geq \frac{\hbar^2}{m\Delta x^2}. \tag{5.28}$$

This is certainly impossible. Indeed, in the Tonks regime, the kinetic energy is essential, whereas (5.28) states that the chemical potential is twice the maximal kinetic energy for the given spatial grid. On the other hand, in the Thomas-Fermi regime, the kinetic energy is small, so that the condition (5.28) may hold. This does not lead to any problems because, in the Thomas-Fermi case, line (5.24) stays far on the right of the insulator lobes.

5.2.2 Upper and lower bounds for Δx

The key question is, if the Bose-Hubbard model can be used in the weak-hopping limit, $J/U \ll 1$ to describe a homogeneous Bose gas. To this end, recall the expression for the 1D interaction constant Eq. (2.3). For $a_{3D} \ll l_\perp$

$$g_{1D} = \frac{2a_{3D}}{l_\perp^2}, \tag{5.29}$$

were a_{3D} is the 3D scattering length, and $l_\perp$ is the quantum lengths related to the radial directions . In terms of the radial frequency $\omega_\perp$,

$$l_\perp = \sqrt{\frac{\hbar}{m\omega_\perp}}. \tag{5.30}$$

A tightly confining trap is assumed here, $l_\perp \ll l$, where l is the quantum length related to the longitudinal direction,

$$l = \sqrt{\frac{\hbar}{m\omega}}. \tag{5.31}$$

To keep the motion one-dimensional, all energies in the problem should stay small compared to the radial quantum, $\hbar\omega_\perp = \hbar^2/ml_\perp^2$.

In physical units, Eq. (5.29) is expressed as,

$$g_{1D} = \frac{2\hbar^2 a_{3D}}{ml_\perp^2}\,. \tag{5.32}$$

The parameter χ then becomes,

$$\chi = \frac{\mu m l_\perp^4}{4\hbar^2 a_{3D}^2} = \frac{\mu}{\hbar\omega}\,\frac{l_\perp^4}{4a_{3D}^2 l^2}\,. \tag{5.33}$$

For the relative hopping strength, one has,

$$\frac{J}{U} = \frac{l_\perp^2}{4a_{3D}\Delta x}. \tag{5.34}$$

Thus, the weak hopping limit is realised if

$$\Delta x \gg \frac{l_\perp^2}{4a_{3D}}. \tag{5.35}$$

Note that, since $a_{3D} \ll l_\perp$, this requires that $\Delta x \gg l_\perp$.

Condition (5.35) sets a lower limit on Δx while inversion of (5.28), which must

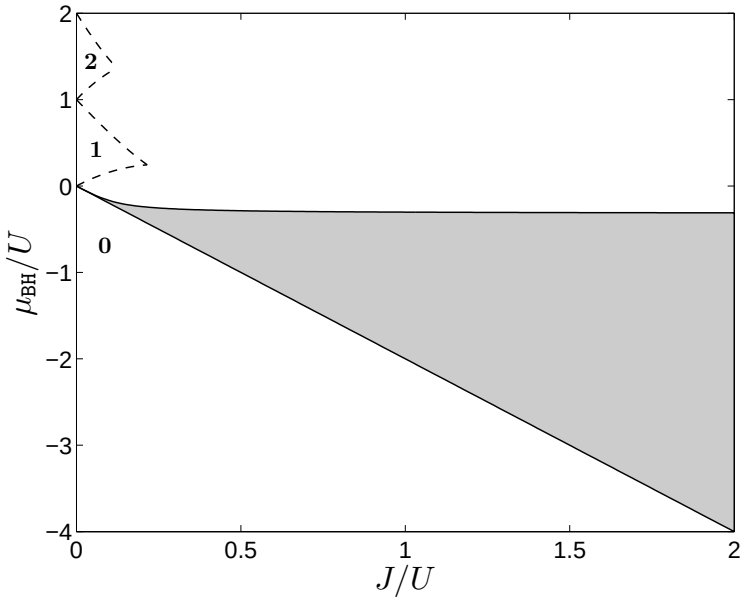

Figure 5.2: The grey shaded area corresponds to the discretized system when mapped onto the Bose-Hubbard-Hamiltonian with a Δx below the coherence length. The coherence length is evaluated in the hypothetical limit $\Delta x \to 0$ which is known from the Lieb-Liniger solution.

hold in the Tonks limit, provides an upper limit. Thus, in the Tonks regime, Δx must obey,

$$\frac{\hbar^2}{m\mu} \gg \Delta x^2 \gg \frac{l_\perp^4}{16 a_{3\mathrm{D}}^2}\,, \tag{5.36}$$

which in turn yields a consistency condition for μ,

$$\mu \ll \frac{16\hbar^2 a_{3\mathrm{D}}^2}{m l_\perp^4}. \tag{5.37}$$

It may be rewritten in two equivalent forms,

$$\frac{\mu}{\hbar\omega_\perp} \ll \frac{16 a_{3\mathrm{D}}^2}{l_\perp^2}\,, \tag{5.38}$$

$$\frac{\mu}{\hbar\omega} \ll \frac{16 a_{3\mathrm{D}}^2 l^2}{l_\perp^4}\,. \tag{5.39}$$

The first form gives better physical insight while the second form is better suited for numerical estimates if using oscillator coordinates in the trap.

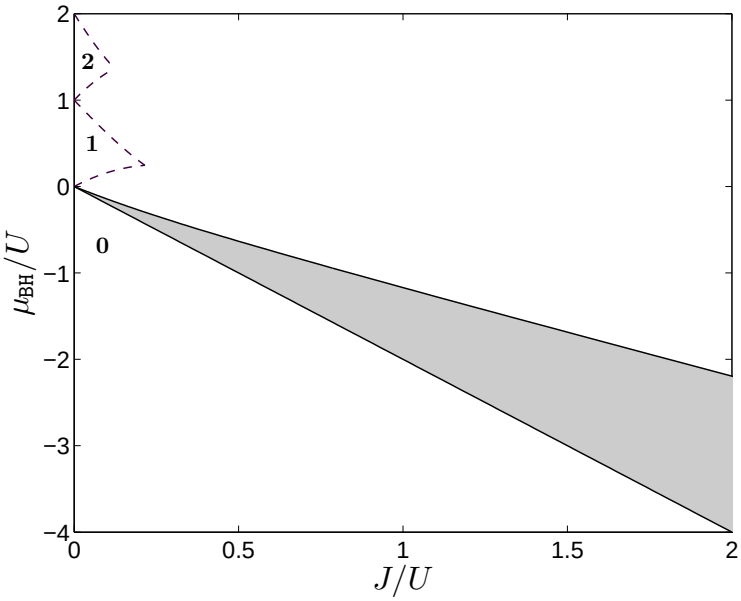

Figure 5.3: The grey shaded area corresponds to the discretized system when mapped onto the Bose-Hubbard-Hamiltonian with a Δx below the healing length. The healing length is evaluated in the hypothetical limit $\Delta x \to 0$ which is known from the Lieb-Liniger solution.

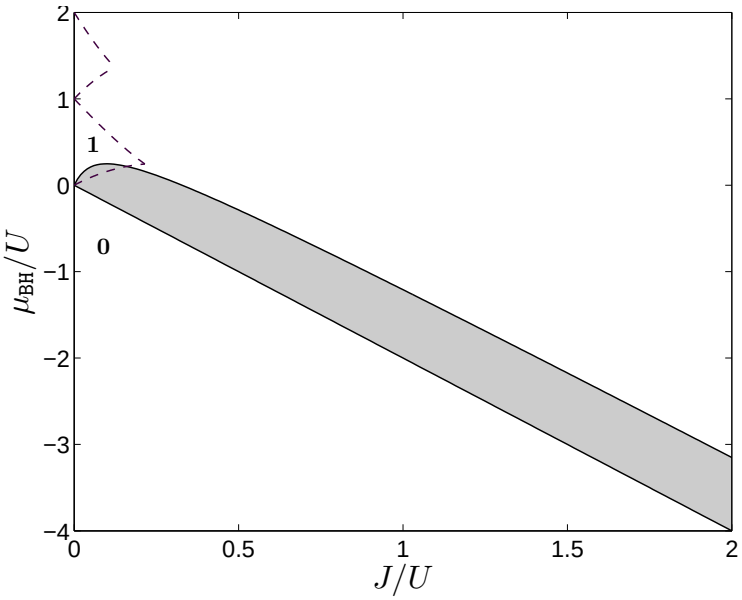

Figure 5.4: The grey shaded area corresponds to the discretized system when mapped onto the Bose-Hubbard-Hamiltonian with a Δx below the inverse density. For the density the hypothetical density in the limit $\Delta x \to 0$ is assumed which is known from the Lieb-Liniger solution. The dashed lines show the borders of the insulator phases for a filling of 1 and 2 of the Bose-Hubbard system.

5.2.3 Physical length scales

The purpose of this section is to examine which points in the Bose-Hubbard-diagram correspond to a Δx smaller than physically relevant lengths like the healing length or the correlation length. Firstly, one notes that the condensate has three parameters $(\Delta x, n, g_{1\mathrm{D}})$ whereas the Bose- Hubbard model has only two $(\bar{J} = J/U, \bar{\mu} = \mu/U)$. This means, that a third parameter must be added to the Bose-Hubbard-diagram to get a proper mapping. It proves to be convenient to chose $g_{1\mathrm{D}}$ as the third parameter. In the parameter-space of $(\bar{J}, \bar{\mu}, g_{1\mathrm{D}})$ Δx is now given by

$$\Delta x = \frac{\hbar^2}{2m g_{1\mathrm{D}} \bar{J}}. \tag{5.40}$$

For the further discussion the Lieb-Liniger-solution is used. This is done most easily by finding the relationship between χ and the Tonks-Girardeau parameter $\gamma = g_{1\mathrm{D}}/\rho$. In the Lieb-Liniger model χ is given by

$$\chi = \frac{1}{2\gamma^2}(3e(\gamma) - \gamma e'(\gamma)) \tag{5.41}$$

where $e(\gamma)$ is the Lieb-Liniger function. By noting that

$$\chi = (\bar{\mu} + 2\bar{J})2\bar{J} \tag{5.42}$$

one finds that γ is only a function of $\bar{\mu}$ and $\bar{J}$.

Two typical physical lengths are the coherence length $l_c = \frac{1}{\sqrt{\rho g_{1\mathrm{D}}}}$ and the healing length $\xi = \hbar/(\sqrt{2m\rho\frac{\partial\mu}{\partial\rho}})$. If these two lengths are compared to Δx the results are

$$\frac{\Delta x}{l_c} = \frac{1}{\sqrt{\gamma} 2\bar{J}} \tag{5.43}$$

$$\frac{\Delta x}{\xi} = \frac{1}{\bar{J}\sqrt{2}}\sqrt{\chi(2-\chi\gamma)}. \tag{5.44}$$

These ratios depend only on $\bar{\mu}$ and $\bar{J}$. Fig. 5.2 shows that one finds Δx smaller than the healing length only below $\bar{\mu}_{\mathrm{BH}} = 0$ in the corresponding Bose-Hubbard system. One stays always away from the insulating phases. Fig. 5.3 shows that staying with Δx below the healing length is even more restrictive. One has to stay close to the zero filling insulator. Another typical distance for the continuous system is the inverse density. One can find from the Lieb-Linger solution that the maximum

width of the quasi-momentum distribution is $2\pi\rho$ for $\gamma \to \infty$. For finite γ it is even less. The quasi-momenta of the Lieb-Liniger solution are a measure of the distance over which the wave function is varying in one simplex of the configuration space. Δx should therefore be much smaller than $1/\rho$. For the hypothetical number of particles per site when the density is inserted in the limit $\Delta x \to 0$ one finds

$$\rho\Delta x = \frac{1}{2\bar{J}\gamma}. \tag{5.45}$$

Fig. 5.4 shows which points in the Bose-Hubbard phase diagram correspond to a Δx below the inverse density. This region hits also the insulator phases which shows that a Δx of approximately $1/\rho$ is not small enough. It should be an order of magnitude smaller. Also it is not possible to reach the insulator phase without making Δx larger than the healing-length. The healing length is especially important when there are fast varying potentials present. Finally one comes to the conclusion that the discretized system must be always close to the zero filling lobe of the BH-phase diagram i.e. the line $\bar{\mu} = -2\bar{J}$ to approximate the continuous system well enough.

5.2.4 Effective Mass

Analysis of the Hamiltonian (4.1) shows, that the limiting case $k \to \infty$, while keeping η constant has an additional interpretation. Namely if one defines $\Delta x = \pi/k$, and introduces the effective mass m^* by setting $J = \frac{\hbar}{2m^*\Delta x^2}$ one finds the correspondence

$$\begin{aligned}\hat{H} &= \int dx\, \hat{\Psi}^\dagger(x) \left[\frac{-\hbar^2\partial^2}{2m\partial x^2} + V_0\left(\sin^2(kx) - \frac{1}{2}\right)\right] \hat{\Psi}(x) \\ &\hat{=} J\sum_j \left[2\hat{b}_j^\dagger\hat{b}_j - \hat{b}_j^\dagger\hat{b}_{j+1} - \hat{b}_j^\dagger\hat{b}_{j-1}\right] \overset{k\to\infty}{\longrightarrow} \int dx\, \hat{\Psi}^\dagger(x) \left[\frac{-\hbar^2\partial^2}{2m^*\partial x^2}\right] \hat{\Psi}(x),\end{aligned} \tag{5.46}$$

which means, that the lattice gas mimics a free gas with a mass different from the original particles if one approaches the limit $k \to \infty$. One finds for the ratio between mass and effective mass

$$\frac{m^*}{m} = \frac{E_R}{J\pi^2}. \tag{5.47}$$

with $E_R = \frac{\hbar^2k^2}{2m}$. If the lattice depth is increased J/E_R will get smaller, hence the effective mass increases with increasing lattice depth. This makes it for example

possible to simulate a strong interacting free-space gas with a weakly interacting lattice gas, see [34].

5.3 Stochastic simulation for $T \approx \hbar\omega$

Although, the stochastic method described in Section 3.1 seems to be quite a general tool for calculating thermal expectation values, it faces many limitations in practice. A first limitation is that low temperatures - in the trap particularly temperatures below $\hbar\omega$ - are not easily accessed. Like many other stochastic methods, the stochastic factorization of the kinetic energy shows worse convergence when the temperature is decreased. Another big problem is that decreasing Δx also has a very negative influence on the convergence. Decreasing Δx is associated with a larger quasi-momentum cut-off and thus leads to larger noise in the simulation of the kinetic energy. However Δx must be chosen small enough, for the discrete system to approximate well the continuous one; the number of particles per site must be small compared to unity. [34, 35].

With the block factorization method and $\Delta x < 1/n(0)$ it is just possible to reach a temperature of $k_{\mathrm{B}}T = \hbar\omega$, corresponding to a temperature where thermal fluctuation just start to destroy the quasi long range order. Still block artefacts, i.e. effects of badly chosen block states, although much reduced by use of the environment, show up especially at low temperature.

In Fig. 5.5 numerical results for the density and the first order correlations in a 1D trap are shown for $k_{\mathrm{B}}T = \hbar\omega$. The densities are compared to the predictions obtained from the Bethe ansatz solutions of Yang and Yang [6] using a local density approximation [i.e. replacing μ by $\mu(x) = \mu - V(x)$]. Also shown is the Tonks-gas limit, $\gamma = \infty$, at the given temperature, which is obtained using the mapping to a free Fermi gas. Apart from the case of $\gamma = 0.8$ where block artefacts are still present, there is very good agreement with the prediction of the Yang-Yang theory in local density approximation. The latter becomes invalid close to the edges of the gas, and thus larger deviations of the numerical simulation from the Yang-Yang theory occur.

The Yang-Yang solution unfortunately does not give any information about the correlations in the system, therefore the corresponding numerical results are compared here to different predictions valid either in the weak or strong interaction limits. The weak-interaction limit is described by a Bogoliubov approximation. Since the temperature is rather low thermal depletion of the quasi-condensate is not taken into account here. In the opposite limit, $\gamma \to \infty$, correlations can be

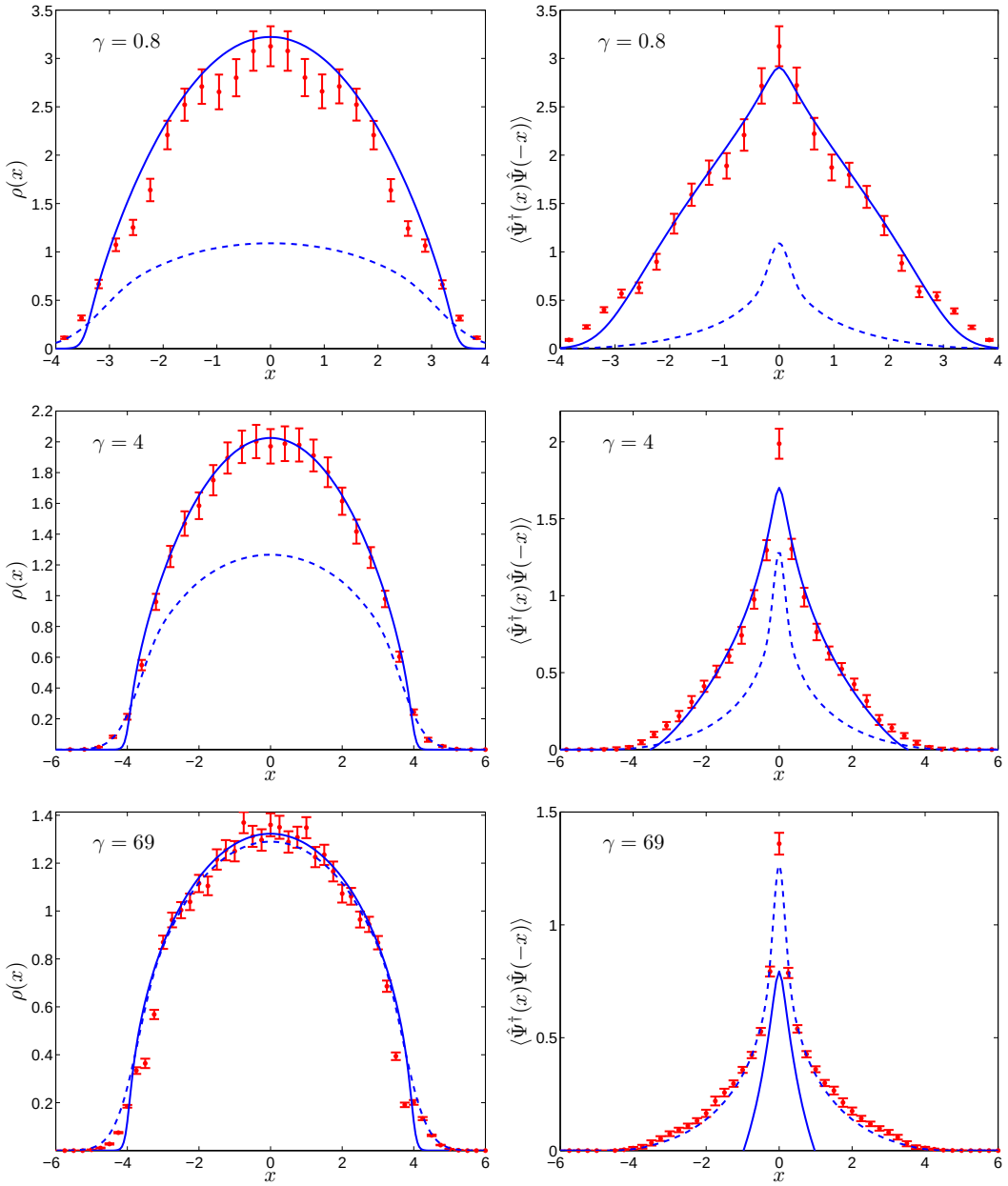

Figure 5.5: Left side: Particle density of the Bose gas in a trap at $k_\mathrm{B}T = \hbar\omega$ for different interaction strengths. Red dots with error bars: Stochastic simulation, solid line: Prediction from Yang and Yang within the local density approximation, and dashed line: Tonks fermionization limit. Right side: First-order correlations in the Bose gas for the same parameter regimes as for the left side. Dots with error bars: Stochastic simulation, solid line: Bogoliubov approximation, and dashed line: Efetov-Larkin approximation.

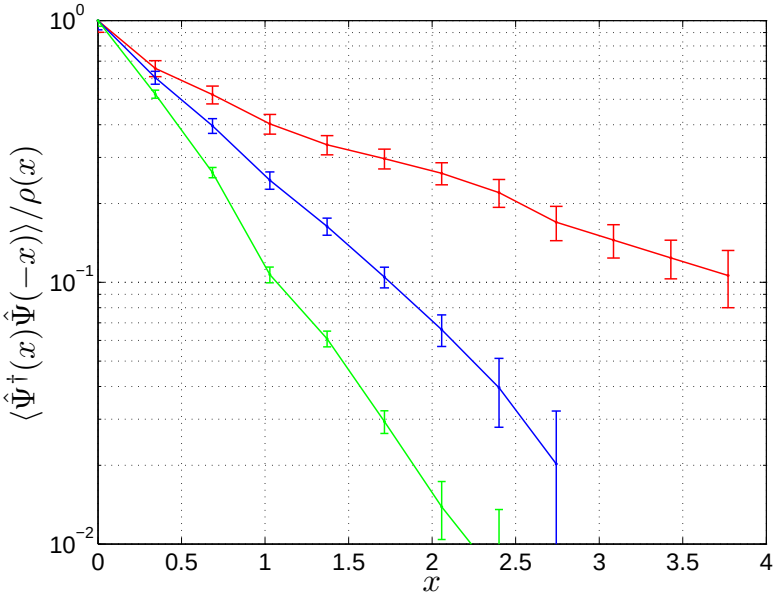

Figure 5.6: First-order correlations for $\gamma = 4$ at different temperatures shown on a logarithmic scale: $k_\mathrm{B}T/\hbar\omega = 3$ (green), $k_\mathrm{B}T/\hbar\omega = 2$ (blue), and $k_\mathrm{B}T/\hbar\omega = 1$ (red). At $k_\mathrm{B}T = \hbar\omega$, a deviation from the exponential behaviour becomes discernible.

calculated by mapping impenetrable bosons $\hat{b}_i, \hat{b}_i^\dagger$ to fermions $\hat{c}_i, \hat{c}_i^\dagger$ via a Wigner-Jordan transformation $\hat{b}_i = \prod_{j<i}(1 - 2\hat{c}_j^\dagger\hat{c}_j)\,\hat{c}_i$, which leads to the expression for first-order correlations found by Efetov and Larkin [36]

$$\langle\hat{b}_i^\dagger\hat{b}_j\rangle = \mathrm{Det}\Big(\mathbf{g}^{ij}\Big), \qquad j < i. \tag{5.48}$$

$\mathbf{g}^{ij}$ is a $(j-i)\times(j-i)$ matrix with elements $(g^{ij})_{n,m} = \langle\hat{c}_n^\dagger\hat{c}_m\rangle - \delta_{nm}/2$, where n and m are running from i to $j-1$. Fig. 5.5 compares the simulated correlations with the Bogoliubov and Efetov-Larkin predictions. The expected transition from the Bogoliubov to the Efetov-Larkin behaviour in the Tonks limit with increasing γ is clearly seen.

To see the asymptotic behaviour of the phase correlations more clearly, in Fig. 5.6 the first-order correlations normalized to the density $\langle\hat{\Psi}(x)^\dagger\hat{\Psi}(-x)\rangle/\rho(x)$ for $\gamma = 4$ are plotted on a logarithmic scale. Numerical results for three different temperatures are shown, $k_\mathrm{B}T/\hbar\omega = 1, 2, 3$. For the lowest temperature which was possible to reach in the simulation, deviations from the pure exponential decay characteristic of higher temperatures can already be seen for intermediate distances. This is consistent with predictions of the Luttinger-liquid model [35], namely, that the asymptotic behaviour of the correlations changes from exponential to a power law if the thermal energy $k_\mathrm{B}T$ becomes much smaller than the

trap energy $\hbar\omega$. (The spatial resolution of our simulations is insufficient to see the short-distance behaviour of the correlations which is not described by the LL model.)

5.4 DMRG calculations of ground state properties

In this section results from a DMRG calculation for a one-dimensional interacting Bose gas in a harmonic trap are compared to the best available analytic solutions. The aim of this section is to show that the DMRG method is able to produce correct results also for inhomogeneous continuous systems. The DMRG method works best for ground state properties, but also some calculations for low temperatures are discussed. From the homogeneous Bose gas the following results have been derived in Section 2.1.2. In the absence of an external trapping potential the Hamiltonian (2.4) is integrable in the thermodynamic limit, i.e. it has an infinite number of constants of motion. The ground-state solution for $T = 0$ which can be obtained by Bethe ansatz [5] shows that the 1D Bose-gas is fully characterized by one parameter $\gamma = \frac{g}{\rho}$, the so-called Tonks parameter. Integrability is no longer given when a (harmonic) trapping potential $V(x)$ is taken into account. An often used approximation to nevertheless describe the local properties in the inhomogeneous case is the local density approximation (LDA) Eq. 2.38. The LDA assumes that the homogeneous solution holds with the chemical potential μ replaced by an effective, local chemical potential $\mu_{\text{eff}}(x) = \mu - V(x)$. As long as the characteristic length of changes is small compared to the healing length the LDA is believed to work well. Within this approximation one finds e.g. for the density of the gas:

$$\rho(x) = \frac{g}{f^{-1}\left(\frac{\mu_{\text{eff}}(x)}{g^2}\right)} \tag{5.49}$$

where f^{-1} is the inverse function of Eq. (2.37).

In order to develop an in principle exact numerical algorithm powerful real-space renormalization methods such as the DMRG [37, 38] is employed here. See Section 3.2. To this end it is necessary to map the continuous to a lattice model. As shown in Section 5.1 this can be done in a consistent way.

The numerical DMRG calculations of the density profile, shown in Fig. 5.7, for Tonks parameters γ ranging from 0.4 to about 70 show excellent agreement with the Lieb-Liniger result with LDA (5.49) apart from a very small region at the

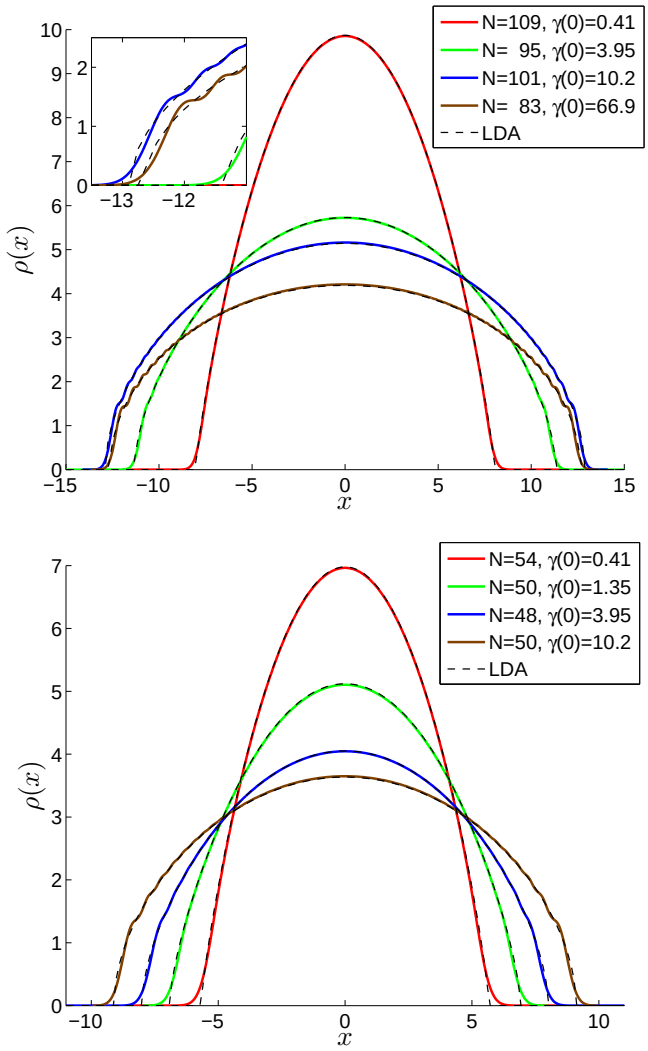

Figure 5.7: Density of the 1D bosonic gas in a trap at $T = 0$. The solid lines are the DMRG results and the dashed lines are the Lieb-Liniger prediction in local density approximation. Excellent agreement is found apart from the edges and some barely visible Friedel oscillations.

trap edges and the barely visible Friedel-type oscillations, which result from the finite number of particles. One recognizes the typical change of the density profile from an inverted parabola in the Bogoliubov regime $\gamma \ll 1$ to the square root of a parabola in the Tonks-Girardeau limit $\gamma \gg 1$ [12].

An important consequence of the Fermion-like behaviour of Bosons in the Tonks limit $\gamma \gg 1$ is a dramatic reduction of the loss rate due to inelastic three-body collisions [39]. The rate is proportional to the local three particle correlation

$$g_3(x) = \frac{\langle \hat{\Psi}^{\dagger 3}(x)\, \hat{\Psi}^3(x) \rangle}{\langle \hat{\Psi}^{\dagger}(x)\, \hat{\Psi}(x) \rangle^3}, \tag{5.50}$$

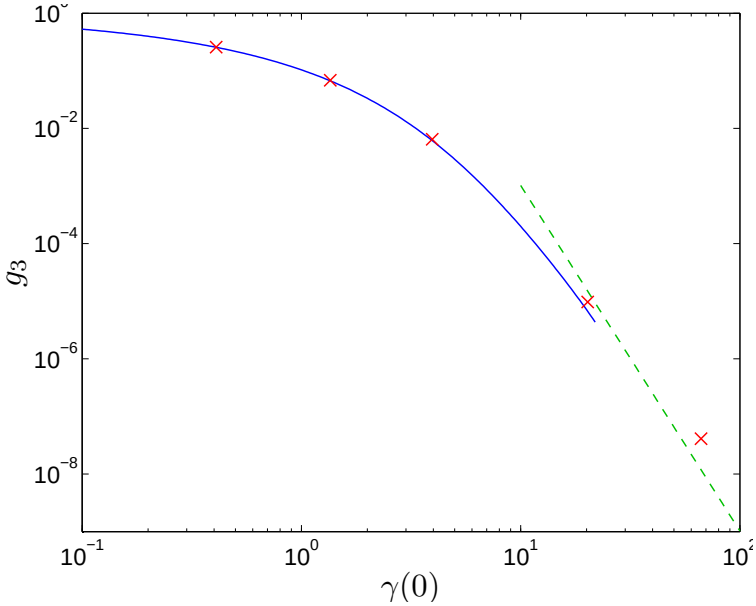

Figure 5.8: Local third-order correlations as function of Tonks parameter at the trap centre (red crosses) compared to prediction from Lieb-Liniger theory with local density approximation (solid line) and Tonks-Girardeau limit (dashed line).

and determines the stability of the Bose gas. Making use of the Hellman-Feynman theorem and the constants of motion of the homogeneous Lieb-Liniger gas Cheianov [40] has found for g_3

$$\begin{aligned} g_3 &= \frac{3}{2\gamma}\epsilon_4' - \frac{5\epsilon_4}{\gamma^2} + \\ &\quad + \left(1+\frac{\gamma}{2}\right)\epsilon_2' - 2\frac{\epsilon_2}{\gamma} - \frac{3\epsilon_2\epsilon_2'}{\gamma} + \frac{9\epsilon_2^2}{\gamma^2}. \end{aligned} \tag{5.51}$$

Fig. 5.8 shows a comparison between the numerical data for $g_3(0)$ at the trap centre with Eq. (5.51) and the asymptotic expression in the Tonks-Girardeau limit with γ taken at the trap centre $\gamma(0) = g/\rho(0)$. One recognizes again excellent agreement except for a small deviation for very large γ, where the numerics is however susceptible to errors due to the smallness of g_3.

In contrast to local quantities, such as the moments of the number density, information about spatial correlations of the homogeneous 1D Bose gas such as $g_1(x_1, x_2) = \langle \hat{\Psi}^\dagger(x_1)\,\hat{\Psi}(x_2)\rangle / \sqrt{\rho(x_1)\rho(x_2)}$ cannot straight-forwardly be obtained from the Lieb-Liniger and Yang-Yang theories. Making use of the Hellmann-Feynman theorem and the asymptotic properties of the Lieb-Liniger wavefunction for large momenta, Olshanii and Dunjko derived the lowest-order terms of the

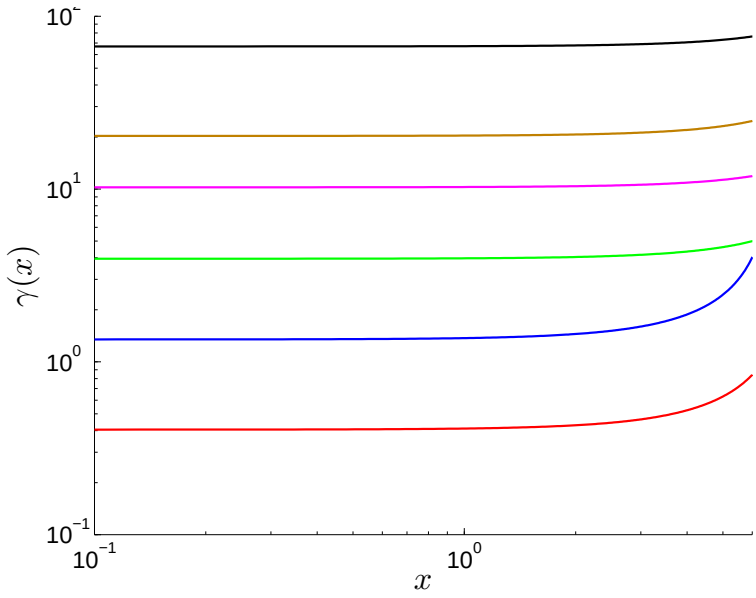

Figure 5.9: Local Tonks parameter $\gamma(x)$ as function of distance from the trap centre for different interaction strength and particle numbers.

Taylor expansion of $g_1(x_1, x_2)$ in $x = x_1 - x_2$ [9]

$$\begin{aligned} g_1(x_1, x_2) &= 1 - \frac{1}{2}\Big(\epsilon_2(\gamma) - \gamma\epsilon'(\gamma)\Big)\rho^2 x^2 \\ &\quad + \frac{1}{12}\gamma^2\epsilon_2'(\gamma)\rho^3|x|^3 + \cdots . \end{aligned} \tag{5.52}$$

In the presence of a trapping potential the Tonks parameter becomes space dependent $\gamma \to \gamma(x)$. Thus Eq. (5.52) cannot be applied straightforwardly. However, as can be seen from Fig. 5.9, in which $\gamma(x) = g/\rho(x)$ is plotted with the densities obtained in LDA, there is only a very weak dependence on x. Thus short-range correlations are expected not to depend on the presence of the confining trap potential. Fig. 5.10 shows a comparison between g_1 obtained from Eq. (5.52) and numerical results for different Tonks parameters at the trap centre. Taking into account that a high resolution of the short-distance behaviour is numerically very difficult the agreement is rather good.

The long-range or low-momentum behaviour of the correlations can be obtained from a quantum hydrodynamic approach [10], the Luttinger liquid theory (see also Section 2.1.3), in which long-wave properties of the 1D fluid are described in terms of two conjugate variables, the local density fluctuations and the phase.

In the homogeneous case one finds that the leading-order term in the asymptotics of first order correlation at temperature T are given by [11]

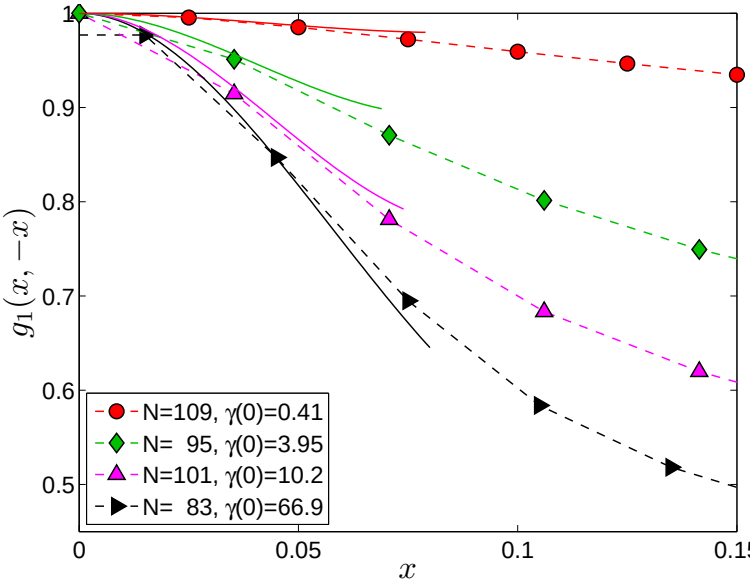

Figure 5.10: First order correlations (dashed lines) compared to analytic short-distance expansion (solid lines) for a homogeneous gas with γ taken at the trap centre.

$$g_1(x_1,x_2) \approx \left(\frac{K/L_T}{\rho \sinh\left(\frac{\pi|x_1-x_2|}{L_T}\right)} \right)^{1/2K} \tag{5.53}$$

where K is the Luttinger parameter and L_T is the thermal correlation length $L_T = \pi\rho/KT$. One recognizes that for $T = 0$ correlations decay asymptotically as a power-law with exponent $1/2K$, while for finite T there is an intermediate power-law behaviour turning into an exponential decay for $|x_1 - x_2| \geq L_T$. For $T = 0$ the exponent $1/2K$ is given by

$$\frac{1}{2K} = \frac{1}{2}\sqrt{-\frac{\gamma^3 f'(\gamma)}{\pi^2}}. \tag{5.54}$$

In Fig. 5.11 the first-order coherence $g_1(x,-x)$ is plotted for symmetric positions with respect to the trap centre for $\gamma = 3.95$ and different temperatures. For comparison the Luttinger-liquid results for the homogeneous case, Eq. (5.53), are also shown with K and ρ taken at the trap centre and for $T = 0$. (The change of K and ρ with T has little effect and is ignored in the comparison). One recognizes two things: First of all the transition from an exponential to a power-law decay happens around $k_B T = 0.1\hbar\omega$ for which $L_T \approx 30l$. Secondly the correlations are rather well described by the homogeneous solution (5.53). A similar observation can be made at $T = 0$. Fig. 5.12 shows the DMRG results for $g_1(x,-x)$ for different

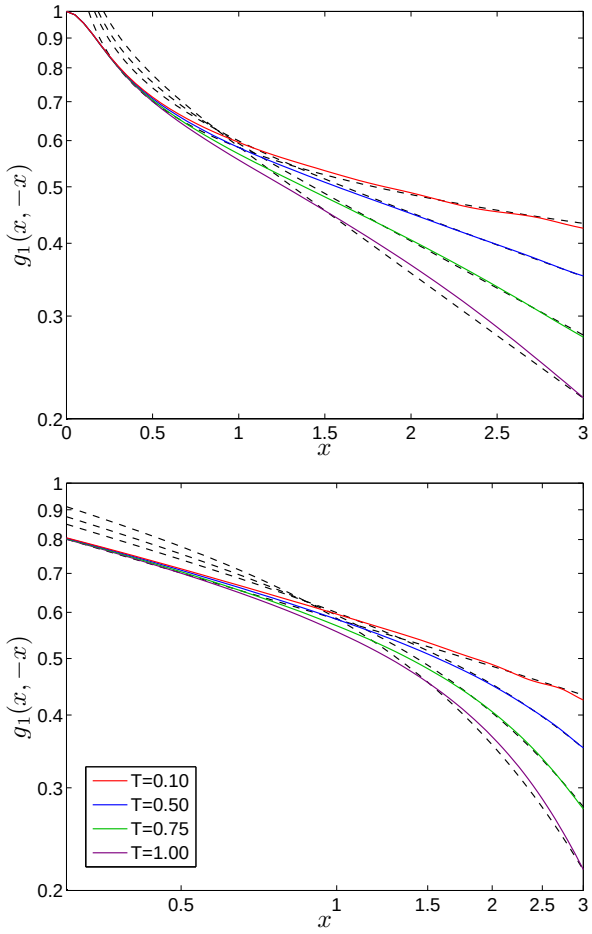

Figure 5.11: First order correlations in the temperature regime between exponential and algebraic decay. *top:* semi-logarithmic plot, *bottom:* double-logarithmic. Solid curves are DMRG calculations in the trap, dashed lines are Luttinger liquid predictions for a homogeneous gas with γ taken at the trap centre. Transition from thermal (exponential decay) to quantum dominated correlations (algebraic decay) at $T \ll \omega$ is apparent. The parameters are: $\gamma = 3.95$, $N = 12$.

interaction strength. The straight lines show the Luttinger liquid predictions for the homogeneous case. Again a rather good agreement is found for $x \leq 3l$. The agreement is less surprising when considering Fig. 5.9. The local Tonks parameter $\gamma(x)$ and thus the local Luttinger parameter $K(x)$ as obtained from (5.54) with $\gamma \to \gamma(x)$ are almost constant within this distance range. Furthermore replacing ρ in the denominator of Eq. (5.53) by $\rho(x)$ and expanding in a power series one finds

$$g_1(x,-x) \sim \left(1 - \frac{1}{4K}\frac{\rho''(x)}{\rho(x)}x^2 + \cdots\right)\left(2x\right)^{-1/2K}. \tag{5.55}$$

Even in the Tonks limit where $K \to 1$ the corrections are small for positions sufficiently far away from the edges of the density distribution.

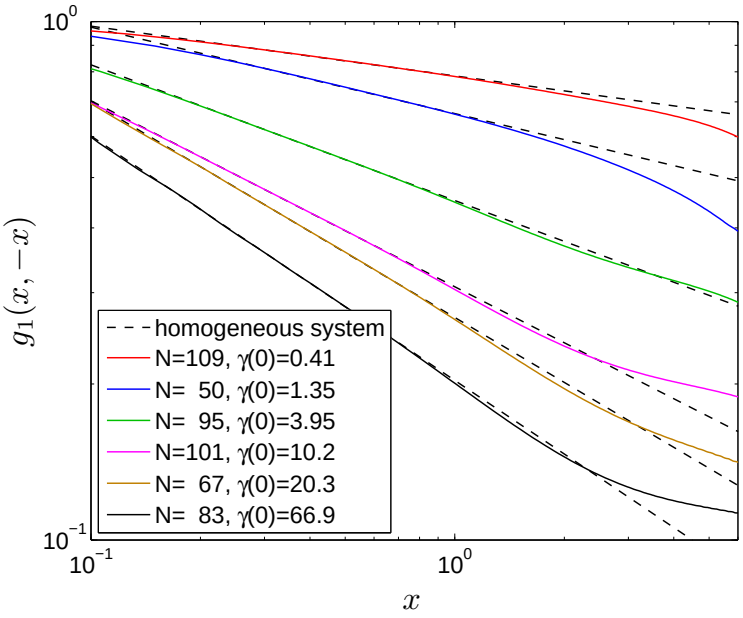

Figure 5.12: Logarithmic plot of first-order correlations for $T = 0$ and various interaction strengths. The dashed lines show power-law prediction from the Luttinger liquid approach with a Luttinger parameter determined by the density at the trap centre.

5.5 Conclusion

In this chapter the stochastic simulation and the DMRG method described in Section 3.1 and 3.2 has been applied to calculate a variety of properties of the one-dimensional Bose-gas in a trap with a local interaction. Since the methods are designed for lattice models, the model of the Bose-gas was discretized, which led to a Bose-Hubbard model with parameters depending on the discretization. The relationship between the continuous and discretized system was examined in detail and conditions on the discretization grid were derived.

The stochastic simulation allowed to calculate the density distribution and first-order correlations in a harmonic trap at temperatures around $\hbar\omega$. The precision of the simulation is rather limited as can be seen by the relative coarse discretization and the visible block artefacts. Nevertheless a quite good agreement with the analytic results from the homogeneous solutions was found and the transition from an exponential to an algebraic decay of first order correlations at low temperature became visible.

For zero temperature calculations as well as for temperatures below $\hbar\omega$ the DMRG method was used which allowed for a much finer discretization than the stochastic simulation. The DMRG allowed to calculate local properties as well

as correlations of a 1D Bose gas in a trapping potential for temperatures up to the oscillator frequency. For local quantities such as the density or the local three-body correlation there was excellent agreement with the predictions from the Lieb-Liniger and Yang-Yang theories with local density approximation. Deviations from LDA were found only in the immediate vicinity of the edges of the gas or for smaller particle numbers where finite size effects come into play. The good agreement with analytic results proved also that the DMRG can be applied successfully to inhomogeneous systems.

Remarkably, first-order correlations for positions away from the edges are well described by the homogeneous theory with parameters taken at the trap centre. In particular the transition from a thermal dominated regime of exponential decay to a power law decay of correlations could be observed, with exponents as predicted by the Luttinger liquid approach in the homogeneous case.

Chapter 6

1D Fermi gas with p-wave interaction in the trap

The purpose of this chapter is to develop and use various numerical methods to calculate properties of interacting spin-polarized fermions. The first part of the chapter will show that the p-wave interaction of this kind of fermions can be modelled by a pseudopotential and that the resulting equations can be mapped to equations of s-wave scattering bosons. This mapping of interacting fermions onto interacting bosons makes numerical methods for bosons also available for fermions.

The second part of this chapter will therefore deal with the question how properties of the fermions can be obtained from bosonic numerical calculations. The well known possibility of mapping non-interacting fermions via a Jordan-Wigner transformation onto hard-core bosons is a special case of this procedure. The general case of arbitrary interaction strength is more involved and needs a careful treatment.

For numerical calculations it is often necessary to discretize the Hamiltonian of a system. Therefore, in the third part of this chapter, the correct discretization of a p-wave interacting fermion gas is derived. It is shown that the resulting Hamiltonian is equivalent to that of hard-core bosons in a lattice with nearest neighbour interaction which is also equivalent to the XXZ model. It is analysed how the parameters of the discretized system must be chosen in order to keep the discretization error as low as possible. A further section analyses the case of infinitely strong interacting fermions, which correspond to non-interacting bosons. Finally, all the different methods are used to calculate density and momentum distributions of fermions in a harmonic trap.

6.1 Polarized fermions with p-wave interaction

Polarized fermions cannot interact by s-wave scattering, because this is forbidden by the Pauli-principle. Thus, the lowest possible scattering channel is p-wave scattering [41]. Like for the s-wave scattering, pseudopotentials can be found to model this interaction [42] . In one dimension the fermion pseudopotential is

$$\hat{V}_F = -2g^F_{1\mathrm{D}}\delta'(x_1 - x_2)(\partial_{x_1} - \partial_{x_2})|_{x_1=x_2+} \tag{6.1}$$

which can also be written in the symmetric form

$$\hat{V}_F = g^F_{1\mathrm{D}}\left(\overleftarrow{\partial}_{x_1} - \overleftarrow{\partial}_{x_2}\right)\delta(x_1 - x_2)\left(\overrightarrow{\partial}_{x_1} - \overrightarrow{\partial}_{x_2}\right)\Big|_{x_1=x_2+} \tag{6.2}$$

where the arrows denote the direction in which the derivation operators act (See [43, 44]). The derivatives here are regularized derivatives which means that the limit $x_1 \to x_2$ is taken after the derivative. This avoids that the derivatives produce a delta-function. The effective interaction constant $g^F_{1\mathrm{D}}$ is related to the p-wave scattering volume V_p and the radial trap frequency $\omega_\perp$ by

$$g^F_{1\mathrm{D}} = 6V_p\omega_\perp\left(1 + \eta V_p\omega_\perp^{3/2}\right)^{-1} \tag{6.3}$$

with $\eta \approx 2.4946\ldots$. The p-wave scattering volume V_p is the natural generalization of the scattering length to p-wave collisions.

6.2 Boson-fermion mapping

When the interaction strength of bosons in one dimension is increased one notices that the bosons show some properties of fermions. This is not so surprising, because strong interaction prevents the bosons to sit at the same place, which is much like the Pauli-principle for fermions. However, this effect is only seen for local properties and in 1D where one particle is like a hard wall for another particle, which is not the case in higher dimensions. It is widely known that bosons in 1D with infinite δ-interaction, so called hard-core bosons, can be mapped one-to-one onto free fermions using the Wigner-Jordan transformation. A not so well known fact is that even bosons with a finite δ-interaction can be mapped onto fermions with a specific local p-wave interaction pseudopotential of the form (6.1). From the hard-core boson case one would expect that the interaction strengths of the bosons and fermions somehow have an inverse relation, leading to zero interaction for the fermions when the bosons interact infinitely strong and vice versa. To derive the

relationship between the bosonic and fermionic interaction constant it is sufficient to review the theory of the two-particle problem . The following discussion in this section will be very close to the formulation in [43]. In the next section the same procedure is then repeated for the discretized system.

For the two particle problem the Hamiltonian in the relative coordinate $x = x_1 - x_2$ reads

$$\hat{H} = \left(-\partial_x^2 + \hat{V}\right) \tag{6.4}$$

where $\hat{V}$ is some pseudopotential representing the interaction of the particles. This pseudopotential will be some point-interaction, thus a discontinuity in $\phi(x)$ of some kind is to be expected at $x = 0$. The second derivative in Eq. (6.4) will then produce in general a delta-function and a derivative of a delta-function:

$$\partial_x^2\phi(x) = \phi''(x \neq 0) + [\phi'(0+) - \phi'(0-)]\,\delta(x) + [\phi(0+) - \phi(0-)]\,\delta'(x). \tag{6.5}$$

Thus, the derivative discontinuity can be chosen to cancel a zero-range even-wave interaction proportional to $\delta(x)$ in the bosonic case. In that case $[\phi(0+) - \phi(0-)] = 0$. In the fermionic case one has $[\phi'(0+) - \phi'(0-)]$=0 and it can cancel an odd-wave pseudopotential proportional to $\delta'(x)$. However, the discontinuities in ϕ can lead to undefined products of delta-function, unless some regularizing operators are included. Let the operators $\hat{\delta}_\pm$ and $\hat{\partial}_\pm$ be defined by

$$\hat{\delta}_\pm\phi(x) = \frac{1}{2}\,[\phi(0+) + \phi(0-)]\,\delta(x), \tag{6.6}$$

$$\hat{\partial}_\pm\phi(x) = \frac{1}{2}\,[\phi'(0+) + \phi'(0-)]\,. \tag{6.7}$$

The bosonic and fermionic pseudopotential operators corresponding to s- and p-wave scattering respectively are:

$$\hat{V}_B = g_{1\mathrm{D}}^B\hat{\delta}_\pm, \tag{6.8}$$

$$\hat{V}_F = -\,4g_{1\mathrm{D}}^F\delta'(x)\hat{\partial}_\pm. \tag{6.9}$$

The factor 4 in front of the fermionic pseudopotential is chosen to absorb the two factors of 1/2 coming from the derivative in relative coordinates. The minus sign is chosen such that the interactions are repulsive if $g_{1\mathrm{D}}^B$ and $g_{1\mathrm{D}}^F$ are positive and attractive otherwise. Furthermore

$$\partial_x \equiv \frac{1}{2}\,(\partial_{x_1} - \partial_{x_2})\,. \tag{6.10}$$

Solving the stationary Schrödinger equation for Hamiltonian (6.4) in the bosonic case requires

$$\phi'_B(0+) - \phi'_B(0-) = g^B_{1\mathrm{D}} \frac{1}{2} \left[\phi_B(0+) + \phi_B(0-)\right] \tag{6.11}$$

and solving it in the fermionic case requires

$$\phi_F(0+) - \phi_F(0-) = -4g^F_{1\mathrm{D}} \frac{1}{2} \left[\phi'_F(0+) + \phi'_F(0-)\right] \tag{6.12}$$

Eq. (6.11) and (6.12) are like boundary conditions for $\phi(x)$. In the following they will however be called contact conditions to distinguish them from the actual physical boundary conditions. One can easily see that Eq. (6.11) and (6.12) are equivalent if

$$\phi_F(x) = \frac{x}{|x|} \phi_B(x) \tag{6.13}$$

and

$$g^F_{1\mathrm{D}} = -1/g^B_{1\mathrm{D}}. \tag{6.14}$$

Indeed the relation between the interaction constants turns out to be inverse. Additionally there is a sign change in the interaction, showing that the repulsive bosons are mapped onto attractive fermions. One easily sees that the limit $g^B_{1\mathrm{D}} \to \infty$ of infinitely strong interacting bosons is equivalent to free fermions. This is the so-called hard-core boson or bosonic Tonks-Girardeau case. In the opposite limit of $g^F_{1\mathrm{D}} \to \infty$ one finds that the infinitely strong interacting Fermi gas is equivalent to a free bosonic gas. Such a gas is called a fermionic Tonks-Girardeau gas.

The validity of the mapping was proven by showing that the wavefunctions which solve the Schrödinger equation are essentially the same. The two particle case can easily be extended to more particles. From now on let

$$x = (x_1, x_2, \ldots, x_N) \tag{6.15}$$

be an N-particle configuration. Configurations where at least two particles are at the same position play an important role in this mapping. Therefore let the set of those configurations be

$$C = \{x \in \mathbb{R}^N : \text{ there exists } i, j, \quad i \neq j \text{ with } x_i = x_j\}. \tag{6.16}$$

The mapping for an arbitrary number N of particles in terms of the wavefunctions between the bosons and fermions in first quantization is then

$$\phi_F(x_1, x_2, \ldots, x_N) = \begin{cases} \prod_{i<j} \frac{x_j - x_i}{|x_j - x_i|} \phi_B(x_1, x_2, \ldots, x_N) & \text{if } x \notin C \\ 0 & \text{if } x \in C. \end{cases} \tag{6.17}$$

This mapping looks almost the same as the known Jordan-Wigner transformation between fermions and hard-core bosons. However, there is one important difference which was not mentioned before. For hard-core bosons the wavefunction is zero for $x \in C$, which is also true for the fermionic wavefunction. Thus, no special care must be taken here. The soft-core case , however, is different. The wavefunction is not zero where two particles are at the same position. It must therefore be explicitly stated, what the mapping does when two particles are at the same position. The fermionic wavefunction has to be 0 in C by definition. Thus, the mapping must set the value of the wavefunction to zero for $x \in C$, while the rest of the wavefunction is only Jordan-Wigner transformed and stays otherwise unaltered to fulfil the necessary differential equations and contact conditions. It should be noted, that there is no conflict with the contact conditions, which are enforced on the wavefunction to be compatible with the local interaction. The contact conditions actually make statements about the wavefunction when one is approaching C, not about the wavefunction directly in C. While the bosonic wavefunction for a delta-interacting gas has the property

$$g^B_{1\mathrm{D}} \phi_B|_{x_{j+1}=x_j} = \left(\frac{\partial}{\partial x_{j+1}} - \frac{\partial}{\partial x_j} \right) \phi_B \Big|_{x_{j+1}=x_j} \tag{6.18}$$

the fermionic wavefunction fulfils

$$\phi_F|_{x_{j+1}=x_j} = -g^F_{1\mathrm{D}} \left(\frac{\partial}{\partial x_{j+1}} - \frac{\partial}{\partial x_j} \right) \phi_F \Big|_{x_{j+1}=x_j} \tag{6.19}$$

with the relation (6.14). That follows from Eq. (6.17) and is also the correct contact condition for replacing the fermionic interaction term (6.1). At this point some questions which naturally arise here should be clarified.

The first question is: How can the value of the wavefunction on C be important when C is of (N-dimensional) measure zero? Even though C is of measure zero, the wavefunction is multiplied by delta-functions, when one wants to calculate expectations values of local multi-particle processes. For example the local two

particle correlation function is

$$g_2 \propto \int \phi_B^*(x)\delta(x_1 - x_2)\phi_B^*(x)dx^N = \int dx_2 dx_3 \dots dx_N |\phi(x_2, x_2, x_3, x_4, \dots, x_N)|^2. \quad (6.20)$$

As one sees, the integral on the right is an integral over the $N-1$ dimensional set C, which is in general not zero.

The second question is: How can this mapping be invertible? At first glance it seems, that the information about the bosonic local correlation functions is lost by the mapping to fermions. This is however not true. The value of the wavefunction can always be reconstructed at the point where two particles are at the same position by the condition that the bosonic wavefunction has to be continuous.

6.3 Simulation of p-wave interacting fermions by mapping to bosons

Although in first quantization the details of the mapping seem straight forward, they help to understand how the mapping is done in second quantization. For that it is helpful to examine what happens if the soft-core bosons are mapped to fermions and from the fermions to hard-core bosons via the Jordan-Wigner-transformation.

$$\phi_B \xrightarrow{\text{Bose-Fermi mapping}} \phi_F \xrightarrow{\text{Jordan-Wigner}} \phi_{\text{HC}} \quad (6.21)$$

The result is that the wavefunction of the hard-core bosons is the same as the one for the soft-core bosons, except that the hard-core boson wavefunction is zero when two particles are at the same position:

$$\phi_{\text{HC}}(x) = \begin{cases} \phi_B(x) & \text{if } x \notin C \\ 0 & \text{if } x \in C \end{cases} \quad (6.22)$$

Removing discontinuities of the hard-core boson wavefunction would reconstruct the soft-core boson wavefunction, because the discontinuities are only on C on which the wavefunction can always be extended in a continuous way. Representing the wavefunction via second quantization leads to

$$\phi_B(x_1, x_2, \dots, x_N) = \frac{1}{\sqrt{N!}} \langle 0|\hat{\Psi}^B(x_1)\hat{\Psi}^B(x_2)\dots\hat{\Psi}^B(x_N)|\phi\rangle. \quad (6.23)$$

The wavefunction for the hard-core bosons is the same as that of the original bosons, as long as two particles are not at the same position. This leads to

$$\langle 0|\hat{\Psi}^B(x_1)\hat{\Psi}^B(x_2)\dots\hat{\Psi}^B(x_N)|\phi_B\rangle = \langle 0|\hat{\Psi}^{\mathrm{HC}}(x_1)\hat{\Psi}^{\mathrm{HC}}(x_2)\dots\hat{\Psi}^{\mathrm{HC}}(x_N)|\phi_{\mathrm{HC}}\rangle \quad (6.24)$$

if $x \notin C$. For the expectation value of a hard-core boson operator A one finds

$$\begin{aligned}
\langle\phi_{\mathrm{HC}}|\hat{P}\hat{A}\hat{P}|\phi_{\mathrm{HC}}\rangle &= \int_{\mathbb{R}} dx^N \phi^*_{\mathrm{HC}}(x)A(x)\phi_{\mathrm{HC}}(x)dx^N && (6.25)\\
&= \int_{\mathbb{R}/C} dx^N \phi^*_{\mathrm{B}}(x)A(x)\phi_{\mathrm{B}}(x) && (6.26)\\
&= \frac{1}{N!}\int_{\mathbb{R}/C} dx^N \langle\phi_B|\Psi^\dagger_B(x_1)\dots\Psi^\dagger_B(x_N)|0\rangle A(x)\langle 0|\Psi_B(x_1)\dots\Psi_B(x_N)|\phi_B\rangle && (6.27)\\
&= \langle\phi_B|\int_{\mathbb{R}/C} dx^N \frac{1}{N!}\Psi^\dagger_B(x_1)\dots\Psi^\dagger_B(x_N)|0\rangle A(x)\langle 0|\Psi_B(x_1)\dots\Psi_B(x_N)|\phi_B\rangle && (6.28)\\
&= \langle\phi_B|\int_{\mathbb{R}} dx^N \hat{P}\frac{1}{N!}\Psi^\dagger_B(x_1)\dots\Psi^\dagger_B(x_N)|0\rangle A(x)\langle 0|\Psi_B(x_1)\dots\Psi_B(x_N)\hat{P}|\phi_B\rangle && (6.29)\\
&= \langle\phi_B|\hat{P}\hat{A}\hat{P}|\phi_B\rangle && (6.30)
\end{aligned}$$

where

$$\hat{A} = \int_{\mathbb{R}} dx^N \frac{1}{N!}\Psi^\dagger_B(x_1)\dots\Psi^\dagger_B(x_N)|0\rangle A(x)\langle 0|\Psi_B(x_1)\dots\Psi_B(x_N) \quad (6.31)$$

and $\hat{P}$ projects onto states which do not have more than one particle on each position in space. In first quantization the operation of $\hat{P}$ is simply that of Eq. (6.22). Thus, the final overall procedure for calculating fermion expectation values in second quantization would be to transform the fermionic operators via Jordan-Wigner-transformation and take the expectation value with the projected boson state. The boson state has of course to be determined in the full Hilbert-space from the soft-core Hamiltonian, even if finally only the hard-core boson part is needed. Starting from the fermions and calculate boson expectation values is equally easy, as long as one does not want to calculate expectation values from local multi-particle terms. In that case one has first to calculate the non-local expectation

values and take the limit, i.e.

$$\langle\phi_B|\hat{\Psi}_B^\dagger(x)\hat{\Psi}_B^\dagger(x)\hat{\Psi}_B(x)\hat{\Psi}_B(x)|\phi_B\rangle = \lim_{\varepsilon\to 0}\langle\phi_{\mathrm{HC}}|\hat{\Psi}_{\mathrm{HC}}^\dagger(x+\varepsilon)\hat{\Psi}_{\mathrm{HC}}^\dagger(x)\hat{\Psi}_{\mathrm{HC}}(x)\hat{\Psi}_{HC}(x+\varepsilon)|\phi_{\mathrm{HC}}\rangle \quad (6.32)$$

Note, that in second-quantization the fermionic state $|\phi_F\rangle$ is identical to the hard-core boson state $|\phi_{\mathrm{HC}}\rangle$, although the wavefunctions are different.

To use hard-core bosons and Jordan-Wigner transformation, actually discretized Hamiltonians must be used. One effect of the discretization is that the state after it has been projected into the hard-core boson subspace it is not normalized anymore. In the continuous limit this is not the case because C is a set of measure zero. Numerical calculations show however, that the discretization error in the norm of the projected state can be extremely large, even when the state, except for the normalization, approximates the continuum limit very well. This effect can be understood by noticing that the discretized equivalent to C

$$\bar{C} = \{z \in \mathbb{Z}_M^N : \text{ there exists } i,j, \quad i \neq j \text{ with } z_i = z_j\}. \quad (6.33)$$

is still quite a large set (M is the number of grid points used to discretize space). In the discretized case the hard-core boson subspace is isomorph to $\mathbb{Z}_M^N \backslash \bar{C}$ which has

$$\frac{M!}{(M-N)!} \quad (6.34)$$

elements. The number of elements of $\mathbb{Z}_M^N$ is M^N which is the number of all possible particle configurations of the particles. In the continuum limit, i.e. $M \to \infty$ the ratio of the number of elements of $\mathbb{Z}_M^N \backslash \bar{C}$ and $\mathbb{Z}_M^N$ should go to 1. This is indeed true, but it turns out to be going very slowly against 1. An estimate can be made by using Stirling's formula for the factorials and one finds that

$$\frac{M!}{M^N(M-N)!} \approx e^{-\frac{N^2}{2M}} \quad (6.35)$$

for large N and M, and M much larger than N. Thus, to have the norm of the hard-core boson part of the state close to 1, M must be much larger than the *square* of N. In numerical calculations it is often impossible to have such a fine discretization. Also it is not necessary, because the discretization needs only two be much smaller than the wavelengths contained in the wavefunction to give

correct results. The normalization loss can be compensated by normalizing the the projected state.

6.4 Numerical simulation of p-wave interacting fermions by direct discretization

In the previous section it was discussed how p-wave interacting fermions can be simulated by mapping to bosons. In this section an alternative method is derived based on a direct discretization of the p-wave interaction (6.1). It will be shown that the discretized Hamiltonian describes hard-core bosons with nearest neighbour interaction. The major part of the discussion will be restricted to the discretized two particle wavefunction in relative coordinates

$$\phi_j = \phi(j\Delta x) \tag{6.36}$$

but everything can be easily translated to arbitrary particle numbers. As a first step the discretization of the derivatives is chosen. It is useful for the further theoretical and numerical treatment if the resulting discretized Hamiltonian contains only nearest neighbour and local terms. Thus, the choice for the discretized derivatives is

$$\bar{\partial}\phi_j = \frac{\phi_{j+1} - \phi_j}{\Delta x} \tag{6.37}$$

$$\bar{\partial}^2\phi_j = \frac{\phi_{j+1} + \phi_{j-1} - 2\phi_j}{\Delta x^2}, \tag{6.38}$$

where $\bar{\partial}$ and $\bar{\partial}^2$ now indicate the discretized first and second derivative respectively. Next, it must be declared how a possible discontinuity around $j = 0$ of the discretized wavefunction is modelled. The assumption here will be that only at the points $j = +1, 0, -1$ the discretized second derivative can produce terms which scale like Δx^{-1} or Δx^{-2}. It is necessary to make this assumption for at least three grid-points because the $\bar{\partial}^2$ extends over three grid-points. The discretized analogon to Eq. (6.5) is found to be

$$\begin{aligned}\bar{\partial}^2\phi_j = \bar{\partial}^2\phi_{j\neq+1,0,-1} + (\delta_{j,-1} + \delta_{j,+1})\,\frac{1}{2}\left[\bar{\partial}^2\phi_1 + \bar{\partial}^2\phi_{-1}\right] \\ + \delta_{j,0}\left[\frac{\bar{\partial}\phi_0 - \bar{\partial}\phi_{-1}}{\Delta x}\right] + (\delta_{j,-1} - \delta_{j,1})\frac{1}{2}\left[\frac{\phi_1 - \phi_{-1}}{\Delta x^2} - \frac{\bar{\partial}\phi_1 + \bar{\partial}\phi_{-2}}{\Delta x}\right].\end{aligned} \tag{6.39}$$

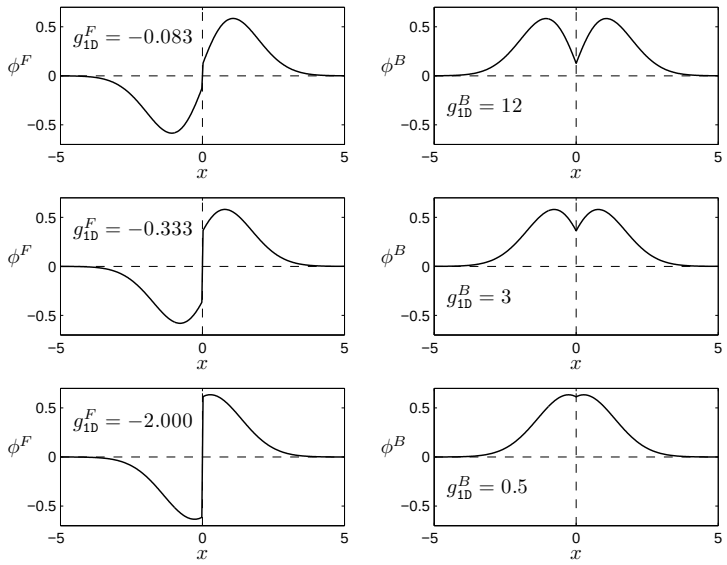

Figure 6.1: Examples of fermionic (left hand side) and bosonic (right hand side) wavefunctions in the two particle case. The results are obtained by numerical diagonalization of the discretized Hamiltonians. A harmonic trapping potential $V(x_1, x_2) = x_1^2 + x_2^2$ was used as in [42]. In [42] a small square well interaction potential was used to obtain the wavefunctions. The agreement with that method shows that the discretization is correct.

For bosons and fermions ϕ_j is either symmetric or antisymmetric and one finds

$$\bar{\partial}^2 \phi^B_j = \bar{\partial}^2 \phi^B_{j\neq 0} + \delta_{j,0} \left[\frac{\bar{\partial}\phi^B_0 - \bar{\partial}\phi^B_{-1}}{\Delta x} \right] \tag{6.40}$$

$$\bar{\partial}^2 \phi^F_j = \bar{\partial}^2 \phi^F_{j\neq +1,0,-1} + (\delta_{j,-1} - \delta_{j,1}) \frac{1}{2} \left[\frac{\phi^F_1 - \phi^F_{-1}}{\Delta x^2} - \frac{\bar{\partial}\phi^F_1 + \bar{\partial}\phi^F_{-2}}{\Delta x} \right]. \tag{6.41}$$

Thus, for the bosons it is possible to absorb pseudopotentials proportional to $\delta_{j,0}$ and for the fermions proportional to $\delta_{j,-1} - \delta_{j,1}$. It is easy to show that the only possible linear pseudopotential operators $\bar{V}^B$ and $\bar{V}^F$ are uniquely defined (up to a prefactor) by the following conditions: They have to be self-adjoint and $\bar{V}^B$ and $\bar{V}^F$ are zero when acting on anti-symmetric respectively symmetric wavefunctions. From this follows that the pseudopotential operators have the form:

$$\left(\bar{V}^B\right)_{j1,j2} = \alpha^B \delta_{j_1,0} \delta_{0,j_2} \tag{6.42}$$

$$\left(\bar{V}^F\right)_{j1,j2} = \frac{\alpha^F}{2} (\delta_{j_1,-1} - \delta_{j_1,1})(\delta_{-1,j_2} - \delta_{1,j_2}). \tag{6.43}$$

Note, that the self-adjointness forbids that any other component of the wavefunction than ϕ_1^F and ϕ_{-1}^F is involved in the fermionic pseudopotential. Thus, derivatives like $\bar{\partial}$ can not appear in the pseudopotential in contrast to the continuous system. Therefore, a remarkable property of the pseudopotentials of the discretized system is that only $\bar{V}^B$ is the direct analogue to its continuous version.

The prefactors α^B and α^F are now to be determined by demanding consistency between the continuous and discretized contact conditions. This means that discretized versions of Eq. (6.11) and (6.12) must be fulfilled. Eq. (6.11) and (6.12) can be simplified to

$$-2\partial_x\phi^B(0+) + g_{1\mathrm{D}}^B\phi(0+)^B = 0 \tag{6.44}$$

$$2g_{1\mathrm{D}}^F\partial_x\phi^F(0+) + \phi^F(0+) = 0 \tag{6.45}$$

by using the symmetry of the wavefunction. There are many different choices for discretizing those equations. The most obvious and simplest one is

$$-2\bar{\partial}\phi_0^B + g_{1\mathrm{D}}^B\phi_0^B = 0 \tag{6.46}$$

$$2g_{1\mathrm{D}}^F\bar{\partial}\phi_1^F + \phi_1^F = 0. \tag{6.47}$$

From (6.46) and (6.47) one can already derive that the expansion of α^B and α^F in Δx starts with

$$\alpha^B = \frac{1}{\Delta x}\left(g_{1\mathrm{D}}^B + \mathcal{O}(\Delta x)\right) \tag{6.48}$$

$$\alpha^F = -\frac{1}{\Delta x^2}\left(1 + \frac{\Delta x}{2g_{1\mathrm{D}}^F} + \mathcal{O}\left(\Delta x^2\right)\right). \tag{6.49}$$

It is interesting, that in the fermionic case the interaction constant $g_{1\mathrm{D}}^F$ does not appear in lowest order in Δx, but only in the next higher order. Obviously this order in Δx can not be neglected because the information about $g_{1\mathrm{D}}^F$ would get lost. In fact the purpose of the Δx^{-2} term is only to completely remove the term of the same order coming from the second derivative, thus Δx^{-1} becoming the lowest order term in the equation. In the next section it will be analysed how the higher orders in Δx^{-2} for α^B and α^F must be chosen to make the discretization error as small as possible.

Finally the results of this section can be generalized to arbitrary particle number. The second-quantized versions of the pseudopotential operators are found to

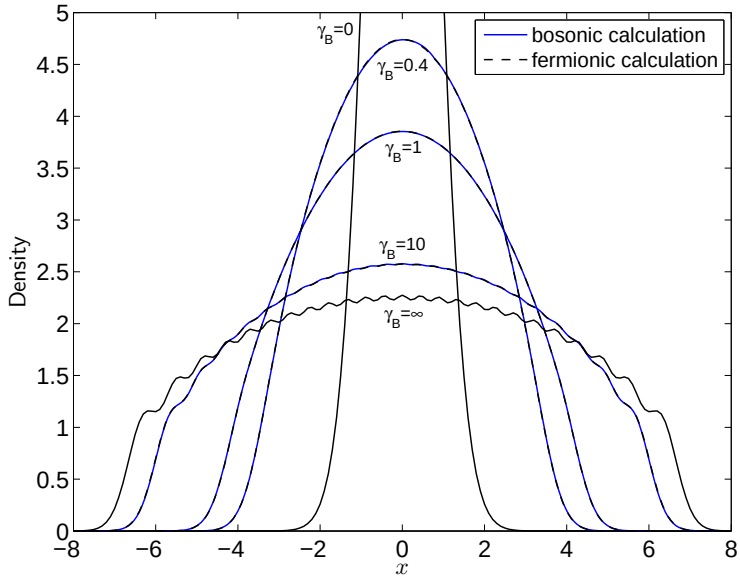

Figure 6.2: Density distribution of bosons and fermions in a harmonic trap using either Hamiltonian (6.52) (blue) or (6.53) (dashed black) for the numerical calculation. The particle number is 25. $\gamma_B = g^B_{1D}/\rho(0), g^F_{1D} = -1/g^B_{1D}$, where $\rho(0)$ is the density in the middle of the trap. Using an extrapolation $\Delta x \to 0$ for the fermions, which is necessary because of the larger discretization error, gives perfect agreement with the bosons. $\gamma_B = 0$ is the $g^B_{1D} \to 0$ limit at constant particle number. The $\gamma_B = \infty$ limit is easily obtained from the density distribution of non-interacting fermions.

be

$$\bar{V}^B = \frac{\alpha_B}{2} \sum_j \hat{a}_j^{\dagger 2} \hat{a}_j^{\dagger} \tag{6.50}$$

$$\bar{V}^F = \alpha_F \sum_j \hat{c}_j^{\dagger} \hat{c}_j \hat{c}_{j+1}^{\dagger} \hat{c}_{j+1} \tag{6.51}$$

Thus, the bosons can be modelled by the Bose-Hubbard model and the fermions by the spinless Fermi-Hubbard model with nearest neighbour interaction. Their discretized Hamiltonians are

$$\bar{H}^B = -J \sum_j \left(\hat{a}_j^{\dagger} \hat{a}_{j+1} + \hat{a}_{j+1}^{\dagger} \hat{a}_j \right) + \frac{\alpha^B}{2} \sum_j \hat{a}_j^{\dagger 2} \hat{a}_j^2 + D_j \hat{a}_j^{\dagger} \hat{a}_j \tag{6.52}$$

$$\bar{H}^F = -J \sum_j \left(\hat{c}_j^{\dagger} \hat{c}_{j+1} + \hat{c}_{j+1}^{\dagger} \hat{c}_j \right) + \alpha^F \sum_j \hat{c}_j^{\dagger} \hat{c}_j \hat{c}_{j+1}^{\dagger} \hat{c}_{j+1} + \sum_j D_j \hat{c}_j^{\dagger} \hat{c}_j \tag{6.53}$$

with

$$J = \frac{1}{2\Delta x^2}, \tag{6.54}$$

$$D_j = V_j + \frac{1}{\Delta x^2}, \tag{6.55}$$

where $V_j = V(j\Delta x)$ is for example the discretized potential of a trap. Fig. 6.2 shows density-distributions of fermions in a harmonic trap. The calculations where done with the discretized Hamiltonians (6.52) and (6.53) using the DMRG.

6.4.1 Optimization of the discretization error

For numerical calculations it is also important of which order in Δx the discretization error is. On the one hand the discretization error can in principle be made arbitrary small by choosing the appropriate discretization of the derivatives and the contact conditions. On the other hand, the choice is limited by demanding that the discretized Hamiltonian should contain only nearest neighbour couplings. The discretized Hamiltonians so far are

$$\bar{H}_B\phi_j^B = \begin{cases} \frac{-\phi_{j+1}^B - \phi_{j-1}^B + 2\phi_j^B}{\Delta x^2} & \text{if } j > 0 \\ \frac{-2\phi_1^B + 2\phi_0^B}{\Delta x^2} + \alpha^B\phi_0^B & \text{if } j = 0 \end{cases} \tag{6.56}$$

$$\bar{H}_F\phi_j^F = \begin{cases} \frac{-\phi_{j+1}^F - \phi_{j-1}^F + 2\phi_j^F}{\Delta x^2} & \text{if } j > 1 \\ \frac{-\phi_2^F + 2\phi_1^F}{\Delta x^2} + \alpha^F\phi_1^F & \text{if } j = 1 \end{cases} \tag{6.57}$$

where $\phi_{-j}^B = \phi_j^B$ and $\phi_{-j}^F = -\phi_j^F$. In order to determine the discretization error the discretized wavefunction must be expanded in a Taylor series, e.g.

$$\phi_{j+1} = \phi(x + \Delta x) = \sum_n \frac{\partial_x^n \phi(x) \Delta x^n}{n!}. \tag{6.58}$$

For α^B and α^F also an expansion of the form

$$\alpha^B(\Delta x) = \sum_{n=-1}^{\infty} \alpha_n^B \Delta x^n, \tag{6.59}$$

$$\frac{1}{\alpha^F(\Delta x)} = \sum_{n=2}^{\infty} \alpha_n^F \Delta x^n \tag{6.60}$$

is assumed. On the points $j > 0$ for the bosons and $j > 1$ for the fermions the discretized equation is

$$\frac{-\phi_{j+1} - \phi_{j-1} + 2\phi_j}{\Delta x^2} - E\phi_j = -\partial_x^2\phi(x) - E\phi(x) - \frac{\Delta x^2}{12}\partial_x^4\phi(x) + \mathcal{O}(\Delta x^4). \quad (6.61)$$

Thus, the discretization error which is made here is of $\mathcal{O}(\Delta x^2)$. This is the optimum which can be achieved with nearest neighbour coupling. Expanding now the equations for the points $j = 0$ (bosons) and $j = 1$ (fermions) one finds

$$\begin{aligned}(\bar{H}_B - E)\phi_0 = \frac{-2\phi_1^B + 2\phi_0^B}{\Delta x^2} + \alpha^B\phi_0^B - E\phi_0 = \\ \frac{1}{\Delta x}\Big[- 2\partial_x\phi^B(0+) + \alpha_{-1}^B\phi^B(0+)\Big] - \partial_x^2\phi(0+) - E\phi(0+) + \mathcal{O}(\Delta x),\end{aligned} \quad (6.62)$$

$$\begin{aligned}(\bar{H}_F - E)\phi_1 = \frac{-\phi_2^F + 2\phi_1^F}{\Delta x^2} + \alpha^F\phi_1^F - E\phi_1 = \\ \alpha^F\Big[(\alpha_2^F + 1)\phi(0+) + \Delta x[\alpha_3^F\phi(0+) + \partial_x\phi(0+)] + \mathcal{O}(\Delta x^2)\Big].\end{aligned} \quad (6.63)$$

It is now easy to see that the $\frac{1}{\Delta x}$ term in (6.62) becomes equal to (6.44) if $\alpha_{-1}^B = g_{1\mathrm{D}}^B$. The next term $-\partial_x^2\phi(0+) - E\phi(0+)$ vanishes. An important point is that the equivalent term in the multi-particle case also vanishes. Thus, the discretization error of the contact condition for the bosons is also of $\mathcal{O}(\Delta x^2)$ because the relative order of the $\mathcal{O}(\Delta x^{-1})$ and $\mathcal{O}(\Delta x^1)$ term is two. The case for the fermions is more complicated. α_F has to be pulled out such that the expansion becomes similar to the bosonic case. It is necessary that $\alpha_2^F = -1$ to remove the highest order term. To get the contact condition (6.45) in the $\mathcal{O}(\Delta x^1)$ term one needs to set $\alpha_3^F = 1/(2g_{1\mathrm{D}}^F)$. The discretization error of the fermionic contact condition remains of $\mathcal{O}(\Delta x^1)$. It cannot be improved to higher order because this would require the knowledge of higher derivatives of the wavefunction. The final result for α_F is thus

$$\alpha^F = -\frac{1}{\Delta x^2}\left(\frac{1}{1 - \frac{\Delta x}{2g_{1\mathrm{D}}^F}}\right). \quad (6.64)$$

It is also instructive to examine which point in the phase diagram of the lattice Hamiltonian (6.53) corresponds to the discretized system. If one maps the

fermionic system onto the spin-1/2 XXZ model then one finds for the anisotropy

$$\Delta = \frac{\alpha_F}{2J} = -\left(1 + \frac{\Delta x}{2g_{1\mathrm{D}}^F} + \mathcal{O}\left(\Delta x^2\right)\right) \tag{6.65}$$

which shows that the system is always near the transition regime between the XY-ferromagnetic and Ising-ferromagnetic phase. For negative $g_{1\mathrm{D}}^F$ one is always on the XY-ferromagnetic side.

6.5 Tonks-Girardeau fermions

Fermions with an infinitely strong interaction are called Tonks-Girardeau (TG) fermions. As Eq. (6.14) shows, fermions with an infinitely strong interaction $g_{1\mathrm{D}}^F = -\infty$ correspond to non-interacting bosons $g_{1\mathrm{D}}^B = 0$. Thus, it should be possible to derive properties of the TG-fermions from non-interacting bosons. In the following some results from [44, 45] are discussed for $g_{1\mathrm{D}}^F = -\infty$. In the second part fermions are considered, whose interaction is only close to infinity but not exactly infinity. Since this regime correspond to weakly interacting bosons, results from mean field-theory can be applied.

If the interaction of the fermions is infinite ($g_{1\mathrm{D}}^F = -\infty$) their wavefunction is simply

$$\phi_F(x_1, x_2, \ldots, x_N) = \sum_{i<j}^{N} \frac{x_i - x_j}{|x_i - x_j|} \phi_0(x_1)\phi_0(x_2)\ldots\phi_0(x_N) \tag{6.66}$$

where

$$\phi_0(x_j) = \frac{1}{\sqrt{\pi}} e^{-\frac{x^2}{2}} \tag{6.67}$$

is the single particle ground state of a boson in a harmonic trap. From this the first-order correlations of the fermions can be determined:

$$\begin{aligned}\langle \hat{\Psi}_F^\dagger(y')\hat{\Psi}_F(y)\rangle = N\phi_0^*(y')\phi_0(y) \int_{\mathbb{R}^{N-1}} \left(\prod_{i=2}^{N} \frac{y - x_i}{|y - x_i|}\frac{y' - x_i}{|y' - x_i|}\right) \\ \times \left(\prod_{1<j<k}^{k=N} \left(\frac{x_j - x_k}{|x_j - x_k|}\right)^2 \phi_0^*(x_k)\phi_0(x_k)\right) dx_2 dx_3 \ldots dx_N\end{aligned} \tag{6.68}$$

Noticing that $\left(\frac{x_j - x_k}{|x_j - x_k|}\right)^2 = 1$ in this expression, the multidimensional integrals can be separated into a product of $N-1$ integrals over each dx_j. The resulting first

order correlations in the limit $g_{1D}^F = -\infty$ reads

$$\langle \hat{\Psi}_F^\dagger(y')\hat{\Psi}_F(y)\rangle = \sqrt{\rho(y')}\sqrt{\rho(y)}\left[1 - \frac{2}{N}\left|\int_y^{y'} \rho(x)dx\right|\right]^{N-1} \tag{6.69}$$

where $\rho(x) = N|\phi_0(x)|^2$ is the density of the bosons. Thus, for the harmonic trap one finds

$$\langle \hat{\Psi}_F^\dagger(y')\hat{\Psi}_F(y)\rangle = \frac{N}{\sqrt{\pi}} e^{\frac{-y'^2-y^2}{2}} \left[1 - |\mathrm{erf}(y') - \mathrm{erf}(y)|\right]^{N-1} \tag{6.70}$$

where $\mathrm{erf}(x) = \frac{2}{\sqrt{\pi}} \int_0^x e^{-t^2} dt$.

So far it was assumed that g_{1D}^F is strictly infinite. In the following it will be assumed that g_{1D}^F is so large that the bosons with $g_{1D}^B = -1/g_{1D}^F$ in a harmonic potential can be described by the Gross-Pitaevskii (GP) equation

$$-\frac{\partial_x^2}{2}\psi(x) + \left(\frac{1}{2}x^2 - \mu\right)\psi(x) + g_{1D}^B|\psi(x)|^2\psi(x) = 0. \tag{6.71}$$

It is well known that this equation, under certain conditions, called the Thomas-Fermi (TF) limit, predicts a density distribution in the harmonic trap which has the form of a parabola which is very different from the density distribution of non-interacting bosons which has a Gaussian shape. The conditions under which the TF approximation holds will be analysed in the following and it will be shown that it is still possible to use this to derive properties of strongly interacting fermions. For analysing the shapes of the solutions predicted by the GP-equation it is instructive to introduce the rescaled functions

$$\tilde{\psi}(z) = \sqrt{\frac{g}{\mu}}\psi(z\sqrt{\mu}). \tag{6.72}$$

Then one finds

$$-\frac{\partial_z^2}{2}\tilde{\psi}(z) + \mu^2\left(\frac{1}{2}z^2 - 1\right)\tilde{\psi}(z) + |\tilde{\psi}(z)|^2\tilde{\psi}(z)] = 0, \tag{6.73}$$

thus g_{1D}^B drops completely from the equation. From that it can be concluded that the principal shape of the function $\psi(x)$ is not changed in the limit $g_{1D}^B \to 0$ and $\mu =$ constant. Furthermore one sees that if μ is large compared to the trap frequency the kinetic energy can be neglected which constitutes the Thomas-Fermi approximation. The other possible limit is taking $g_{1D}^B \to 0$ and keeping the particle number constant rather than the chemical potential. This limit however inevitable leads into the small μ regime. Then the Thomas Fermi-approximation breaks down

and $\psi(x)$ has the shape of a non-interacting bosonic gas, i.e. a Gaussian function in the trap. In the Thomas-Fermi approximation the equation can be easily solved for the density and one finds

$$\left|\tilde{\psi}_{\mathrm{TF}}(z)\right|^2 = 1 - \frac{z^2}{2}. \tag{6.74}$$

In the TF-approximation the kinetic energy is proportional to z and thus consistent with the assumption that he kinetic energy can be neglected if z is small. If $z \gtrsim \sqrt{2}$ the TF-density gets small and finally becomes negative, which shows that the TF approximation also breaks down at the edges of the particle cloud. In this area the density is actually very small, i.e. $|\tilde{\psi}(z)|^2 \ll 1$, so that the interaction term $|\tilde{\psi}(z)|^2\tilde{\psi}(z)$ can be neglected. Thus, in areas of low density the wavefunction in a trap can be described by parabolic cylinder functions, which are for large z proportional to $e^{-\frac{x^2}{2}}x^{-\mu}$. If the particle cloud becomes very narrow, that is when μ is small compared to the trap energy, the Gaussian shape of a non-interacting Bose-gas appears. Both cases are however well described by the GP-equation. For this equation to hold it is only necessary that the interaction is sufficiently weak such that higher correlations factorize approximatively , i.e.

$$\langle \hat{a}_i^\dagger \hat{a}_j^\dagger \hat{a}_k \hat{a}_l \rangle \approx \langle \hat{a}_i^\dagger \hat{a}_k \rangle \langle \hat{a}_j^\dagger \hat{a}_l \rangle \tag{6.75}$$

where $\langle\rangle$ denotes the ground state expectation value. From that follows also that first order correlations can be written as

$$\langle \hat{a}_i^\dagger \hat{a}_j \rangle \approx \sqrt{\langle \hat{a}_i^\dagger \hat{a}_i \rangle}\sqrt{\langle \hat{a}_j^\dagger \hat{a}_j \rangle}. \tag{6.76}$$

It is therefore possible to calculate the correlations from the density. If this result is inserted into the Jordan-Wigner transformation then the correlations of the fermionic gas in the continuum limit are obtained to be

$$\langle \hat{\Psi}_F^\dagger(y')\hat{\Psi}_F(y)\rangle = \sqrt{\rho(y')}\sqrt{\rho(y)}\exp\left(-2\left|\int_y^{y'}\rho(x)dx\right|\right) \tag{6.77}$$

where $\rho(x)$ is the density of the gas. Note that Eq. (6.69) and (6.77) are identical in the limit $N \to \infty$.

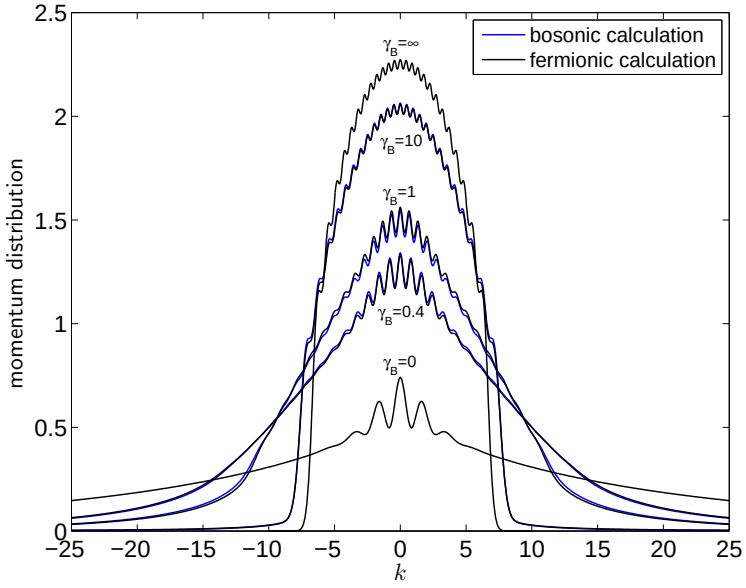

Figure 6.3: Momentum distribution of fermions in a harmonic trap using either Hamiltonian (6.52) (blue) or (6.53) (black) for the numerical calculation. The particle number is 25. $\gamma_B = g^B_{1D}/\rho(0), g^F_{1D} = -1/g^B_{1D}$, where $\rho(0)$ is the density in the middle of the trap. $\gamma_B = 0$ is the $g^B_{1D} \to 0$ limit of infinitely strong interacting fermions, where Eq. (6.70) together with (6.78) was used to calculate the momentum distribution . The $\gamma_B = \infty$ limit is easily obtained from the momentum distribution of non-interacting fermions.

6.6 Momentum distribution of p-wave interacting fermions in a harmonic trap

In the previous sections of this chapter it was demonstrated, that properties of p-wave interacting fermions can be calculated by either using s-wave interacting bosons or a proper discretization of the fermionic Hamiltonian. Using both methods to calculate the density made it possible to validate the equivalence of fermions and bosons if $g^F_{1D} = -1/g^B_{1D}$, because in that case, the density distribution of fermions and bosons is just the same. However, first order correlations of bosons and fermions are fundamentally different. A physical property which is directly related to the first order correlations in space is the momentum distribution. The momentum distribution is given by

$$\langle \hat{\Psi}(k)^\dagger \hat{\Psi}(k) \rangle = \frac{1}{2\pi} \int dx \int dy \langle \hat{\Psi}(x)^\dagger \hat{\Psi}(y) \rangle e^{ik(x-y)}, \tag{6.78}$$

where $\hat{\Psi}(x)$ is either the bosonic or fermionic field operator. Still, bosons can be used to calculate the fermionic momentum distribution, if the numerical method which is used allows to calculate the expectation value of the operators which one gets from the Jordan-Wigner transformation

$$\langle \hat{c}_i^\dagger \hat{c}_j \rangle = \left\langle \hat{P}\hat{b}_i^\dagger \prod_{l=i+1}^{j-1} \exp\left(i\pi \hat{b}_l^\dagger \hat{b}_l\right) \hat{b}_j \hat{P} \right\rangle \tag{6.79}$$

(assuming $i < j$). The expectation value on the right side of Eq. (6.79) is calculated with the state obtained from the calculation with the (soft-core) bosons. $\hat{P}$ projects onto states with not more than one particle at the same position. With DMRG methods the expectation value of the right side of Eq. (6.79) is easily calculated. After that the Fourier transformation given by Eq. (6.78) must be performed to get the momentum distribution of the fermions. The results are shown in Fig. 6.3 and compared to those obtained from a direct discretization as well. Also shown is the analytic expression (6.70) for the Fermi-Tonks gas ($\gamma_B = 0$, $g_{1D}^B \to 0$ or $g_{1D}^F \to -\infty$). One recognizes perfect agreement.

6.7 Summary

The present chapter discussed spin-polarized fermions with p-wave interaction in one dimension. Such fermions with an attractive interaction of strength g_{1D}^F are equivalent to s-wave interacting bosons with repulsive interaction strength $g_{1D}^B = -1/g_{1D}^F$. This offers the possibility to use bosonic numerical methods to calculate properties of the fermions. It was shown how fermionic expectation values can be calculated from a bosonic wave function. A further way of calculating fermionic properties was explored that uses a discretization of the fermionic Hamiltonian. The discretized fermionic Hamiltonian maps to a Hamiltonian describing hard-core bosons with attractive nearest neighbour interaction in a lattice which is also equivalent to the spin-1/2 XXZ model. The parameters of the discretized Hamiltonian were determined and the discretization error discussed. In the limit of infinite strong interaction the fermions correspond to weakly interacting bosons. Thus, non-interacting bosons and the Gross-Pitaevskii equation for weakly interacting bosons can be used to calculate properties of the fermions. Finally density and momentum distributions of the fermions in a harmonic trap were calculated using either the boson-fermion mapping or the direct discretization of the fermions. The results were compared and the agreement of the different methods verified.

Part III

Meta-stable particle pairs in periodic potentials

Chapter 7

Repulsively bound pairs of particles in lattices

Recently, Winkler *et al.* [46] have observed an interesting lattice effect: the binding of *repulsively* interacting bosons into close pairs which are dynamically stable in the absence of dissipation. Repulsively bound composite objects are a general phenomenon, appearing in various periodic systems possessing a band gap at the relevant "dissociation" energy. Electrons have been shown to pair, via Coulomb repulsion, in arrays of tunnel-coupled quantum dots [47]. Analogous effects have been predicted for strongly interacting mixtures of bosonic and fermionic atoms in an optical lattice [48], or photons forming gap solitons in non-linear photonic band-gap structures [49].

In this chapter a periodic potential loaded with even numbers of bosons at each site is studied, in the experimentally relevant regime [46] where on-site repulsion between particles exceeds the inter-site tunnelling rate. An effective Hamiltonian for repulsively bound particle pairs ("dimers") which exhibits occupation-dependent tunnelling and nearest-neighbour interactions is derived. One finds that the attractive interaction between the dimers always exceeds their kinetic energy thereby binding them into clusters with minimum surface area and uniform density, which represent incompressible "droplets" of a lattice liquid. When the system contains at most one dimer per site, the effective Hamiltonian takes the form of the extended Hubbard model, which can be mapped onto the well-known spin-$\frac{1}{2}$ XXZ model in a magnetic field, exhibiting a phase transition from a "droplet" to a "gas" phase at some critical temperature.

7.1 Monomer-dimer description of the Bose-Hubbard model

In the following it will be shown that it is in principle possible to distinguish between particle pairs (dimers) and unpaired particles (monomers) within the framework of the Bose-Hubbard-model. At first glance the Bose-Hubbard model gives no hint that some particles can be regarded as paired particles and some as unpaired ones. However, a very simple idea turns out to provide a consistent way of accomplishing this distinction: If there are n particles on a lattice site then the number of particle pairs is just the maximum number of pairs which can be formed of the particles. That means that at most one particle remains unpaired on a lattice site, exactly when the number of particles on the given lattice site is odd. So far this pairing is purely formal. In the following it is shown that this formal pairing also makes physically sense by mapping the Bose-Hubbard Hamiltonian exactly onto a Hamiltonian which describes he dimers and the monomers as two distinct particle species.

To understand how such a mapping works a single lattice site in the number state $|n\rangle$ is considered first. The action of the bosonic annihilation operator $\hat{a}$ on that state would be $\hat{a}|n\rangle = \sqrt{n}|n-1\rangle$. Formally one can introduce particle pairs by declaring the number of pairs to be $m = \left\lfloor \frac{n}{2} \right\rfloor$, where $\lfloor * \rfloor$ denotes rounding to the nearest smaller integer. The number of monomers is then given by $k = n \bmod 2$ which can either be 0 or 1. If a state which contains m dimers and k monomers is denoted by $|m,k\rangle$ a one-to-one mapping between the single particle number state and the dimer+monomer state is established, which can be written as

$$|n\rangle \leftrightarrow \left| \left\lfloor \frac{n}{2} \right\rfloor, n \bmod 2 \right\rangle . \tag{7.1}$$

With that mapping it is now easy to define creation and annihilation operators for the dimers and monomers. The action of the annihilation operator $\hat{b}$ on the state $|m,k\rangle$ is that it annihilates the monomer if it is present or is 0 if no monomer is residing on the lattice site. Remember that according to the definition there can be at most one monomer at a lattice site. This means the monomers are hard-core bosons with the property

$$\hat{b}|m,k\rangle = \begin{cases} 0 & \text{if } k = 0 \\ |m,0\rangle & \text{if } k = 1. \end{cases} \tag{7.2}$$

The annihilation operator for the dimers is a usual bosonic operator with the

property

$$\hat{d}|m,k\rangle = \sqrt{m}|m-1,k\rangle. \tag{7.3}$$

From that definitions it is clear that $\hat{b}$ and $\hat{d}$ commute. The number operators for the single, dimer and monomer particles are denoted by

$$\hat{n} = \hat{a}^\dagger\hat{a}, \quad \hat{m} = \hat{d}^\dagger\hat{d}, \quad \hat{k} = \hat{b}^\dagger\hat{b}. \tag{7.4}$$

The number operator of the monomers is a projector onto the states with odd particle number and has the property $\hat{k}^2 = \hat{k}$. The aim of the following is to express $\hat{a}$ solely by $\hat{b}$ and $\hat{d}$. For that it seems reasonable to divide $\hat{a}$ into a part acting on states with even number of particles and a part acting on states with odd number of particles. This can be achieved by writing

$$\hat{a} = \hat{a}\hat{k} + \hat{a}(1-\hat{k}) = \hat{a}\hat{k} + \hat{k}\hat{a} \tag{7.5}$$

One finds that

$$\hat{a}\hat{k} = \hat{b}\sqrt{\hat{n}} = \hat{b}\sqrt{2\hat{m}+\hat{k}} \tag{7.6}$$

and

$$\hat{k}\hat{a} = \hat{k}(\hat{a}^\dagger\hat{a})^{-1}\hat{a}^\dagger\hat{a}\hat{a} = \hat{k}(\hat{a}^\dagger\hat{a})^{-1/2}\hat{a}^\dagger(\hat{a}^\dagger\hat{a}+1)^{-1/2}\hat{a}^2 = \sqrt{2}\hat{b}^\dagger\hat{d} \tag{7.7}$$

where it was used that $\hat{k}(\hat{a}^\dagger\hat{a})^{-1}\hat{a}^\dagger = \hat{k}\hat{b}^\dagger = \hat{b}^\dagger(1-\hat{k}) = \hat{b}^\dagger$ and $(1-\hat{k})(2(\hat{a}^\dagger\hat{a}+1))^{-1/2}a^2 = (1-\hat{k})\hat{d}$. The inverse of $\hat{a}^\dagger\hat{a}$ poses no problems for zero particles because the operator $\hat{k}$ projects onto states with odd number of particles. The inverse can be understood as if taken in the subspace of odd particle-number-states. $\hat{a}$ expressed by $\hat{b}$ and $\hat{d}$ is then found to be

$$\hat{a} = b\sqrt{2\hat{m}+\hat{k}} + \sqrt{2}\hat{b}^\dagger\hat{d}. \tag{7.8}$$

If (7.8) is inserted into the Bose-Hubbard Hamiltonian (2.74) a new two species

Hamiltonian is found:

$$\hat{H} = -J \sum_{\langle i,j \rangle} \Big(\sqrt{2\hat{m}_i + 1}\hat{b}_i^\dagger \hat{b}_j \sqrt{2\hat{m}_j + 1} \tag{7.9a}$$

$$+ \sqrt{2\hat{m}_i + 1}\hat{b}_i^\dagger b_j^\dagger \hat{d}_j \sqrt{2} + \sqrt{2}\hat{d}_j^\dagger \hat{b}_j \hat{b}_i \sqrt{2\hat{m}_i + 1} \tag{7.9b}$$

$$+ 2\hat{d}_i^\dagger \hat{b}_i \hat{b}_j^\dagger \hat{d}_j \Big) \tag{7.9c}$$

$$+ \frac{U}{2} \sum_i \Big(2\hat{m}_i(2\hat{m}_i - 1) + 4\hat{m}_i \hat{k}_i \Big) \tag{7.9d}$$

$$+ \sum_i \varepsilon_i \Big(\hat{m}_i + \frac{1}{2}\hat{k}_i \Big) \tag{7.9e}$$

The term (7.9a) describes monomer hopping, (7.9b) creation (destruction) of a dimer from (to) two monomers, (7.9c) describes tunnelling of dimers mediated by monomers and(7.9d) contains the interaction of the dimers and monomers. ε_i is an additional potential ($\varepsilon_i = 2D_i$ in (2.74)).

7.2 Effective single-particle dynamics of dimers

In this section a periodic potential loaded with even numbers of bosons at each site is studied, which is in the experimentally relevant regime [46] where on-site repulsion between particles exceeds the inter-site tunnelling rate.

Considering two particles in a periodic potential, according to Eq. (2.74), the state $|2_j\rangle$ with two particles localized at the same site has an energy offset U from the state $|1_j\rangle |1_i\rangle$ with $i \neq j$. The transition between states $|1_j\rangle |1_i\rangle$ and $|2_j\rangle$ is therefore non-resonant and is suppressed when $U \gg J$. If initially the particles occupy different sites, each particle can tunnel freely from site to site, until it encounters the other particle at a neighbouring site. At this point the two particles undergo elastic scattering and separate again, since the maximal kinetic energy $4dJ$ of the two particles is below the potential barrier U associated with two particles occupying the same site. Note that, in second-order in the small parameter J/U, an adiabatic elimination of the non-resonant states $|2_j\rangle$ and $|2_i\rangle$ yields an effective energy shift of state $|1_j\rangle |1_i\rangle$ with two particles at the adjacent sites $\langle j, i\rangle$, given by $-4J^2/U$. This effective attraction between a pair of particles at the neighbouring sites is, however, small compared to the single-particle tunnelling rate J, and therefore can not bind the particles together. Conversely, if the system is initially prepared in state $|2_j\rangle$, then in order for the two particles to separate ($|2_j\rangle \rightarrow |1_j\rangle |1_i\rangle$) via the last term of Eq. (2.74), energy of the order of U would

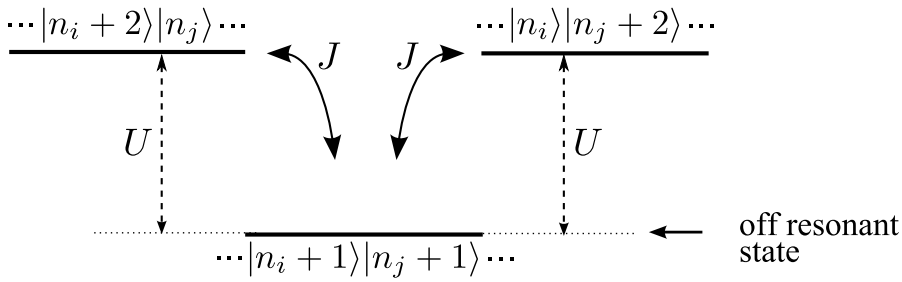

Figure 7.1: Energy level diagram and tunnel couplings employed in the adiabatic elimination of nonresonant states with odd occupation numbers. $\cdots|n_i\rangle|n_j\rangle\cdots$ denotes a state with $n_i = 2m_i$ bosons at site i and $n_j = 2m_j$ bosons at site $j = i + 1$.

have to be discarded. In the absence of dissipation, this is not possible, so the two particles are repulsively bound as a dimer [46].

An important aspect of the problem is the dimer mobility. Although the first-order transition $|2_j\rangle \to |1_j\rangle\,|1_i\rangle$ (with $\langle j, i\rangle$) effected by the last term of Eq. (2.74) is nonresonant, in the second order in J, the transition $|2_j\rangle \to |2_i\rangle$ via the virtual intermediate state $|1_j\rangle\,|1_i\rangle$ is resonant. An adiabatic elimination [50, 51] of the intermediate state $|1_j\rangle\,|1_i\rangle$ then yields an effective tunnelling rate for a dimer as a whole, given by $J^{(2)} \equiv 2J^2/U \ll J$. Note also that the adiabatic elimination of $|1_j\rangle\,|1_i\rangle$ results in an energy shift of the dimer states $|2_j\rangle$ equal to $J^{(2)}$, which constitutes a correction to the dimer energy $\varepsilon + U$. In analogy to the single particle case, the effective tunnelling with the rate $J^{(2)}$ implies a narrow Bloch band for single dimers, of width $4dJ^{(2)}$ centred around $\varepsilon + U + 2dJ^{(2)}$.

The exact wave function and dispersion relation for single dimers can be obtained analytically in 1D [46, 52]. As a tutorial for the derivation of the effective many-dimer Hamiltonian in the following section, one can analyse the single dimer dynamics perturbatively for small J/U [53]. Given a dimer centred at site j, in 1D its "internal" state $|D_j\rangle$ is

$$|D_j\rangle = A_{j,0}\,|2_j\rangle + \sum_r \Big(A_{j,r}\,|1_j\rangle\,|1_{j+r}\rangle + A_{j,-r}\,|1_{j-r}\rangle\,|1_j\rangle\Big), \tag{7.10}$$

where $r = 1, 2, \ldots$ is the distance in sites one of the constituent particles of the dimer has tunnelled away from the other. In zeroth order in J, one has $A_{j,0} = 1$ and all $A_{j,\pm r} = 0$. In the successive higher orders in J/U it is easy to see that $A_{j,\pm r} \simeq \sqrt{2}\left(-\frac{J}{U}\right)^r A_{j,0}$. The corresponding probability of finding the dimer constituents separated by r sites is $P_{j,r} = |A_{j,r}|^2 + |A_{j,-r}|^2 = 4P_{j,0}\left(\frac{J^2}{U^2}\right)^r$, while $P_{j,0} = |A_{j,0}|^2$.

For $|J/U| \ll 1$, the normalization condition $\sum P_{j,r} = 1$ then yields

$$A_{j,0} \simeq \sqrt{\frac{U^2 - J^2}{U^2 + 3J^2}}, \quad A_{j,\pm r} \simeq (-1)^r \sqrt{2} A_{j,0} \left(\frac{J}{U}\right)^r . \tag{7.11}$$

Note the alternating sign of the amplitudes $A_{j,\pm r}$ between the sites r. Expressing the tunnelling probabilities $P_{j,r}$ as

$$P_{j,r} = 4P_{j,0} \exp\left[\ln\left(\frac{J^2}{U^2}\right)^r\right] = 4P_{j,0}\, e^{-r/\zeta}, \tag{7.12}$$

the localization (or "bond") length of the dimer is found to be $\zeta = [2\ln(U/J)]^{-1}$, so that $\zeta < 1$ for $U/J > \sqrt{e}$. These results agree with the exact expressions in the limit $J \ll U$, and they can be extended to higher dimensions, which are less tractable by the exact methods. Thus, for example, in 2D one obtains

$$A_{j,0} \simeq \sqrt{\frac{U^2 - 3J^2}{U^2 + 5J^2}}, \tag{7.13}$$

$$\begin{aligned} P_{j,r} &\simeq 8P_{j,0}\left[\frac{\Gamma(r+\frac{1}{2})}{\sqrt{\pi}\Gamma(r+1)} 4^r - 1\right]\left(\frac{J^2}{U^2}\right)^r \\ &< 8P_{j,0} \exp\left[\ln\left(\frac{4J^2}{U^2}\right)^r\right] = 8P_{j,0}\, e^{-r/\zeta}, \end{aligned} \tag{7.14}$$

where the localization length is $\zeta = [2\ln(U/2J)]^{-1}$. One can conclude that for $U/J > \sqrt{e}$ the dimer can be considered as a localized object, i.e. the relative motion of its atomic constituents is frozen out.

7.3 Effective many-body Hamiltonian for a system of dimers

7.3.1 Derivation of the effective Hamiltonian

So far, the properties of a single repulsively bound dimer in a periodic potential have been discussed. The goal here will be to describe the dynamics of a system of dimers. To this end it is instructive to extend the discussion of the previous section to two dimers occupying adjacent sites $\langle j, i\rangle$. Their potential energy is lower by the amount $8J^{(2)}$ than that of two dimers separated by one or more lattice sites (see Eq. (7.26)). In analogy with the case of two particles forming a dimer, one can calculate the wavefunction $|Q_{ji}\rangle$ of the dimer pair perturbatively in the effective

tunnelling $J^{(2)}$. To that end, one can expand the wavefunction $|Q_{ji}\rangle$ as

$$\begin{aligned} |Q_{ji}\rangle &= B_{ji,0}\left|1_j^D\right\rangle\left|1_i^D\right\rangle + \sum_r \Big(B_{ji,r}\left|1_j^D\right\rangle\left|1_{i+r}^D\right\rangle \\ &\quad + B_{ji,-r}\left|1_{j-r}^D\right\rangle\left|1_i^D\right\rangle\Big), \end{aligned} \tag{7.15}$$

where $r = 1, 2, \ldots$ is the number of sites separating the dimers. One then obtains $B_{ji,\pm r} \simeq (-1/8)^r B_{ji,0}$, which, upon requiring the normalization $\sum P_{ji,r} = 1$, where $P_{ji,r} = |B_{ji,r}|^2 + |B_{ji,-r}|^2$, yields

$$B_{ji,r} \simeq \sqrt{\frac{63}{65}}\left(-\frac{1}{8}\right)^r. \tag{7.16}$$

One therefore has $P_{ji,r} \simeq 2e^{-r/\xi}$ with the localization length $\xi = (\ln 64)^{-1} \simeq 0.24$. Hence, two dimers localized at adjacent lattice sites are closely bound to each other. It can be shown that this conclusion also holds in 2D and 3D. Thus one expects an interesting many-body dynamics mediated by the dimer-dimer interaction.

In the next step the states with an odd number of particles on any given lattice site will be eliminated adiabatically. Let $\hat{P}$ be the projection operator onto the states which have an even number of particles per lattice site and $\hat{Q} = 1 - \hat{P}$ the orthogonal projection. The Hamilton operator can then be expanded into four parts

$$\hat{H} = \hat{H}_{PP} + \hat{H}_{PQ} + \hat{H}_{QP} + \hat{H}_{QQ} \tag{7.17}$$

where $\hat{H}_{PP} = \hat{P}\hat{H}\hat{P}$ is the Hamilton operator projected into the subspace of particle pairs, $\hat{H}_{PQ} = \hat{P}\hat{H}\hat{Q}$ and $\hat{H}_{QP} = \hat{Q}\hat{H}\hat{P}$ contain processes which change the number of particles from even to odd numbers on some lattice site and $\hat{H}_{QQ} = \hat{Q}\hat{H}\hat{Q}$ contains all process between states with odd particle numbers at some sites. One important property of the Bose-Hubbard model is that

$$\hat{P}\hat{a}_j^\dagger\hat{a}_i\hat{P} = 0 \text{ if } j \neq i \tag{7.18}$$

$$\hat{P}\hat{a}_j^\dagger\hat{a}_j\hat{Q} = \hat{Q}\hat{a}_j^\dagger\hat{a}_j\hat{P} = 0 \tag{7.19}$$

$$\hat{P}\hat{a}_j^\dagger\hat{a}_j^\dagger\hat{a}_j\hat{a}_j\hat{Q} = \hat{Q}\hat{a}_j^\dagger\hat{a}_j^\dagger\hat{a}_j\hat{a}_j\hat{P} = 0. \tag{7.20}$$

Thus, $\hat{H}_{PP}$ contains only local parts and no hopping, whereas $\hat{H}_{QP}$ and $\hat{H}_{PQ}$ contain only the hopping and no local parts. Only $\hat{H}_{QQ}$ contains contributions

from both. The effective Hamiltonian for a state of energy E is in general

$$\hat{H}_{\text{eff}} = \hat{H}_{PP} + \hat{H}_{PQ}\frac{1}{E - \hat{H}_{QQ}}\hat{H}_{QP}. \tag{7.21}$$

See [54]. It can be seen now that a second order perturbation theory in J is equivalent to neglecting the hopping contained in $\hat{H}_{QQ}$. Furthermore E can be replaced by operators which automatically give the correct energy for a given state. The operator $\hat{E}$ which gives the energy for a number state is

$$\hat{E}(\hat{n}_1, \hat{n}_2, \ldots, \hat{n}_M) = \frac{U}{2}\sum_j \hat{n}_j(\hat{n}_j - 1) \tag{7.22}$$

If the matrix element $\langle p|\, \hat{H}_{\text{eff}}\, |p\rangle$ is considered for a number state $|p\rangle$ with even number of particles per site with the intermediate virtual processes of the form $|n_i\rangle\,|n_{i+1}\rangle \rightarrow |n_i - 1\rangle\,|n_{i+1} + 1\rangle \rightarrow |n_i\rangle\,|n_{i+1}\rangle$, where n_i and n_{i+1} are even, then E can be replaced by the operator $\hat{E}(\ldots, \hat{n}_i + 1, \hat{n}_{i+1} - 1, \ldots)$. Non-diagonal matrix elements $\langle p'|\, H_{\text{eff}}\, |p\rangle$ with the intermediate virtual process $|n_i + 2\rangle\,|n_{i+1}\rangle \rightarrow |n_i + 1\rangle\,|n_{i+1} + 1\rangle \rightarrow |n_i\rangle\,|n_{i+1} + 2\rangle$ will only belong to resonant processes when $|p\rangle$ and $|p'\rangle$ have the same energy, which is only the case for $n_i = n_{i+1}$. Otherwise an energy of nU with $n > 1$ would be necessary for this process which can be neglected in comparison to energy U which is assumed to be large compared to J here. In second order in J/U the resulting effective Hamiltonian is

$$\begin{aligned}\hat{H}_{\text{eff}} &= \sum_j \varepsilon_j \hat{m}_j + U\sum_j \hat{m}_j\Big(2\hat{m}_j - 1\Big) \\ &\quad + J^{(2)}\sum_{\langle j,i\rangle} \hat{d}_j^\dagger\, \hat{T}\Big(\hat{m}_j, \hat{m}_i\Big)\, \hat{d}_i \\ &\quad + J^{(2)}\sum_{\langle j,i\rangle} \hat{S}\Big(\hat{m}_j, \hat{m}_i\Big),\end{aligned} \tag{7.23}$$

where $J^{(2)} \equiv 2J^2/U$, and $\hat{T}$ and $\hat{S}$ are defined as

$$\hat{T}\Big(\hat{m}_j, \hat{m}_i\Big) = \delta_{\hat{m}_i \hat{m}_j}\sqrt{\Big(2\hat{m}_j + 1\Big)\Big(2\hat{m}_i + 1\Big)}, \tag{7.24a}$$

$$\hat{S}\Big(\hat{m}_j, \hat{m}_i\Big) = \frac{\hat{m}_i\Big(2\hat{m}_j + 1\Big)}{2\hat{m}_i - \Big(2\hat{m}_j + 1\Big)}. \tag{7.24b}$$

The third term on the right-hand side of (7.23) describes dimer tunnelling between adjacent sites. This tunnel-interaction is resonant only between states of the form

$\left|m_j^D\right\rangle\left|(m+1)_i^D\right\rangle$ and $\left|(m+1)_j^D\right\rangle\left|m_i^D\right\rangle$, i.e. for which the occupation numbers of the adjacent sites differ by one; the corresponding matrix element is equal to $J^{(2)}(m+1)(2m+1)$. The last term of Eq. (7.23), containing the energy shift function $\hat{S}$, is responsible for the nearest-neighbour interaction, which, depending on the values of m_j and m_i, can be positive or negative. Adding the two interaction terms between adjacent sites i and j, one arrives at

$$\hat{S}\big(\hat{m}_j,\hat{m}_i\big)+\hat{S}\big(\hat{m}_i,\hat{m}_j\big)=\frac{2\hat{m}_j^2+2\hat{m}_i^2+\hat{m}_j+\hat{m}_i}{4\big(\hat{m}_j-\hat{m}_i\big)^2-1}. \tag{7.25}$$

Thus, when $m_j = m_i$ the interaction energy of neighbouring sites is negative, otherwise it is positive resulting in an attractive interaction of pairs. These effects can be understood as the level shifts of the dimer states, due to "level repulsion" from virtual states having odd occupation numbers.

The Hamiltonian (7.23) describes the effective dynamics of dimers in a 1D, 2D or 3D periodic potential, in the strong coupling regime. Its key features are occupation-dependent tunnelling and nearest-neighbour interactions, as well as strong on-site repulsion via the term proportional to U.

The tunnelling $\hat{T}$ and the nearest neighbour interactions $\hat{S}$ are responsible for competing processes: While tunnelling favours dispersed centre of mass wavefunctions of dimers with long-range coherence, the nearest neighbour attraction tends to balance the population of neighbouring sites and to minimize the surface area between regions of different occupation number. Since, the interaction term is always larger than the competing tunnelling term, the ground state will be dominated by attractively bound clusters of uniform occupation number and minimal surface area, thus representing incompressible "droplets" of a quantum lattice liquid.

7.3.2 Effective Hamiltonian for $m \leq 1$

In the following the important special case of a system containing at most one dimer per site ($m = 0$ or 1 for all j) is considered. Thus, it is assumed that the periodic potential can be loaded initially only with zero or two particles per site, at effectively infinite U/J which is then adiabatically lowered to a large but finite value, as implemented in the optical lattice experiment of Winkler *et al.* [46]. Just as dimers are energetically forbidden to dissociate in the absence of dissipation, the single-site dimer occupation numbers will never exceed unity, for this would require a large energy input of the order of $5U$. Under these conditions, the effective

Hamiltonian (2.74) can be recast simply as

$$H_{\rm eff}^{(0,1)} = \sum_j \left[\varepsilon_j + U + 2dJ^{(2)}\right]\hat{m}_j + J^{(2)} \sum_{\langle j,i\rangle} \hat{d}_j^\dagger \hat{d}_i - 4J^{(2)} \sum_{\langle j,i\rangle} \hat{m}_j \hat{m}_i, \tag{7.26}$$

where the only allowed values of m are 0 or 1 and thus the $\hat{d}_j$ are now hard-core boson operators. Thus, in addition to the tunnelling interaction with negative effective mass, there is a stronger attractive interaction between dimers localized at neighbouring sites, which can bind them together. Note that (7.26) has the form of an extended Hubbard model, like that which describes electrons in a crystal lattice or quantum dot array [47]. There, however, the nearest-neighbour interaction is repulsive, while in the present case it is attractive. Also note, that related effects have been predicted for strongly interacting mixtures of bosonic and fermionic atoms in an optical lattice [48], wherein the fermions tend to pair with one or more bosons, forming composite fermions with nearest-neighbour interaction.

To verify the validity of the perturbative approach in the limit of $J/U \ll 1$, the Schrödinger equation was solved numerically for the cases of one and two dimers in a 1D lattice of 20 sites, using the Bose-Hubbard Hamiltonian (2.74), and the effective Hamiltonian (7.23) [or (7.26)]. As shown in Fig. 7.2, the dynamics of the system obtained from the exact and effective Hamiltonians is very similar; the difference between the exact and effective models decreases for smaller values of J/U, as expected. In the inset of Fig. 7.2**a** the projection of the system wavefunction $|\Psi(t)\rangle$ onto the states $|2_j\rangle$ with two particles per site was plotted. As seen, $\sum_j |\langle 2_j|\Psi\rangle|^2 \simeq 1$ at all times, attesting to the fact that the two particles forming a dimer are strongly bound to each other, even though the centre-of-mass wavefunction of the dimer disperses with time due to the tunnelling $J^{(2)}$. Figs. 7.2**c**,**d** reveal the greatly reduced dispersion for a pair of neighbouring dimers attractively bound to each other: the two-dimer pair can only tunnel collectively in fourth order in the fundamental J (second order in $J^{(2)}$).

The above reasoning can be extended to the case of more dimers. Since each dimer is attracted to its immediate neighbour, for a given number of dimers, the configuration that minimizes the energy of the system would correspond to clustering of the dimers together in such a way as to maximize the number of the nearest–neighbour (attractive) interactions. Thus, in 1D all the dimers would stick together in a line without voids, while for 2D or 3D square lattices, the dimers would tend to arrange themselves in a square (2D) or a cube (3D), as shown in Fig. 7.3. (Be-

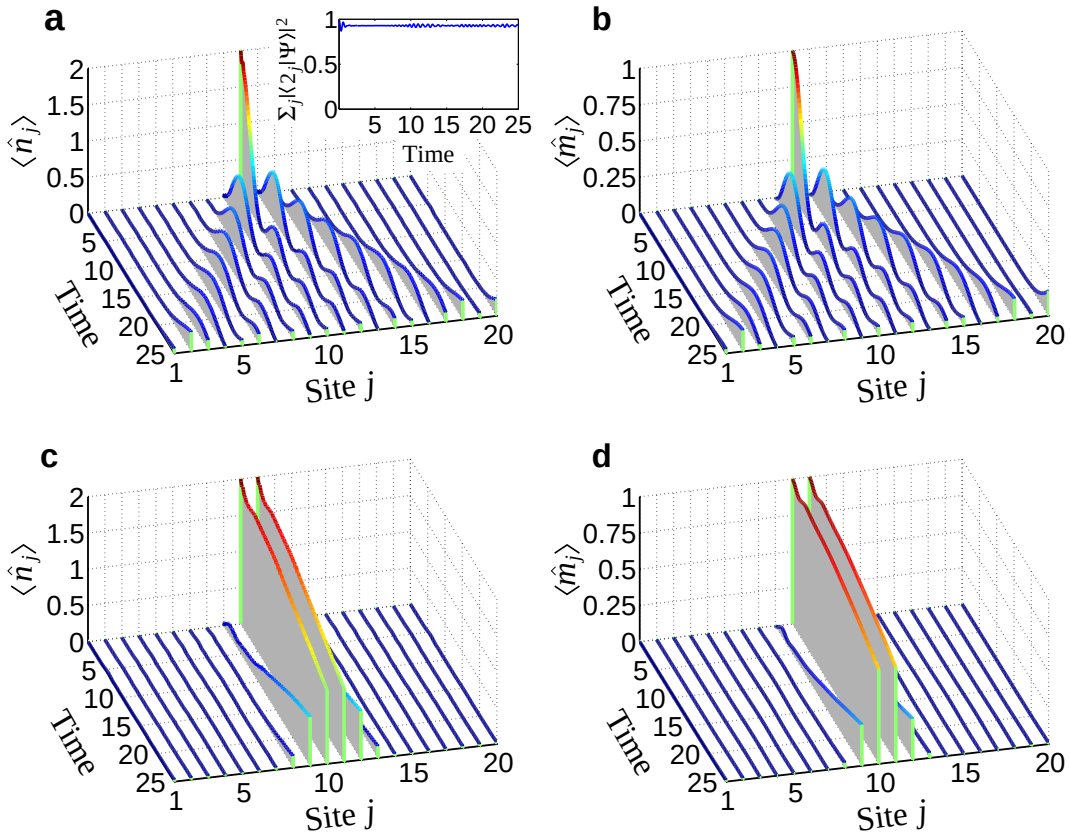

Figure 7.2: Dynamics of one dimer, **a** and **b**, and two dimers, **c** and **d**, in a 1D lattice of 20 sites, for $J/U = 0.1$. **a** and **c** are numerical solutions of the Schrödinger equation with the Bose-Hubbard Hamiltonian (2.74), while **b** and **d** are obtained with the effective Hamiltonian (7.23) [or (7.26)]. Inset in **a** shows the time-evolution of $\sum_j |\langle 2_j|\Psi\rangle|^2$, where $|\Psi(t)\rangle$ is the system wavefunction. Time is in units of J^{-1}.

cause of the discretized perimeter metric in the lattice, minimal surfaces of these "droplets" are rectangular rather than round.)

7.4 Phase diagram of the grand canonical ensemble

In order to understand the ground-state properties of the effective Hamiltonian (7.23), the grand canonical ensemble described by the operator

$$\hat{K} = \hat{H}_{\text{eff}} - \mu \sum_j \hat{m}_j, \tag{7.27}$$

is considered here, where μ is the chemical potential assumed uniform for all sites. The corresponding phase diagram, calculated numerically for a small 1D lattice

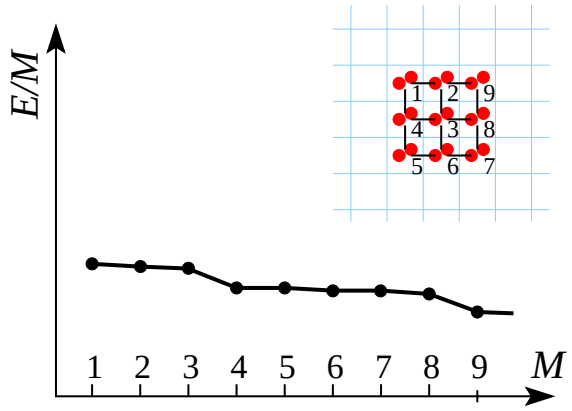

Figure 7.3: Energy per dimer E/M versus the number of dimers M forming a cluster in 2D square lattice. As seen, E/M abruptly drops once a square droplet with the dimension $\sqrt{M} \times \sqrt{M}$ is formed, since the addition of the last dimer results in the formation of two "bonds".

at zero temperature, is shown in Fig. 7.4. Since the tunnelling interaction is always smaller than the attractive interaction between neighbouring sites with equal occupation numbers, only incompressible phases are observed, with uniform, commensurate filling. All systems with incommensurate dimer filling lie on the border lines between the incompressible phases, which verifies the qualitative discussion of the last section. When adding a dimer to the system, it is energetically favourable for this dimer to be bound to an already existing cluster or droplet rather than to move freely.

This picture changes, however, when a finite temperature T is considered. If T is sufficiently large the minimum free energy may be attained when the dimers move freely rather than being bound to a cluster. Thus it can be expected that the system shows a first-order phase transition from a "quantum-droplet" phase to a "gas" phase at some critical temperature T_c.

The system described by the effective Hamiltonian $H_{\text{eff}}^{(0,1)}$ is equivalent to the well-known spin-$\frac{1}{2}$ XXZ model in a magnetic field [55, 56] (see also Section 2.4). Indeed, with the mapping $|0_j\rangle \to |\downarrow_j\rangle$ and $|1_j\rangle \to |\uparrow_j\rangle$ and simple algebraic manipulations, Eq. (7.26) can be cast as

$$\hat{H}_{\text{spin}} = C + \sum_j \frac{h_j}{2}\hat{\sigma}_j^z + \frac{J^{(2)}}{4}\sum_{\langle j,i\rangle}\left(\hat{\sigma}_j^x\hat{\sigma}_i^x + \hat{\sigma}_j^y\hat{\sigma}_i^y\right) - J^{(2)}\sum_{\langle j,i\rangle}\hat{\sigma}_j^z\hat{\sigma}_i^z, \quad (7.28)$$

where C is an unimportant constant, $h_j = \varepsilon_j + U - 6dJ^{(2)}$ is an effective magnetic field, and $\hat{\sigma}_j^x$, $\hat{\sigma}_j^y$ and $\hat{\sigma}_j^z$ are the Pauli spin matrices. Note that, unlike the usual situation in spin systems, here the total "magnetization" of the system $\sum_j\langle\hat{\sigma}_j^z\rangle$ is fixed by the condition $\langle\hat{m}\rangle = (1 + \langle\hat{\sigma}^z\rangle)/2$, where $\langle\hat{m}\rangle$ is the dimer filling factor.

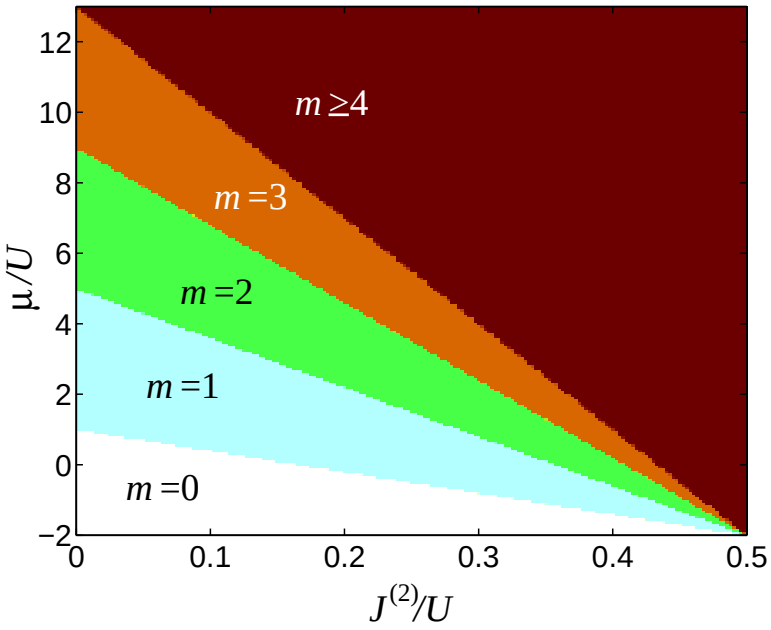

Figure 7.4: Phase diagram of the grand canonical ensemble obtained from exact diagonalization of Eq. (7.27). The Hilbert space is restricted by five sites (periodic boundary conditions), with each site occupation number in the range of $0 \leq m \leq 4$. The areas of integer filling are tightly adjoined to each other, with no significant extent of fractional filling phase.

In this description, ferromagnetic spin coupling is present described by the last term of Eq. (7.28), which dominates over the spin-exchange interaction. At low temperatures ($k_{\mathrm{B}}T < J^{(2)}$), the "spins" therefore form a ferromagnetic domain with the spins pointing up, surrounded by the remaining spins pointing down. At a certain critical temperature T_c, the spin domains disappear and a random distribution of the $|\uparrow_j\rangle$ and $|\downarrow_j\rangle$ states emerge. In order to estimate T_c, note that in the above spin Hamiltonian the ZZ coupling is significantly larger than the XX and YY couplings, which, to a reasonable approximation, can be neglected. Eq. (7.28) then reduces to the Ising Hamiltonian [57], whose analytic properties in 2D are well known. In Fig. 7.5 the finite–temperature phase diagram of the 2D Ising model is shown. The shaded ferromagnetic spin domains at low temperatures correspond to the "droplets" of the present model. The boundary of that region $\langle\hat{\sigma}^z\rangle_c(T)$ is defined through

$$\langle\hat{\sigma}^z\rangle_c(T) = \left[1 - \sinh^{-4}\left(\frac{2J^{(2)}}{k_{\mathrm{B}}T}\right)\right]^{1/8}.$$

As temperature is increased, for $\langle\hat{\sigma}^z\rangle \neq 0$ the system undergoes a first-order phase transition from the "droplet' to the "gas" phase. For $\langle\hat{\sigma}^z\rangle = 0$, the transition is a

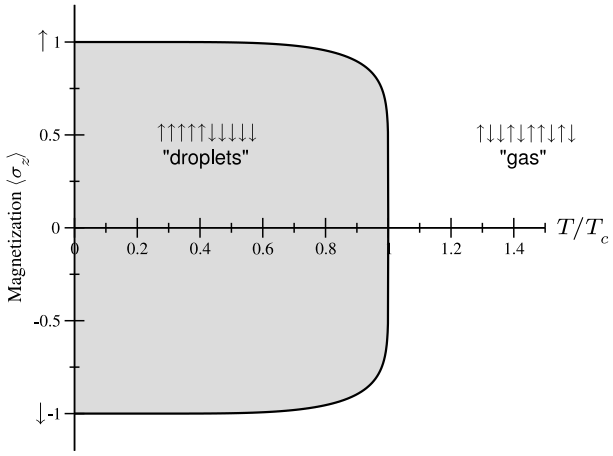

Figure 7.5: Temperature phase diagram of the 2D Ising model. In the shaded area, the ferromagnetic spin domains are formed. As temperature is increased, for $\langle\hat{\sigma}^z\rangle \neq 0$, the system undergoes a first-order phase transition to the "gas" phase, while at $\langle\hat{\sigma}^z\rangle = 0$ it is a second order phase transition. See text for more details.

monotonous second order phase transition, for which the critical temperature T_c corresponds to $\langle\hat{\sigma}^z\rangle_c(T_c) = 0$ which yields $k_{\mathrm{B}}T_c/J^{(2)} = 2/\mathrm{arcsinh}(1) = 2.2692$

7.5 Experimental issues

As was stated in the beginning of this chapter, the most relevant experimental situation for the present study is realized by cold bosonic atoms loaded into an optical lattice [46]. Initially, pairs of atoms (^{87}Rb) are adiabatic converted with near unit efficiency into chemically bound molecules (Rb_2) using a magnetic field sweep across a Feshbach resonance. This step is then followed by removing all chemically unbound atoms with combined radio-frequency and optical purification pulses. Finally, the dimer molecules are adiabatically converted back into pairs of atoms localized at the same site, with no significant admixture of unpaired atoms. In the case of strong on-site repulsion $U \gg J$, these pairs of atoms form the dimers studied in this chapter. When the lattice sites are occupied by more than one dimer, the three- and four body collisions will presumably be the dominant loss mechanism for the atoms. In a recent study, Campbell *et al.* [58] have experimentally realized a Mott insulator phase of cold ^{87}Rb atoms with particle numbers per site of $n = 1, 2, 3, 4, 5$ in successive spatial shells, and determined the lifetime of each shell. The observation for $n = 2$ was around 100 s, and for $n \geq 3$ around 0.5 s. On the other hand, the rate of dimer tunnelling $J^{(2)}$ estimated from [46] is about $10 - 20$ s^{-1} which is thus three orders of magnitude larger than the loss rate for

$n = 2$ (i.e., $m = 1$), and an order of magnitude larger than the loss rate for $n = 4$ (i.e., $m = 2$).

In the experiment of Winkler *et al.* [46], in order to determine the fraction of the remaining dimers for various experimental conditions and hold times, the authors repeat the above sequence (i.e., conversion of atoms pairs into molecules, purification, and reverse conversion) and then use the conventional absorption imaging. With minor modification, this method can be employed to experimentally verify the formation of clusters of dimers. Recall that dimers forming a cluster become immobile, while individual unbound dimers are mobile, moving around the lattice with the tunnelling rate $J^{(2)}$. Assume that at the boundaries of the lattice of linear dimension l there exists some dimer loss mechanism (see below). Then, if the dimers are not bound to each other, after a sufficient time of the order of $t_{\text{escape}} \sim l/J^{(2)}$, they will escape from the lattice, while immobile dimers bound in a cluster will remain in the lattice, which can be verified by the same absorption imaging. The loss mechanism at the boundaries of the lattice can be an atom evaporation by focused laser beams. Alternatively, if the lattice potential is created by strongly focused (blue-detuned) laser field, then away from the central region, where the intensity of the field falls off, the tunnelling barriers become lower. As a result, the dimer mobility increases, and eventually even individual atoms can move practically freely, quickly escaping the lattice.

In the above discussion on the properties of repulsively bound pairs of particles in a periodic potential, the effects of energy dissipation in the system have been neglected. Assuming small temperature and a dimer filling factor $\langle \hat{m} \rangle \leq 1/2$ (average particle filling factor $\langle \hat{n} \rangle \leq 1$), it is obvious that in the presence of energy relaxation with a characteristic rate γ (such as from spontaneous emission of phonons in a solid, or inelastic collisions with a cold background gas for atoms in an optical lattice), the lifetime of repulsively bound pairs will be limited by γ^{-1}. But for an initial random distribution of dimers in the lattice, dissipation on shorter time scales than γ^{-1} will drive formation of multi-dimer clusters, to minimize the energy of the dimer system. Furthermore, once a cluster is formed, dimer dissociation becomes a surface process only, because dissociation of a dimer inside the cluster would mean forming a "trimer" at an adjacent site, which requires energy input U, instead of energy release. Note also that the collision of a single unpaired particle with a dimer involves resonant single-particle exchange. States of the form $|n_j\rangle\,|(n \pm 1)_i\rangle$ and $|(n \pm 1)_j\rangle\,|n_i\rangle$ (with $\langle j, i \rangle$) are resonantly coupled to each other via single particle tunnelling. But by assuming that only even number of particles per site are present initially in the system, such events have

been explicitly excluded . The admixture of single particles thus brings a complicated interplay between dimer dissociation and bound dimer collisions with single particles. Detailed understanding of fluctuations and dissipation in the liquid-like phase of clustered dimers will require further investigation, bringing the physics of first-order phase transitions into the arena of ultra-cold atoms.

7.6 Summary

This chapter discussed meta-stable pairs of particles in periodic potentials. Despite the repulsion of the particles the pairs cannot dissociate due to the energy gap of the periodic potential. It was shown that the Bose-Hubbard model can be mapped onto a Hamiltonian describing particle pairs (dimers) and single particles (monomers). An effective Hamiltonian for the dimers was derived when no other single particles are present. It was found that the dimer-dimer interaction includes strong on-site repulsion and nearest-neighbour attraction which always dominates over the dimer kinetic energy at low temperatures. The dimers thus can form incompressible, minimal-surface "droplets" of a quantum lattice liquid. For low lattice filling, the effective Hamiltonian can be mapped onto the spin-1/2 XXZ model with fixed total magnetization which exhibits a first-order phase transition from the droplet to a gas phase for non vanishing magnetization and a second-order transition for zero magnetization respectively.

Chapter 8

Attractively bound pairs of particles in lattices

In Chapter 7 and [59] an effective model for particle pairs in an optical lattice was derived. The case where the interaction between the particles is repulsive was investigated, which is remarkable because of the counter-intuitive fact that the particle pairs are meta-stable despite repulsion. The band-gap did not allow the pairs to dissociate. For strong atom-atom interaction, either attraction or repulsion, the dimer constituents are well co-localized [60], and an ensemble of such dimers in a lattice can be accurately described by an effective Hamiltonian which has the form of the spin-1/2 anisotropic XXZ model. The derivation of the effective Hamiltonian is given in Chapter 7 and [59] where also its properties for the case of repulsive atom-atom interactions are discussed. Since the resulting nearest-neighbour attraction of dimers dominates the kinetic energy it causes the formation of minimal surface "droplets" of dimers on a lattice below a critical temperature. In the case of attractive atom-atom interaction considered here, the interaction between the nearest neighbour dimers is a strong repulsion. It is then found that the ground state of the system in a grand canonical ensemble exhibits incompressible phases, corresponding to an empty and a fully filled lattice as well as a half-filled alternating density crystal. These phases are separated from each other by compressible phases.

In this chapter the ground state phase diagram is calculated numerically and analytically for this system in 1D. The critical points can be obtained with the help of a Bethe ansatz making use of the correspondence to the XXZ model [25, 26]. In a finite lattice and close to half filling the compressible phases show characteristic oscillatory modulations on top of the anti-ferromagnetic density profile. A simple kink model is derived which explains the density profiles as well as number-number

correlations in the compressible phases. The long-range correlations of the dimer system show a Luttinger liquid behaviour. First-order and density correlations are calculated in a finite system from a field theoretical model, which show excellent agreement with numerical data. The corresponding Luttinger parameter is obtained from solving the Bethe integral equations. Finally the phase diagram in higher dimension is discussed within a strong-coupling approximation and the differences to the 1D case illuminated.

8.1 Effective dimer model

In the following attractively-bound dimers on a d-dimensional isotropic lattice are considered. Because of the strong on-site atom-atom interaction $U < 0$ it is energetically impossible to break the dimers, which effectively play the role of hard core bosons on the lattice. Via a second order process in the original atom hopping J the dimers carry a nearest neighbour interaction and can tunnel to neighbouring sites. The effective Hamiltonian for the system has been derived in Chapter 7 (see also Ref. [59])

$$\begin{aligned}\hat{H}_{\text{eff}} &= \sum_j \left(U - 2dJ^{(2)} + \varepsilon_j\right)\hat{m}_j - J^{(2)} \sum_{\langle j,i\rangle} \hat{d}_j^\dagger \hat{d}_i \\ &\quad + 4J^{(2)} \sum_{\langle j,i\rangle} \hat{m}_j \hat{m}_i \end{aligned} \tag{8.1}$$

where $\hat{d}_j^\dagger$ and $\hat{d}_j$ are the creation and annihilation operators of hard-core bosons (dimers), and $\hat{m}_j = \hat{d}_j^\dagger \hat{d}_i$ is the number operator for a dimer at site j. The effective repulsive nearest neighbour interaction is fixed at four times the dimer tunnelling $J^{(2)} \equiv -2J^2/U > 0$ between adjacent sites $\langle j, i\rangle$. Therefore, the kinetic energy of one dimer in the second term of Eq. (8.1) spans the interval $[-2dJ^{(2)}, 2dJ^{(2)}]$ corresponding to a Bloch band of a d dimensional square lattice. In comparison, bringing dimers close together on neighbouring sites requires an energy of $8J^{(2)}$ due to the strong repulsive interaction in the last term. The local potential energy ϵ_j from the confining potential is modified by an additional 'internal energy" term $\left(U - 2dJ^{(2)}\right)$, which is negative for attractive interactions.

Since the dimers are effectively hard-core bosons it is possible to map the above Hamiltonian onto an anti-ferromagnetic spin system like it is explained in Section 2.4. The mapping to an anti-ferromagnetic spin system yields

$$H_{\text{spin}} = \sum_j \frac{h_j}{2}\hat{\sigma}_j^z - \frac{J^{(2)}}{4} \sum_{\langle j,i\rangle} \left(\hat{\sigma}_j^x \hat{\sigma}_i^x + \hat{\sigma}_j^y \hat{\sigma}_i^y\right) + J^{(2)} \sum_{\langle j,i\rangle} \hat{\sigma}_j^z \hat{\sigma}_i^z, \tag{8.2}$$

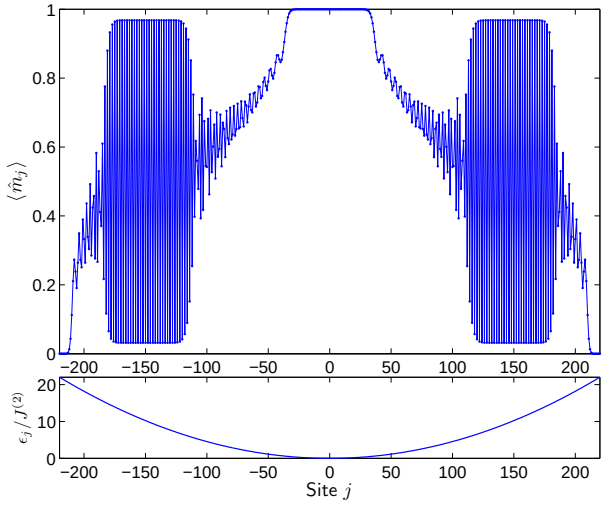

Figure 8.1: Density of dimers in a 1D lattice with additional harmonic confinement potential obtained from a DMRG simulation, with $\tilde{\mu}/J^{(2)} = 18.5$ and $\epsilon_j/J^{(2)} = j^2/2200$. One clearly recognizes the existence of an incompressible phase with homogeneous filling of one in the trap centre, and two anti-ferromagnetic phases separated by compressible intermediate regions.

with an effective field of $h_j = \varepsilon_j + U + 6dJ^{(2)}$. This is the XXZ-model with a fixed anisotropy of 4, i.e. the Ising-like interactions dominate the behaviour. A given total number of dimers corresponds in the XXZ model to a fixed total magnetization. Thus many properties of the dimer system in one dimension can be determined via a mapping to the integrable XXZ model. An interesting general property of the dimer model (8.1) is that the ratio of interaction to kinetic energy has a fixed value larger than one. As a consequence the ground-state of the system is interaction dominated giving rise to interesting correlation properties.

8.2 1D ground-state phase diagram

In a grand canonical ensemble Eq. (8.1) is replaced by $\hat{K} = \hat{H}_{\text{eff}} - \mu \sum_j \hat{m}_j$, with μ being the chemical potential. In a homogeneous system the first term in (8.1) can be absorbed into μ and thus the ground-state of the system depends only on a single parameter $\mu/J^{(2)}$. The corresponding phase diagram can be completely mapped out in an experiment by adding an external trapping potential with sufficiently small confinement such that the local density approximation is valid and $\mu \to \mu_j \equiv \mu - \epsilon_j$. In this way different regions in the trap correspond to different chemical potentials.

In Fig. 8.1 the average number of dimers in a one-dimensional lattice in the presence of an additional harmonic trapping potential is plotted obtained by a

numerical calculation using the density matrix renormalization group DMRG [37]. One clearly recognizes three types of regions: In the trap centre where the local chemical potential is largest there is a unit filling of dimers. Separated by a spatial region of monotonously decreasing average filling follows a region where the latter is exactly one half and the dimers form a periodic pattern with period 2 and almost maximum modulation depth. Towards the edge of the dimer cloud the average density decreases again monotonously to zero. In terms of the equivalent spin system the central region corresponds to a gapped phase of full spin polarization caused by the large negative effective magnetic field. The region of exactly one half average filling corresponds to another gapped phase with anti-ferromagnetic order induced by the nearest neighbour repulsion $4J^{(2)} > 0$ in (8.1). The intermediate regions are compressible.

The critical values of the chemical potential for the transitions between compressible and incompressible phases in 1D are known from the work of Yang and Yang [25, 26] on the XXZ model. For the parameter of the current system one finds with $\widetilde{\mu} = \mu - U + 2J^{(2)} = \mu + |U| + 2J^{(2)}$

$$\begin{aligned}
\widetilde{\mu}_{\uparrow}/J^{(2)} &= 18, && (8.3)\\
\widetilde{\mu}_{\mathsf{AF}+}/J^{(2)} &= 8 + 2\sqrt{15}\sum_{n=-\infty}^{\infty}\frac{(-1)^n}{\cosh(n\,\mathrm{arccosh}(4))} \\
&\approx 12.31638.., && (8.4)\\
\widetilde{\mu}_{\mathsf{AF}-}/J^{(2)} &= 8 - 2\sqrt{15}\sum_{n=-\infty}^{\infty}\frac{(-1)^n}{\cosh(n\,\mathrm{arccosh}(4))} \\
&\approx 3.68361.., && (8.5)\\
\widetilde{\mu}_{\downarrow}/J^{(2)} &= -2. && (8.6)
\end{aligned}$$

These values agree very well with those obtained from an exact diagonalization on a small lattice with $M = 10$ sites and periodic boundary conditions as well as a DMRG simulation with up to $M = 300$ and boxed (i.e. open) boundary conditions. They also correspond to the different regions shown in Fig. 8.1

8.3 Mott-insulating phases

Phases with zero or full filling correspond to ferromagnetic phases in terms of the spin Hamiltonian with a simple form of the ground state wavefunctions

$$\begin{aligned}
|\psi_{\downarrow}\rangle &= |\downarrow,\downarrow,\downarrow,\ldots,\downarrow\rangle\,, && (8.7)\\
|\psi_{\uparrow}\rangle &= |\uparrow,\uparrow,\uparrow,\ldots,\uparrow,\rangle\,. && (8.8)
\end{aligned}$$

Particle hole excitations are not possible in this state and inserting or removing one particle carries a finite energy cost corresponding to flipping a spin. Hence these phases are incompressible.

For half filling the situation corresponds most closely to an anti-ferromagnetic phase. However, in this case the simple "Néel" state

$$\left|\psi_{\mathsf{AF}}^{(0)}\right\rangle \;=\; |\ldots,\downarrow,\uparrow,\downarrow,\uparrow,\downarrow,\uparrow,\downarrow,\uparrow,\ldots\rangle\,, \tag{8.9}$$

is not an exact eigenstate of the Hamiltonian, since a dimer can tunnel from an occupied site to a neighbouring, previously unoccupied site, corresponding to a flip of two neighbouring spins, resulting in a state of the form

$$|\psi_1\rangle \;=\; |\ldots,\downarrow,\uparrow,\downarrow,\downarrow,\uparrow,\uparrow,\downarrow,\uparrow,\ldots\rangle\,, \tag{8.10}$$

If periodic boundary conditions are assumed and an even number of lattice sites M, there are $i = 1,\ldots,M$ different states $|\psi_1^i\rangle$ of type (8.10), one for each link where two neighbouring spins can be flipped. Each of those states $|\psi_1^i\rangle$ has a larger Ising interaction energy, which is increased by $8J^{(2)}$ relative to $\left|\psi_{\mathsf{AF}}^{(0)}\right\rangle$. Treating the smaller hopping as a perturbation it is therefore possible to determine the ground state in first order perturbation theory as

$$\begin{aligned} |\psi_{\mathsf{AF}}\rangle \;&\approx\; \left|\psi_{\mathsf{AF}}^{(0)}\right\rangle + \sum_{i=1}^{M} \frac{|\psi_1^i\rangle\,\langle\psi_1^i|\,H_{\mathsf{hop}}\left|\psi_{\mathsf{AF}}^{(0)}\right\rangle}{E_0 - E_i} \\ &\approx\; \left|\psi_{\mathsf{AF}}^{(0)}\right\rangle + \frac{1}{8}\sum_{i=1}^{M}\left|\psi_1^i\right\rangle \end{aligned} \tag{8.11}$$

which can be normalized by a factor of $1/\sqrt{1+M/64}$. Other states only contribute to order 1/64 or higher, so that they can be neglected for most purposes. The state $|\psi_{\mathsf{AF}}\rangle$ in Eq. (8.11) is in very good agreement with the numerical results. The admixture of the states of type $|\psi_1\rangle$ explains the finite modulation depth of the dimer density in the AF phase in Fig. 8.1. Even though the ground state always implicitly contains excitations of type $|\psi_1\rangle$, the addition or removal of a particle relative to half filling still costs a relatively large energy of $8J^{(2)}$, which makes the anti-ferromagnetic phase incompressible.

8.4 Properties of compressible phases

In the following the properties of the compressible phases are analysed, in particular in the vicinity of the AF phase. This will be done using two different approaches. The first is perturbative in nature and makes use of the fact that the dimer hopping is smaller than the nearest neighbour interaction by a factor of 1/8. It is shown that the system can approximately be described as a non-interacting gas of kinks that behave like hard-core bosons. Alternatively long-range correlations can be described in a Luttinger-liquid model. The relevant Luttinger parameter can be obtained by Bethe ansatz considering the equivalent XXZ model.

8.4.1 Non-interacting kink approximation

In Fig. 8.2 the density distribution of dimers in a lattice of length 99 is plotted, obtained from DMRG simulations for different number of dimers N. Since the hard-wall boundaries prefer either a particle or a hole at both ends of the lattice an odd number M of lattice sites is considered here. For $N = 50$ the ground state has almost perfect anti-ferromagnetic order. The slight deviation from the perfect anti-ferromagnetic order can in principle be calculated by Eq. (8.11). Adding one, two and three dimers leads to a modulated dimer distribution with a regularly spaced number of nodes of the envelope corresponding to 2 times the number of additional particles. In the following a simple theoretical understanding for this effect will be provided.

Without hopping, i.e. setting the small second term in Eq. (8.1) equal to zero, the ground state for half filling is the anti-ferromagnetic state $\left|\psi_{\mathsf{AF}}^{(0)}\right\rangle$ given in Eq. (8.9). This state is twofold degenerate. The anti-ferromagnetic order with period 2 effectively doubles the unit cell.

Without hopping, adding a dimer to $\left|\psi_{\mathsf{AF}}^{(0)}\right\rangle$ costs exactly an energy of $8J^{(2)} + h$, resulting in a state of the form

$$|\psi_{\mathsf{AF}}^{(+1)}\rangle \in \begin{cases} |\ldots,\uparrow,\downarrow,\uparrow,\uparrow,\uparrow,\downarrow,\uparrow,\downarrow,\uparrow,\downarrow,\ldots\rangle \\ \text{or} \\ |\ldots,\uparrow,\downarrow,\uparrow,\uparrow,\downarrow,\uparrow,\uparrow,\downarrow,\uparrow,\downarrow,\ldots\rangle \\ \vdots \end{cases}, \tag{8.12}$$

The total magnetization m is related to the number of dimers $N = M/2+m$, where $m = +1$ in Eq. (8.12). The additional dimer causes effective domain walls, which can be placed anywhere in the system and effectively play the role of a moving kink between anti-ferromagnetic regions with different orientation. Interestingly,

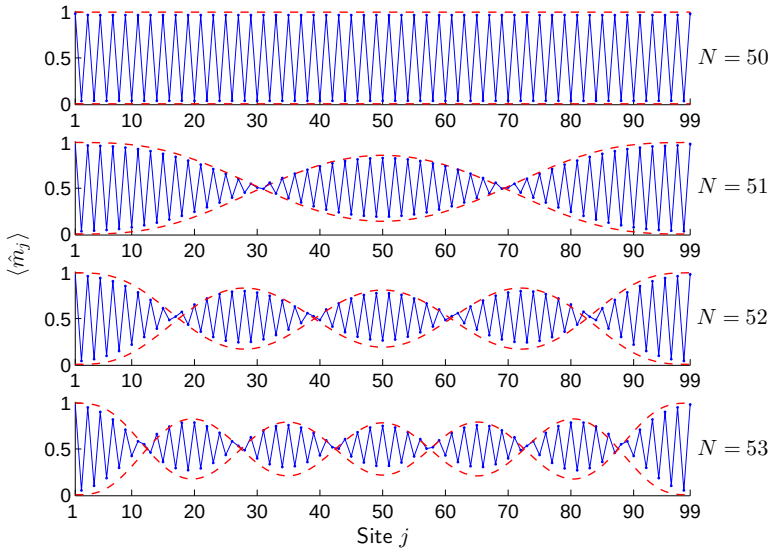

Figure 8.2: Density profile for a lattice with attractively bound dimers with hard-wall boundaries and an odd number of lattice sites. For half filling (here 50 sites occupied) the ground state has almost perfect AF order. Adding dimers leads to modulations with the number of nodes equal twice the number of additional particles.

without hopping any number of dimers above half filling can be created at the critical field $h = -8J^{(2)}$, which can be placed in an arbitrary arrangement of domain walls between anti-ferromagnetic regions and spin-up ferromagnetic regions, leading to a huge degeneracy at that point of states with any $m \geq 0$ as long as no two neighbouring lattice sites are empty. The analogous statements are also true at the upper critical field $h = 8J^{(2)}$, where the degenerate subspace is defined as states where no two neighbouring spins may point up. This degeneracy implies that the transition from the anti-ferromagnetic incompressible phase to the ferromagnetic incompressible phases is infinitely sharp at the effective critical magnetic fields. However, the hopping will lift this degeneracy as will be seen below. Therefore, the hopping is crucial for the stability of the incompressible phase over a finite range as observed in Fig. 8.1.

The hopping is also responsible for the wave patterns observed in Fig. 8.2. Starting from the anti-ferromagnetic state in Eq. (8.9), now a finite number of kinks is considered by inserting more and more particles above half-filling. The state $|\psi_{\mathsf{AF}}^{(+1)}\rangle$ can be considered as an AF-state (8.9) with a pair of kinks, one at even sites and one at odd sites. E.g. the state $|\downarrow,\uparrow,\downarrow,\uparrow,\uparrow,\uparrow,\downarrow,\uparrow,\downarrow,\uparrow,\ldots\rangle$ corresponds to a kink at sites 4 and 5, while $|\downarrow,\uparrow,\downarrow,\uparrow,\uparrow,\downarrow,\uparrow,\uparrow,\downarrow,\uparrow,\ldots\rangle$ corresponds to a kink at sites 4 and 7. It is easy to see that without hopping all states with the same number

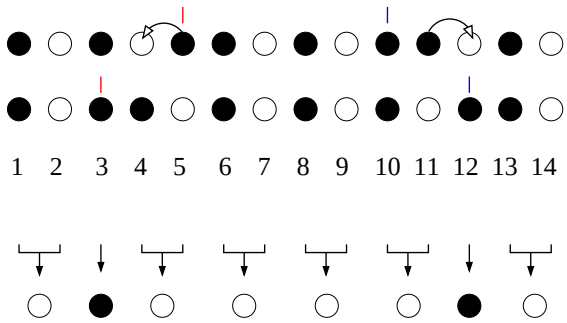

Figure 8.3: *top:* 1D chain with one particle added to the AF states creating a pair of an odd kink (red) and an even kink (blue). The hopping Hamiltonian leads to a motion of the odd and even kinks on odd or even sites respectively. Interchange of odd and even-site kinks is not possible. *bottom:* mapping to effective lattice with lattice constant 2.

of kinks are energetically degenerate. There are non-vanishing matrix elements of $\hat{H}_{\text{hop}}$ within the subspace of fixed number of kinks. Within this manifold a dimer hopping describes the free motion of kinks, where an even-site kink moves on even sites only and respectively an odd-site kink only on odd sites. E.g. hopping of a dimer from sites 4 to 3 can transfer the 4-7 kink state $|\downarrow,\uparrow,\downarrow,\uparrow,\uparrow,\downarrow,\uparrow,\uparrow,\downarrow,\uparrow,\ldots\rangle$ into the 2-7 kink state $|\downarrow,\uparrow,\uparrow,\downarrow,\uparrow,\downarrow,\uparrow,\uparrow,\downarrow,\uparrow,\ldots\rangle$, while hopping of a dimer from site 2 to 3 would create two new kinks and thus would lead out of the considered subspace. Furthermore the even and odd site kinks cannot exchange their relative order. The kink hopping is illustrated in the top part of Fig. 8.3.

The hopping Hamiltonian projected to the sub-space of fixed number of kinks can be mapped to the free motion of pairs of hard-core bosons with lattice constant 2. To see this consider in the following chain kinks caused by addition of dimers, i.e. consider a dimer filling larger than 1/2. The opposite case follows from particle-hole symmetry. Let the positions of the kinks be $j_1 < j_2 < \ldots < j_N$. If j_1 is even (odd) then $j_3, j_5, j_7, \ldots$ are also even (odd) and $j_2, j_4, j_6, \ldots$ are odd (even). It is now possible to map onto a new lattice which is called the kink lattice. The quasi position k_n of the nth kink is then

$$k_n = \begin{cases} \frac{j_n+n-1}{2} & \text{if } j_1 \text{ is even} \\ \frac{j_n+n}{2} & \text{if } j_1 \text{ is odd} \end{cases} \tag{8.13}$$

This mapping is illustrated in the lower part of Fig. 8.3.

Evaluating the matrix elements of the hopping Hamiltonian $\hat{H}_{\text{hop}}$ in the sub-space of states with constant number of kinks one finds that the latter can be considered as hard-core bosons or non-interacting fermions on the kink lattice if

only the absolute value of the wavefunction is considered. The corresponding hopping strength on the period-2 lattice is again $J^{(2)}$. The exchange symmetry cannot be determined straightforwardly and thus this approximation is employed only to determine the density distribution of dimers. For simplicity fermionic exchange symmetry is chosen.

Assume that the lattice is large and consider a dimer filling close to the AF case. In this limit the kinks can be regarded as moving on a continuum. This means that solving the dynamics of the kinks is now equivalent to solving the Schrödinger-equation of non-interacting fermions. For $N = M/2 + 1$ i.e. one additional dimer, one has a pair of kinks whose ground-state wave function is

$$\begin{aligned}\Psi_2(x_1, x_2) = & \\ = \frac{\sqrt{2}}{L}\left[\sin(\pi\frac{x_1}{L})\sin(2\pi\frac{x_2}{L}) - \sin(\pi\frac{x_2}{L})\sin(2\pi\frac{x_1}{L})\right]\end{aligned} \tag{8.14}$$

The left-most kink shall move on odd sites. A dimer is sitting on an even site j if and only if one chain kink is to the left of j. Thus the density of dimers on even sites reads

$$\langle\hat{m}(x)\rangle = 2\int_0^x \mathrm{d}y_1 \int_x^L \mathrm{d}y_2\, \Psi_2^*(y_1, y_2)\Psi_2(y_1, y_2) \tag{8.15}$$

The factor of two emerges here because the integral occurs twice with interchanging roles of y_1 and y_2. Although it is rather straightforward an analytic expression of (8.15) is not given here since it is rather long. At the odd sites one gets accordingly

$$\begin{aligned}\int_0^x \mathrm{d}y_1 \int_0^x \mathrm{d}y_2\, \Psi_2^*(y_1, y_2)\Psi_2(y_1, y_2) + \int_x^L \mathrm{d}y_1 \int_x^L \mathrm{d}y_2\, \Psi_2^*(y_1, y_2))\Psi_2(y_1, y_2) & \\ = 1 - \langle\hat{m}(x)\rangle.\end{aligned} \tag{8.16}$$

For q additional dimers the fermionic ground state wavefunction of the $2q$ kinks is

$$\Psi_{2q}(x_1, \ldots, x_{2q}) = \sum_P \frac{\mathrm{sgn(P)}}{\sqrt{(2q)!}} \prod_{n=1}^{2q} \phi_{P(n)}(x_n) \tag{8.17}$$

where the sum is over all permutations P of the numbers $\{1, 2, 3, \ldots, 2q\}$ and

$$\phi_n(x) = \sqrt{\frac{2}{L}} \sin\left(\pi n \frac{x}{L}\right). \tag{8.18}$$

This results in the density distribution

$$\langle \hat{m}(x) \rangle = \sum_{k=0}^{q-1} \sum_{P,Q} \Big[\frac{\mathrm{sgn}(P)\,\mathrm{sgn}(Q)}{(2k+1)!(2q-2k-1)!} \prod_{n=1}^{2k+1} I(0,x,P(n),Q(n)) \prod_{n=2k+2}^{2q} I(x,L,P(n),Q(n)) \Big]. \quad (8.19)$$

with

$$I(a,b,n,m) = \int_a^b \mathrm{d}x\, \phi_n^*(x) \phi_m(x) \quad (8.20)$$

and $n, m \in \{1, 2, 3, \ldots, 2q\}$. In Eq. (8.19) it is taken into account that there are $\frac{(2q)!}{(2q-2k-1)!(2k+1)!}$ possibilities of choosing $2k+1$ kinks to be left of j. P and Q are permutations of the numbers $\{1, 2, 3, \ldots, 2q\}$.

The dashed red lines in Fig. 8.2 show the analytic results for the dimer density in a box potential for a filling slightly above one half obtained from the kink approximation. The agreement with the numerical DMRG data is rather good. The kink model explains also in a very natural way the pairwise appearance of nodes with adding of a dimer to the lattice.

In the same manner particle-number correlations can be derived. For two even sites at position j_1 and j_2, those configuration contribute to the correlations, where an odd number of particles is left of j_1, an even number is in between j_1 and j_2 and an even number is right of j_2. In that way one obtains for the density-density-correlation of the dimers

$$\langle \hat{m}(x_1)\hat{m}(x_2) \rangle = \sum_{k_1,k_2,k_3=0}^{k_1+k_2+k_3 \leq (q-1)} \sum_{P,Q} \Big[\frac{\mathrm{sgn}(P)\,\mathrm{sgn}(Q)}{(2k_1+1)!(2k_2)!(2k_3+1)!} \prod_{n=1}^{2k_1+1} I(0,x_1,P(n),Q(n)) \prod_{n=2k_1+2}^{2k_1+2k_2+1} I(x_1,x_2,P(n),Q(n)) \prod_{n=2k_1+2k_2+2}^{2q} I(x_2,L,P(n),Q(n)) \Big], \quad \text{for } x_1 < x_2, \quad (8.21)$$

In Fig. 8.4 the density-density correlation of dimers is plotted obtained from a DMRG calculation (blue solid line) and the kink model (dashed red lines). One again recognizes very good agreement.

Within the approximation of non interacting kinks first order correlations exist only between neighbouring sites. They can thus not accurately be described in this perturbative model.

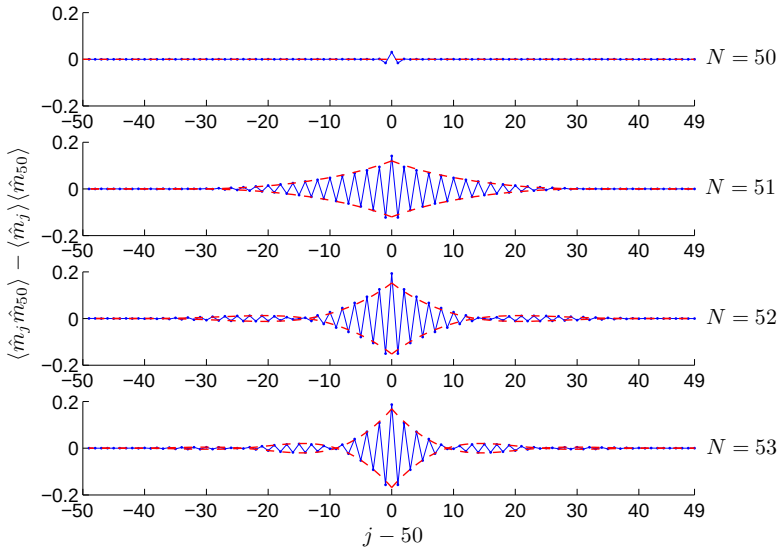

Figure 8.4: Density-density correlations for a lattice with attractively bound dimers with hard-wall boundaries, and 99 lattice sites for different particle number. The blue lines correspond to numerical DMRG results, the red dashed line to the predictions of the kink approximation.

8.4.2 Field theoretical approach

At zero magnetization $s^z := \langle \hat{\sigma}^z \rangle / 2 = 0$, the model (8.2) is gapped since the anisotropy is larger than one. However, as described in Section 8.2, the gap can be closed by a field larger than some critical value, $h > h_c = (8 - \tilde{\mu}_{\mathsf{AF}-})J^{(2)} = (4.31638\ldots)J^{(2)}$. In other words, the system is critical for any finite magnetization away from the fully magnetized case. In this regime, the leading low-energy effective theory is a Luttinger liquid with two parameters, the spin velocity u and the Luttinger parameter K. These are functions of the magnetization per site s^z and the anisotropy Δ [61](which for the particular dimer model here is fixed, $\Delta = 4$).

In order to calculate correlation functions, $K\,(s^z)$ is of particular interest. The XXZ-model in one dimension can be solved by Bethe ansatz and K can be obtained from it. The details of the Bethe ansatz solution of the XXZ model [62] will not be discussed here, but it is very similar to the Bethe ansatz which was discussed in Section 2.1.2 to solve the one-dimensional Bose gas. Finally the result is also a set of integral equations describing the density $\rho(k)$ of quasi-momenta. Analogous to Eq. (2.23) and (2.35) one finds for the XXZ model the two equations

$$\rho(x) = d(x) + \int_{-B}^{B} \kappa(x-y)\rho(y)\,\mathrm{d}y, \tag{8.22}$$

$$s^z = \int_{-B}^{B} \rho(x)\mathrm{d}x - \frac{1}{2}, \tag{8.23}$$

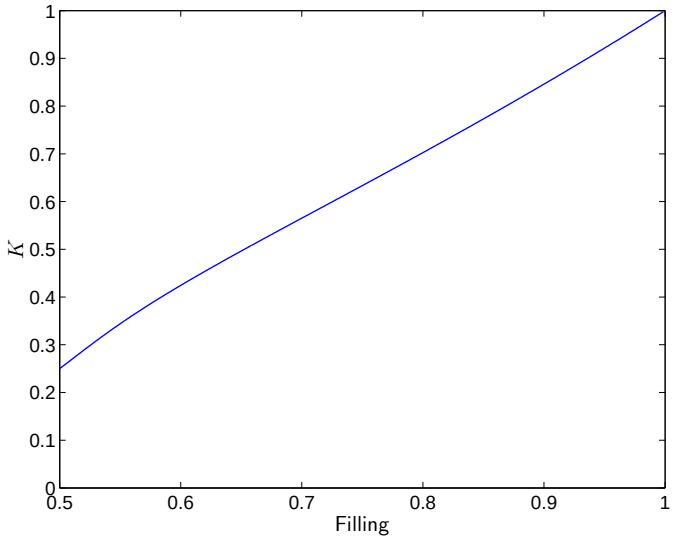

Figure 8.5: Dependence of the Luttinger parameter K on the filling $\langle \hat{m}_j \rangle$ for $\Delta = 4$.

which contain two unknowns: The function $\rho(x)$ and the integration boundary B. The magnetization per lattice site s^z, the driving term $d(x)$ and the integration kernel $\kappa(x)$ are given (see below). The two above equations determine $\rho(x)$ and B. Then the Luttinger parameter K is calculated from another function $\xi(x)$:

$$\xi(x) = 1 + \int_{-B}^{B} \kappa(x-y)\xi(y)\,\mathrm{d}y \tag{8.24}$$

$$K = \xi^2(B)\,. \tag{8.25}$$

The driving term and the integration kernel in Eq. (8.22,8.24) read:

$$\kappa(x) = \frac{1}{\pi}\frac{\sinh 2\eta}{\cos 2x - \cosh 2\eta}, \qquad \Delta = \cosh\eta, \Delta > 1 \tag{8.26}$$

$$d(x) = \frac{1}{\pi}\frac{\sinh \eta}{\cos 2x - \cosh \eta}, \qquad \Delta = \cosh\eta, \Delta > 1 \tag{8.27}$$

Eq. (8.22,8.23,8.24,8.25) are solved numerically by discretizing the integral and inverting the resulting matrix equation. Fig. 8.5 shows the dependence of K on the lattice filling $\langle \hat{m} \rangle = s^z + \frac{1}{2}$ for $\Delta = 4$.

Within the Luttinger liquid approach, one- and two-point correlation functions can be calculated using the standard mode expansion of bosonic fields [63] for open boundary conditions [64]. Then the spin-spin correlation function in the ground

state reads

$$\begin{aligned}\langle\hat{\sigma}^z(x)\hat{\sigma}^z(y)\rangle &= \langle\hat{\sigma}^z\rangle^2 - B\frac{K}{8(L+1)^2}\left(\frac{1}{\left(\sin\frac{\pi(x-y)}{2(L+1)}\right)^2}+\frac{1}{\left(\sin\frac{\pi(x+y)}{2(L+1)}\right)^2}\right)\\ &\quad +C_1\frac{\cos\left[(2k_F+\pi/(L+1))x+\varphi_1\right]}{\left(\sin\frac{\pi x}{L+1}\right)^K}\\ &\quad +C_2\frac{\cos\left[(2k_F+\pi/(L+1))y+\varphi_2\right]}{\left(\sin\frac{\pi y}{L+1}\right)^K}\\ &\quad +D\frac{\cos\left[(2k_F+\pi/(L+1))x+\delta\right]}{\left(\sin\frac{\pi x}{L+1}\,\sin\frac{\pi y}{L+1}\right)^K}\left[\frac{\sin\frac{\pi}{2(L+1)}(x+y)}{\sin\frac{\pi}{2(L+1)}(x-y)}\right]^{2K} \qquad (8.28)\end{aligned}$$

with the Fermi wave vector $k_F := \pi(1+2s^z)/2$. Here the amplitudes $B, C_{1,2}, D$ and the phases $\varphi_{1,2}, \delta$ are so far unknown, and result from bosonizing the operators on the lattice. The constants in Eq. (8.28) are considered here as parameters that are fixed numerically by fitting to DMRG data. The exponents however are obtained from the Luttinger liquid parameter K, which is fixed by the Bethe ansatz. Fig. 8.6 shows the nice agreement between the the two approaches. Also note the shift in the wave vectors of the oscillations by $\pi/(L+1)$, that has been observed also in the context of density oscillations in the open Hubbard model [65]. This is a pure lattice effect which is absent for the analogous correlation functions in open quantum gases [35].

The corresponding result for the first-order correlation function in the ground state is

$$\begin{aligned}\langle\hat{d}^\dagger(x)\hat{d}(y)\rangle &= \left[\frac{\sqrt{\sin\frac{\pi x}{L+1}\sin\frac{\pi y}{L+1}}}{\sin\frac{\pi(x+y)}{2(L+1)}\sin\frac{\pi(x-y)}{2(L+1)}}\right]^{\frac{1}{2K}}\times\\ &\quad\left(B\frac{\cos\left[2k_F+\pi/(L+1))(x-y)+\delta\right]}{\left(\sin\frac{\pi x}{L+1}\,\sin\frac{\pi y}{L+1}\right)^K}\left[\frac{\sin\frac{\pi}{2(L+1)}(x+y)}{\sin\frac{\pi}{2(L+1)}(x-y)}\right]^{2K}\right.\\ &\quad +C_1\frac{\cos\left[2k_F+\pi/(L+1))x+\varphi_1\right]}{\left(\sin\frac{\pi x}{L+1}\right)^K}\\ &\quad\left.+C_2\frac{\cos\left[(2k_F+\pi/(L+1))y+\varphi_2\right]}{\left(\sin\frac{\pi y}{L+1}\right)^K}\right). \qquad (8.29)\end{aligned}$$

Similarly to Eq. (8.28), the constants are considered as fitting parameters. The resulting curves are shown in Fig. 8.7.

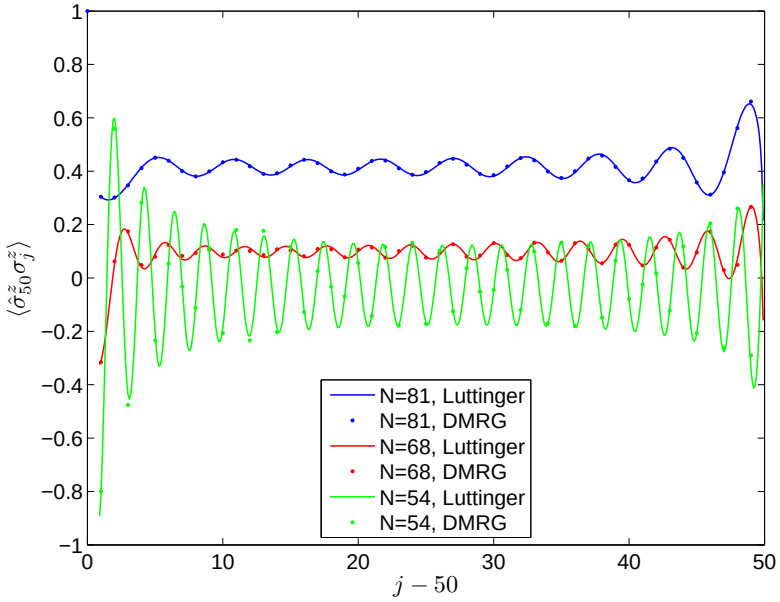

Figure 8.6: $\langle\sigma^z_{50}\sigma^z_j\rangle$ correlations obtained from DMRG and according to Luttinger-liquid approximation.

8.5 Phase diagram in higher dimensions

In order to obtain the phase boundaries in two and three dimensions the strong-coupling approach [66] is used in the following. This means, that the hopping term in (8.1) is treated as small perturbation.

8.5.1 Zero-hopping limit

For vanishing hopping the grand canonical operator is apart from an uninteresting constant term isomorphic to the Ising model in an external magnetic field

$$\hat{K} = \left(4dJ^{(2)} - \frac{1}{2}\widetilde{\mu}\right)\sum_j \hat{\sigma}^z_j + J^{(2)}\sum_{\langle i,j\rangle}\hat{\sigma}^z_i\,\hat{\sigma}^z_j \tag{8.30}$$

In this (formal) limit the model has two critical points

$$\widetilde{\mu}^{(0)}_{\uparrow}/J^{(2)} = 16d, \tag{8.31}$$

$$\widetilde{\mu}^{(0)}_{\downarrow}/J^{(2)} = 0. \tag{8.32}$$

where the superscript (0) denotes zeroth order in ϵ. For very small values of the chemical potential, $\mu < \mu^{(0)}_{\downarrow}$, all spins will be polarized in the $-z$ directions, which corresponds in the dimer language to a state with zero dimer number at each lattice cite. For intermediate values of the chemical potential, $\mu^{(0)}_{\downarrow} < \mu < \mu^{(0)}_{\uparrow}$, the

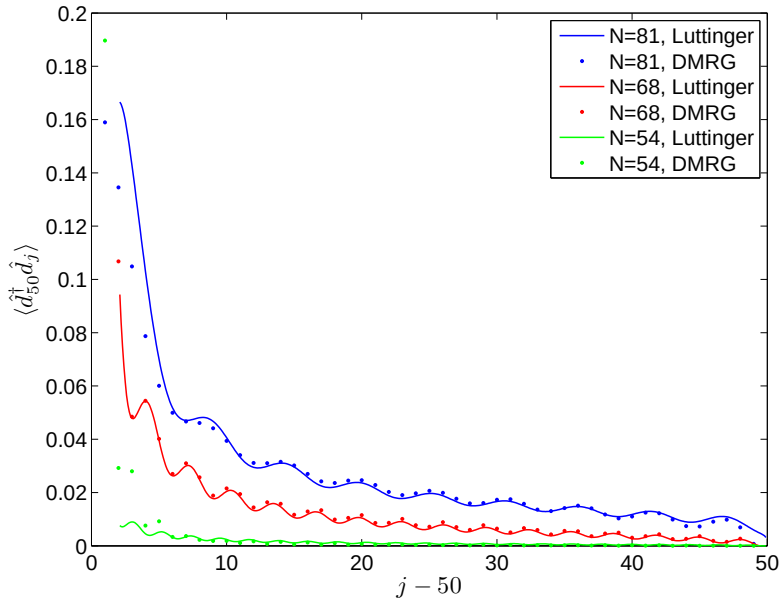

Figure 8.7: $\langle \hat{d}_{50}^{\dagger} \hat{d}_j \rangle$ correlations obtained from DMRG and according to Luttinger-liquid approximation.

ground state is twofold degenerate and has anti-ferromagnetic order. Finally for sufficiently large values of the chemical potential, $\mu > \mu_{\uparrow}^{(0)}$ all spins are aligned in the $+z$ direction, i.e. one has unit filling of dimers.

8.5.2 Boundaries of ferromagnetic phases

When a finite hopping term is switched on, the two critical points extend to two critical regions in which the system is compressible. In the following the chemical potentials will be determined at which the transition between the compressible and incompressible phases takes place employing a strong-coupling expansion in the hopping [66]. To this end the particle-hole excitation energies of a finite lattice with an even number M of lattice sites are calculated from (8.1) for zero, half and full filling.

Since there is no contribution from the interaction energy in the cases of a single dimer or a single hole in the entire lattice one finds immediately without resorting to a perturbation approximation

$$\begin{aligned} E(N=0) &= 0, \\ E(N=1) &= (-|U| - 2dJ^{(2)}) - 2dJ^{(2)}, \end{aligned}$$

where N denotes the total number of dimers, and similarly

$$E(N=M) = (-|U| - 2dJ^{(2)})M + 8dJ^{(2)}M, \tag{8.33}$$

$$E(N=M-1) = (-|U| - 2dJ^{(2)})(M-1) + 8dJ^{(2)}(M-2) - 2dJ^{(2)}. \tag{8.34}$$

From this one finds the critical chemical potentials $\mu_\downarrow$ and $\mu_\uparrow$ for the transition from the compressible phases to an empty lattice, corresponding to a fully polarized spin system in $-z$ direction ($\downarrow$), or a lattice with unity filling, corresponding to a fully polarized spin system in $+z$ direction ($\uparrow$):

$$\widetilde{\mu}_\uparrow/J^{(2)} = 18d, \tag{8.35}$$

$$\widetilde{\mu}_\downarrow/J^{(2)} = -2d. \tag{8.36}$$

It should be noted that the hopping Hamiltonian does not lead to any modification of the corresponding states in the two insulating phases, i.e. within these phases there are no fluctuations of the dimer number; it is exactly one respectively zero per site.

8.5.3 Boundaries of anti-ferromagnetic phase

The calculation of the upper and lower critical chemical potentials $\mu_{\mathsf{AF}\pm}$ for the anti-ferromagnetic (AF) phase is more involved. At exactly half filling, i.e. for $N = M/2$ the ground state is a perfect anti-ferromagnet with an alternating density structure. In lowest order of the hopping the energies of the half-filled state and the states with one additional dimer or dimer-hole are given by

$$E^{(0)}\left(\frac{M}{2}\right) = \left(-|U| - 2dJ^{(2)}\right)\frac{M}{2}, \tag{8.37}$$

$$E^{(0)}\left(\frac{M}{2}+1\right) = \left(-|U| - 2dJ^{(2)}\right)\left(\frac{M}{2}+1\right) + 8J^{(2)}\cdot 2d, \tag{8.38}$$

$$E^{(0)}\left(\frac{M}{2}-1\right) = \left(-|U| - 2dJ^{(2)}\right)\left(\frac{M}{2}-1\right). \tag{8.39}$$

For the case of two spatial dimensions the single particle and single hole states are indicated in Fig. 8.8. It should be noted that in contrast to the 1D case a hopping of the added dimer or dimer hole itself is not allowed since this would lead to a double occupation of sites.

In second order of the hopping amplitude dimers adjacent to a particle kink (see left side of Fig. 8.8) lead to different contributions than all others. Likewise

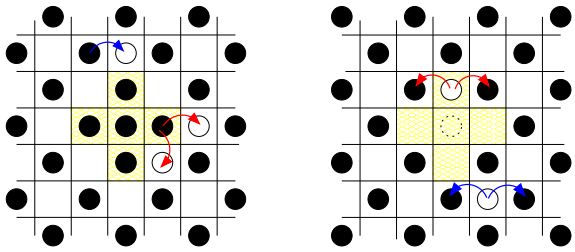

Figure 8.8: Anti-ferromagnetic state in 2D with particle (left) and hole kink (right). Virtual hopping of dimers (holes) adjacent to a kink (red) and in the bulk (blue) lead to different second-order energy contributions. Hopping of the additional particle (hole) is not allowed.

dimer-holes near to a hole-kink (see right side of Fig. 8.8) behave differently than those in the bulk. For exactly half filling every dimer can make $2d$ different hops to off-resonant states with matrix element $J^{(2)}$. The corresponding energy difference is determined by the number of occupied neighbouring sites in the initial and finite states. One finds for exact half filling

$$E^{(2)}\left(\frac{M}{2}\right) = E^{(0)}\left(\frac{M}{2}\right) - \frac{\left(J^{(2)}\right)^2}{8J^{(2)}(2d-1)}\,\frac{M}{2}\,2d$$

and likewise for the kink states

$$E^{(2)}\left(\frac{M}{2}\pm 1\right) = E^{(0)}\left(\frac{M}{2}\pm 1\right) - \frac{\left(J^{(2)}\right)^2}{8J^{(2)}(2d-1)}\left(\frac{M}{2}-2d\right)2d - \frac{\left(J^{(2)}\right)^2}{8J^{(2)}(2d-2)}\,2d\,(2d-1). \quad (8.40)$$

From this one finds the upper and lower critical chemical potential for the anti-ferromagnetic phase

$$\widetilde{\mu}_{\mathsf{AF}+}/J^{(2)} = 16d - \frac{d}{4(2d-1)(2d-2)}, \quad (8.41)$$

$$\widetilde{\mu}_{\mathsf{AF}-}/J^{(2)} = \frac{d}{4(2d-1)(2d-2)}. \quad (8.42)$$

8.6 Summary

This chapter considered a periodic lattice loaded with pairs of bosonic atoms tightly bound to each other via a strong attractive on-site interaction that exceeds the inter-site tunnelling rate. An ensemble of such lattice-dimers is accurately de-

scribed by an effective Hamiltonian corresponding to the extended Hubbard model with strong repulsive interaction between the nearest neighbour sites corresponding to the anisotropic anti-ferromagnetic XXZ model. The ground-state phase diagram was calculated numerically and analytically for this system exhibiting incompressible phases, corresponding to an empty and a fully filled lattice (ferromagnetic phases) and a half-filled alternating density crystal (anti-ferromagnetic phase), separated from each other by compressible phases. In a 1D finite lattice the compressible phases show characteristic oscillatory modulations on top of the anti-ferromagnetic density profile and in density-density correlations. A kink model was derived which provides a simple and quantitative explanation of these features. The large-wavelength properties of the system can be described in terms of a Luttinger liquid. The relevant Luttinger parameter K was obtained exactly using the Bethe ansatz. The corresponding Bethe ansatz calculations were done by Michael Bortz. Density-density as well as first-order correlations were calculated and shown to be in excellent agreement with numerical results obtained with density matrix renormalization group methods.

Part IV

Other quantum multi-particle systems

Chapter 9

Atom-molecule mixtures in optical lattices

In the emerging field of ultra-cold molecules, the conversion of atomic into molecular Bose-Einstein condensates is a central issue. A series of recent experiments on the creation of molecular quantum gases rely on the application of Feshbach resonances (see e.g. [67] for a review). As a more general method, a stimulated optical Raman transition can directly produce deeply bound molecules [68, 69] .

The aim of this chapter is to analyse the phase diagram of atoms in a lattice which are able to form dimer molecules via photoassociation. The general Hamiltonian describing such a system cannot be solved exactly. However, from the special cases of vanishing conversion between atoms and molecules or when the hopping of the atoms can be neglected, the main structure of the phase diagram can be concluded. In the case of non-vanishing hopping a mean-field approximation will be used for the calculations.

9.1 Bosonic atom-dimer Hamiltonian

Atoms which can form dimers via photoassociation will be modelled in the following by a Bose-Hubbard type Hamiltonian. The atoms and molecules are treated as two different particle species. The conversion between atoms and dimers is described by a term which creates a dimer by the annihilation of two atoms and also by a term for the reverse process. It is assumed that the hopping of the molecules is negligible . The chemical potential is defined such, that it is associated with the total number of atoms, where one dimer counts as two atoms. Furthermore, the molecules are energetically detuned from the atoms, which is described by the

parameter Δ. The model Hamilton is for bosonic atoms

$$\hat{H} = \sum_i \Big[- J(\hat{a}_i^\dagger \hat{a}_{i+1} + \hat{a}_i^\dagger \hat{a}_{i-1}) + \frac{U_{\mathrm{aa}}}{2} \hat{a}_i^{\dagger 2} \hat{a}_i^2 - \mu \hat{a}_i^\dagger \hat{a}_i + \frac{U_{\mathrm{dd}}}{2} \hat{d}_i^{\dagger 2} \hat{d}_i^2 - 2\mu \hat{d}_i^\dagger \hat{d}_i + \Delta \hat{d}_i^\dagger \hat{d}_i + \frac{g}{2} (\hat{a}_i^{\dagger 2} \hat{d}_i + \hat{d}_i^\dagger \hat{a}_i^2) + U_{\mathrm{ad}} \hat{a}_i^\dagger \hat{a}_i \hat{d}_i^\dagger \hat{d}_i \Big], \quad (9.1)$$

where the $\hat{a}_j$ are the atomic and the $\hat{d}_j$ the molecular annihilation operators. The atom-atom interaction U_{aa} is used as the energy scale and therefore set to one. g defines the strength of the atom-dimer conversion and U_{dd} is the dimer-dimer and U_{ad} the atom-dimer coupling constant relative to the atom-atom coupling-constant. U_{ad} depends in general not only on the scattering length of the atoms, but also on the so called three body parameter. The question if U_{dd} depends on an additional third parameter seems still to be open. For a detailed discussion on this topic, see [70]. This suggests it is reasonable to assume, that all coupling constants are independent parameters.

Hamiltonian (9.1) includes already the chemical potential μ. There is only a single chemical potential and not a separate one for the atoms and the molecules, because the only conserved particle number is

$$N = \left\langle \sum_j \left(\hat{a}_j^\dagger \hat{a}_j + 2\hat{d}_j^\dagger \hat{d}_j \right) \right\rangle. \quad (9.2)$$

9.2 Vanishing atom hopping and no conversion

As a starting point in understanding the phases of the atom-dimer system one can have a look at the simplest possible case where the atomic hopping J and the conversion rate g is zero. In this case the Hamiltonian (9.1) defines an energy-paraboloid

$$E = \frac{1}{2} n(n-1) + \frac{U_{\mathrm{dd}}}{2} m(m-1) + U_{\mathrm{ad}} nm - \mu(2m+n) + \Delta m \quad (9.3)$$

where n and m is the number of atoms and molecules per site respectively. For the Hamiltonian to be bounded from below it is sufficient to assume, that

$$U_{\mathrm{dd}} > U_{\mathrm{ad}}^2. \quad (9.4)$$

There are also some cases, where the Hamiltonian is bounded from below for $U_{\mathrm{dd}} = U_{\mathrm{ad}}^2$, but in order to make the following discussion not too complicated this case will be ignored here.

The minimum of the paraboloid defined by (9.3) depends linearly on μ:

$$n_{\min} = A_a \mu + B_a m, \tag{9.5}$$

$$m_{\min} = A_d \mu + B_d, \tag{9.6}$$

$$\tag{9.7}$$

with the constants given by

$$A_a = \frac{U_{\mathrm{dd}} - 2U_{\mathrm{ad}}}{U_{\mathrm{dd}} - U_{\mathrm{ad}}^2}, \tag{9.8}$$

$$A_d = \frac{2 - U_{\mathrm{ad}}}{U_{\mathrm{dd}} - U_{\mathrm{ad}}^2}, \tag{9.9}$$

$$B_a = \frac{U_{\mathrm{ad}}U_{\mathrm{dd}} - U_{\mathrm{dd}} - 2U_{\mathrm{ad}}\Delta}{2(U_{\mathrm{dd}} - U_{\mathrm{ad}}^2)}, \tag{9.10}$$

$$B_d = \frac{U_{\mathrm{dd}} - U_{\mathrm{ad}} - 2\Delta}{2(U_{\mathrm{dd}} - U_{\mathrm{ad}}^2)}. \tag{9.11}$$

If $n_{\min} > 0$ and $m_{\min} > 0$, then one of the four nearest integer points $(n, m) \in \mathbb{Z}^2$ is the ground state. Therefore, $1/|A_a|$ and $1/|A_d|$ give estimates for the width of the insulating phases in μ-direction. A_a and A_d can also be negative, but the case where the total number of atoms per site $N_0 = 2m + n$ decreases with increasing μ is not possible as the calculation of $N_{\min} = n_{\min} + 2m_{\min}$ shows:

$$N_0 = A\mu + B \tag{9.12}$$

$$A = \frac{U_{\mathrm{dd}} + 4 - 4U_{\mathrm{ad}}}{U_{\mathrm{dd}} - U_{\mathrm{ad}}^2} \tag{9.13}$$

$$B = \frac{2U_{\mathrm{ad}}\Delta + 3U_{\mathrm{dd}} - 2U_{\mathrm{ad}} - U_{\mathrm{ad}}U_{\mathrm{dd}} - 4\Delta}{2(U_{\mathrm{dd}} - U_{\mathrm{ad}}^2)} \tag{9.14}$$

From condition (9.4) follows that A is always positive.

9.3 Vanishing atom hopping and non-zero conversion rate

For the case of a non-zero atom-molecule-conversion ($g \neq 0$) but zero hopping ($J = 0$) the problem is still local and can be solved numerically very easily. Examples

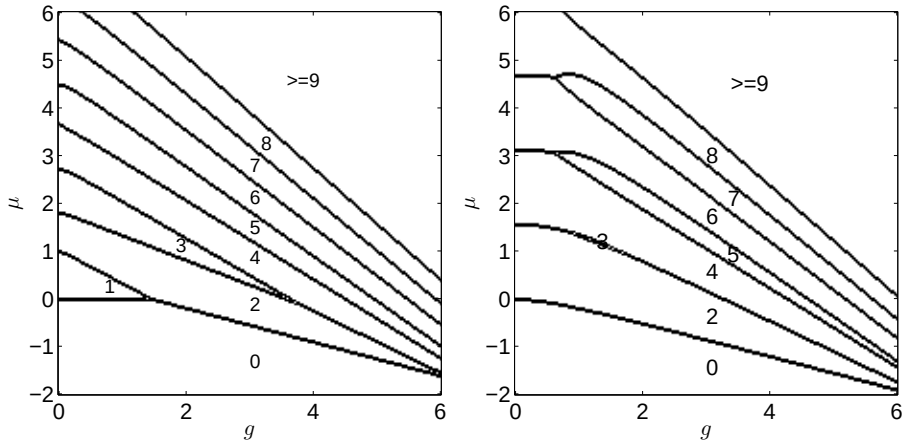

Figure 9.1: Phase diagram of the atom-molecule mixture for $J = 0$. The left picture ($U_{\rm dd} = 3.6$,$U_{\rm ad} = 1.7$,$\Delta = 1.1$) shows only phases which exist also for $g = 0$. Some of them, however, do not exist for large g. The right picture ($U_{\rm dd} = 3.1$,$U_{\rm ad} = 1.7$,$\Delta = 0$) shows some phases which do exist only for larger g and not for $g = 0$.

are shown in Fig. 9.1. For small particle numbers it is even possible to solve it analytically. In this case one can make use of the fact, that the local ground state is an eigenstate of the local particle number operator $\hat{N}_0 = \hat{a}^\dagger\hat{a} + 2\hat{d}^\dagger\hat{d}$. Thus, it can be written in the form

$$|\phi\rangle = \sum_{m=0}^{\lfloor N_0/2\rfloor} c_m |N_0 - 2m\rangle|m\rangle. \tag{9.15}$$

One derives easily the matrix representation of the operators in the basis $|N_0 - 2m\rangle|m\rangle$ as

$$\hat{d}^\dagger\hat{d} = m\delta_{m'm}, \tag{9.16}$$

$$\hat{a}^\dagger\hat{a} = (N_0 - 2m)\delta_{m'm}, \tag{9.17}$$

$$\hat{a}^{\dagger 2}\hat{d} = \sqrt{m(N_0 - 2m + 1)(N_0 - 2m + 2)}\delta_{m'm-1}, \tag{9.18}$$

where $0 \leq m \leq \lfloor N_0/2\rfloor$. For $N_0 \leq 7$ it is in principle possible to find the eigenvectors and eigenstates analytically because the dimension of the Hilbert space is smaller than 5. The calculations show, that the phases which are present for $g = 0$ have a continuation in the $g \neq 0$ regime. A phase for $g = 0$ is given by a combination of n and m defined by the ground-state. For $g \neq 0$ a single phase does not have separately fixed atom and dimer number anymore but preserves its total number of particles per site $N_0 = \langle\hat{a}^\dagger\hat{a}\rangle + 2\langle\hat{d}^\dagger\hat{d}\rangle$. However, for $g = 0$ not all

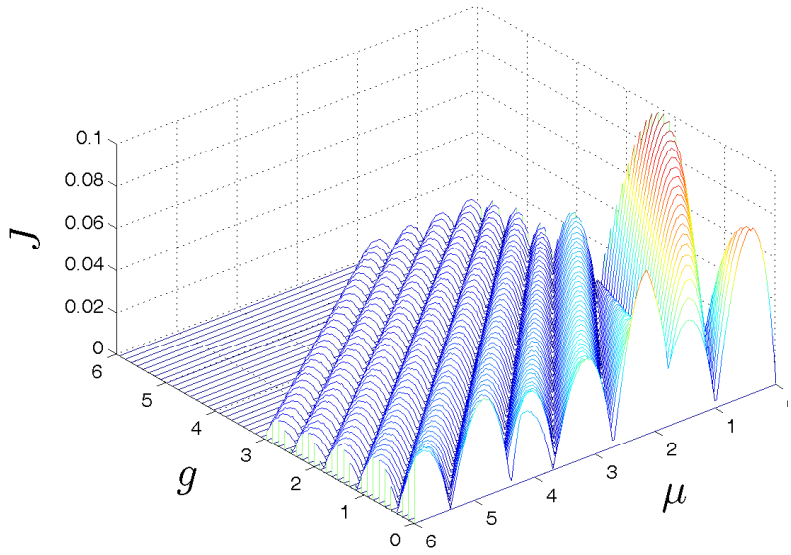

Figure 9.2: Boundaries of the Mott-insulator phases for the atom molecule mixture with $J > 0$ obtained from mean field calculations. The parameters are $\Delta = 1.1$, $U_{\mathrm{dd}} = 3.6$, $U_{\mathrm{ad}} = 1.7$. From right to left the lobes belong to the total particle number $2m + n = 1, 2, 3, \ldots, 11$. On the left the diagram is cut off because the numerical calculation was limited to $2m + n \leq 11$.

combinations of n and m are possible and some N_0 do not occur. It is then possible that those combinations occur only for $g \neq 0$. In conclusion it is seen, that every phase can be characterized by its total particle number $N_0 = \langle \hat{a}^\dagger \hat{a} \rangle + 2\langle \hat{d}^\dagger \hat{d} \rangle$ found for $J = 0$. It is expected that for $J > 0$ this phases just start to shrink. This will be investigate in the next section by using a mean-field approach.

9.4 Finite atomic hopping and conversion in a mean field approach

In this section the same mean-field ansatz as in [24], which was described in Sec. 2.3.1 is applied to the Hamiltonian (9.1). This means that the hopping term of the atoms in (9.1) is replaced by

$$-Jz\alpha(\hat{a}_i^\dagger + \hat{a}_i), \tag{9.19}$$

where z is the number of nearest neighbours. α is determined by the self-consistency condition $\langle \hat{a} \rangle = \alpha$, where the expectation value is taken with respect to the ground-state. It can be shown that this ansatz is equivalent to assuming

that the ground state is a so called Gutzwiller state which means that it factorizes site-wise. Regarding the local Hamiltonian as functional of α, the expectation value $h(\alpha) = \langle \hat{a} \rangle$ becomes a function of α. In general there are more than one solution to the problem $h(\alpha) = \alpha$ with $\alpha = 0$ being always a solution. If this solution is stable the system is in the Mott-insulator-phase. The stability of the $\alpha = 0$ solution can be determined by calculating the first derivative of h at $\alpha = 0$. If $\frac{\partial h}{\partial \alpha}|_{\alpha=0} < 1$ then the zero-solution is stable. One example of a phase diagram obtained by this approach is shown in Fig. 9.2.

9.5 Summary

The present chapter discussed the phase diagrams of atom-molecule mixtures in a periodic potential where two bosonic atoms can form a molecule via photoassociation. The model used for the numerical analysis was a Hubbard-type Hamiltonian. Since the model is difficult to treat exactly the special case of zero hopping was considered first from which the location of the Mott insulator phases can be determined. Every such phase is characterized by the number $N_0 = 2m + n$ where n and m are the number of atoms and molecules per site respectively. This characterization can be extended to non-zero hopping of the atoms. Examples of phase diagrams were calculated numerically where for the case of non-zero hopping a mean-field approximation was used. It is found that for some sets of parameters some of the Mott insulator phases exist only above a critical non-zero value of the conversion rate between atoms and molecules.

Chapter 10

Two-component 1D Bose-gas

This chapter explores how the solution of the one-dimensional interacting Bose gas of Section 2.1.2 can be used to derive results for the case of two different species of bosons that interact which each other. It is not known to the author if the Bethe ansatz can be extended to a two-species Bose-gas by which one would obtain an exact solution. In the following it will be shown however that already a much simpler approximative ansatz allows to derive properties of a two component gas. The approximation will be made in the interspecies interaction, which will be treated in the mean-field limit . The advantage of this approach is that the exact results of the single species case can be employed straightforwardly, i.e. the intraspecies interaction is treated exactly. This results in a phase diagram showing the regimes of phase separation.

10.1 Two-species Bose gas with mean-field interspecies interaction

The 1D-delta-interacting Bose gas can be solved exactly in the homogeneous case, at least for energy and density. The Energy E of such a gas is given by

$$E = \frac{N}{2}\rho^2\epsilon_2(g/\rho) \tag{10.1}$$

where $\rho = N/L$ is the particle density of the gas, $g = g_{1\mathrm{D}}$ the 1D interaction constant of the bosons and ϵ_2 is the Lieb-Liniger function (2.34). To make use of this results for two-component gases, it is assumed in the following that the energy of each component is given by the above expression and that the interaction energy

between the components is just given by

$$E_{\text{int}}/L = g_{12}\rho_1\rho_2. \tag{10.2}$$

This assumes that the ground-state is factorizable in the two components. For the total energy density one obtains

$$E/L = \frac{\rho_1^3}{2}\epsilon_2\left(\frac{g_1}{\rho_1}\right) + \frac{\rho_2^3}{2}\epsilon_2\left(\frac{g_2}{\rho_2}\right) + g_{12}\rho_1\rho_2. \tag{10.3}$$

Minimizing this energy under the condition of fixed average particle numbers yields the equations

$$\mu_1 = g_1^2 f\left(\frac{g_1}{\rho_1}\right) + g_{12}\rho_2 \tag{10.4}$$

$$\mu_2 = g_2^2 f\left(\frac{g_2}{\rho_2}\right) + g_{12}\rho_1 \tag{10.5}$$

where μ_1 and μ_2 are the chemical potentials of the two particle species and f is defined by Eq. (2.37). To be a minimum the matrix

$$\begin{pmatrix} -\frac{g_1^3}{\rho_1^2}f'(\frac{g_1}{\rho_1}) & g_{12} \\ g_{12} & -\frac{g_2^3}{\rho_2^2}f'(\frac{g_2}{\rho_2}) \end{pmatrix} \tag{10.6}$$

must be positive definite. This is exactly the case when

$$\frac{g_1^3}{\rho_1^2}f'\left(\frac{g_1}{\rho_1}\right)\frac{g_2^3}{\rho_2^2}f'\left(\frac{g_2}{\rho_2}\right) > g_{12}^2. \tag{10.7}$$

If there is no such solution then the possible minima of the energy can only be $\rho_1 = 0$ or $\rho_2 = 0$. To have for example a minimum at $\rho_1 = 0$ the first derivative of the energy with respect to ρ_1 must be positive and one must have a local minimum with respect to ρ_2. The first condition leads to $\rho_2 > \frac{\mu_1}{g_{12}}$. The second to $\mu_2 = g_2^2 f(\frac{g_2}{\rho_2})$. This extrema is always a minimum because $-\frac{g_2^3}{\rho_2^2}f'(\frac{g_2}{\rho_2}) > 0$ is always fulfilled.

10.2 Phase diagram of a two component one-dimensional Bose-gas

In the following the phase diagram of the mixture will be derived. For simplicity the following notations are introduced: $\gamma_1 = \frac{\rho_1}{g_1}$, $\gamma_2 = \frac{\rho_2}{g_2}$, $\chi_1 = \frac{\mu_1}{g_1^2}$, $\chi_2 = \frac{\mu_2}{g_2^2}$,

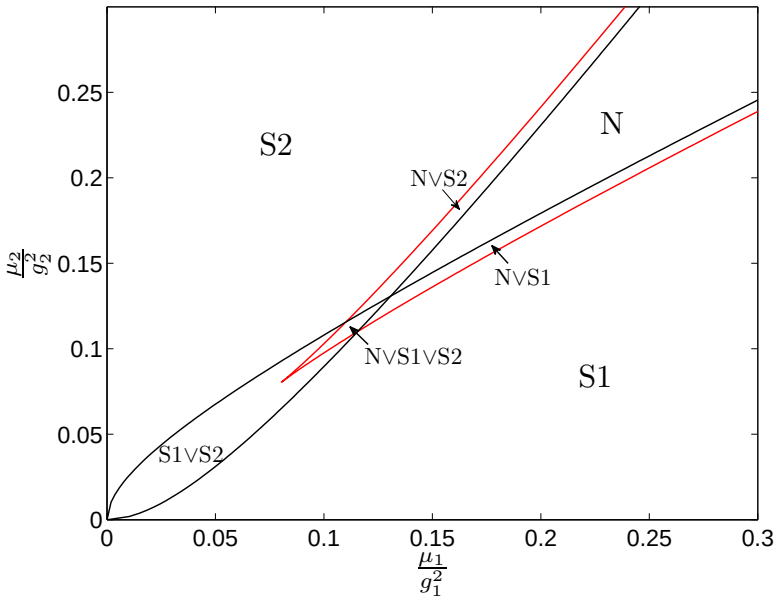

Figure 10.1: Phase diagram of a two-component one-dimensional Bose-gas. N: Phase with $\rho_1 > 0$ and $\rho_2 > 0$; S_1: Phase with $\rho_2 = 0$ and $\rho_1 \geq 0$; S_2: Phase with $\rho_1 = 0$ and $\rho_2 \geq 0$. The symbol $\vee$ means phase separation between the denoted phases.

$\kappa_1 = \frac{g_{12}g2}{g_1^2}$, $\kappa_2 = \frac{g_{12}g1}{g_2^2}$, $\kappa_{12} = \kappa_1\kappa_2 = \frac{g_{12}}{g_1 g_2}$. The parameters of the phase diagram will be χ_1 and χ_2. So far it was shown that for $\rho_1 > 0$, $\rho_2 > 0$ the solution is given by

$$\chi_1 = f(\gamma_1) + \frac{\kappa_1}{\gamma_2} \tag{10.8}$$

$$\chi_2 = f(\gamma_2) + \frac{\kappa_2}{\gamma_1} \tag{10.9}$$

This solution is stable if

$$\gamma_1^2 f'(\gamma_1)\gamma_2^2 f'(\gamma_2) > \kappa_{12} \tag{10.10}$$

The left hand side of Eq. (10.10) is always smaller than 1. So if $\kappa_{12} > 1$ the condition can not be fulfilled and no phase with $\rho_1 > 0$ and simultaneously $\rho_2 > 0$ exists. Stable solutions with $\rho_1 = 0$ are present if

$$\chi_1 < \frac{\kappa_1}{f^{-1}(\chi_2)} \tag{10.11}$$

and stable solutions with $\rho_2 = 0$ are present if

$$\chi_2 < \frac{\kappa_2}{f^{-1}(\chi_1)}. \tag{10.12}$$

As the above discussion shows the system has three pure phases. Two of them are the cases when the density of one of the particle species is zero. The third one allows for a non-zero density of both species, which is however only possible when $\kappa_{12} < 1$. If conditions (10.10)(10.11)(10.12) are drawn into the phase diagram, one arrives at the picture shown in Fig. 10.1. Fig. 10.1 also reveals that the regimes of the pure phases overlap. This phenomenon is a so-called phase-separation. It means that the gas can show spatially separated domains of different phases. If one counts all possible combinations of the pure phases, the total number of phases is seven. A non-zero density of both species is only possible above a certain critical value of the chemical potentials which depends on the interaction strengths.

A trap potential can make parts of the phase diagram visible. If the two-component gas is in a trap the effective chemical potential $\mu - V(x)$ draws a line through the phase diagram given by

$$\chi_2 = \frac{\mu_2 - \mu_1}{g_2^2} + \frac{g_1^2}{g_2^2}\chi_1, \tag{10.13}$$

where χ_1 starts with some value at the trap centre and goes to zero.

10.3 Summary

The present chapter discussed the mixture of two bosonic particle species in one dimension at zero temperature. While the intra-species interaction was treated exactly by using results from the exact solution of a single component gas the inter-species interaction was approximated by a mean-field Hamiltonian. By minimizing the energy of the two-component gas different solutions for the density at given chemical potentials could be found. The system exhibits three pure phases and the possibility for phase separation between them. From the results of the single component gas the phase diagram of the two-component gas could be determined, which shows the location of the phase-separated phases.

Bibliography

[1] K. B. Davis, M. O. Mewes, M. R. Andrews, N. J. van Druten, D. S. Durfee, D. M. Kurn, and W. Ketterle. Bose-einstein condensation in a gas of sodium atoms. *Phys. Rev. Lett.*, 75(22):3969–3973, Nov 1995.

[2] M. H. Anderson, J. R. Ensher, M. R. Matthews, C. E. Wieman, and E. A. Cornell. Observation of Bose-Einstein Condensation in a Dilute Atomic Vapor. *Science*, 269(5221):198–201, 1995.

[3] M. Greiner, O. Mandel, T. Esslinger, T. W. Hänsch, and I. Bloch. Quantum phase transition from a superfluid to a mott insulator in a gas of ultracold atoms. *Nature*, 415:39–44, 2002.

[4] Guifré Vidal. Efficient simulation of one-dimensional quantum many-body systems. *Phys. Rev. Lett.*, 93(4):040502, Jul 2004.

[5] E. H. Lieb and W. Liniger. Exact analysis of an interacting bose gas. *Phys. Rev.*, 130(4):1605, 1963.

[6] C. N. Yang and C. P. Yang. Thermodynmics of a one-dimensional system of bosons with repulsive delta-function interaction. *J. Math. Phys.*, 10(7):1115, 1969.

[7] D. S. Petrov, G. V. Shlyapnikov, and J. T. M. Walraven. Regimes of quantum degeneracy in trapped 1d gases. *Phys. Rev. Lett.*, 85(18):3745, 2000.

[8] D. L. Luxat and A. Griffin. Dynamic correlation functions in one-dimensional quasicondensates. *Phys. Rev. A*, 67(043603), 2003.

[9] M. Olshanii and V. Dunjko. Short-distance correlation properties of the lieb-liniger system and momentum distributions of trapped one-dimensional atomic gases. *Phys. Rev. Lett.*, 91(9), 2003.

[10] F. D. M. Haldane. Effective harmonic-fluid approach to low-energy properties of one-dimensional quantum fluids. *Phys. Rev. Lett.*, 47(25):1840–1843, Dec 1981.

[11] M. A. Cazalilla. Bosonizing one-dimensional cold atomic gases. *J. Phys. B: At. Mol. Opt. Phys.*, 37:S1–S47, 2004.

[12] M. Olshanii. Atomic scattering in the presence of an external confinement and a gas of impenetrable bosons. *Phys. Rev. Lett.*, 81(5), 1998.

[13] Kerson Huang and C. N. Yang. Quantum-mechanical many-body problem with hard-sphere interaction. *Phys. Rev.*, 105(3):767–775, Feb 1957.

[14] Mingzhe Li, Haixiang Fu, Yu-Zhu Wang, Jincan Chen, Lixuan Chen, and Chuanhong Chen. Pseudopotential operator for hard-sphere interactions in any-dimensional space. *Phys. Rev. A*, 66(1):015601, Jul 2002.

[15] E. P. Gross. Structure of quantized vortex. *Nuovo Cimento*, 20(454), 1961.

[16] Eugene P. Gross. Hydrodynamics of a superfluid condensate. *Journal of Mathematical Physics*, 4(2):195–207, 1963.

[17] L. P. Pitaevskii. Vortex lines in an imperfect bose gas. *Soviet Physics JETP-USSR*, 13(2):451–454, 1961.

[18] M. Girardeau. Relationship between systems of impenetrable bosons and fermions in one dimension. *Journal of Mathematical Physics*, 1(6):516–523, 1960.

[19] Lewi Tonks. The complete equation of state of one, two and three-dimensional gases of hard elastic spheres. *Phys. Rev.*, 50(10):955–963, Nov 1936.

[20] C. W. Gardiner. *Handbook of Stochastic Methods*. Springer-Verlag, New York Berlin Heidelberg, second edition, 1985.

[21] C. W. Gardiner, W. Crispin, and P. Zoller. *Quantum Noise*. Springer, Berlin, 2., corr. printing edition, 2004.

[22] J. K. Freericks and H. Monien. Phase diagram of the Bose-Hubbard Model. *EPL (Europhysics Letters)*, 26(7):545–550, 1994.

[23] L. I. Plimak, M. K. Olsen, and M. Fleischhauer. Occupation number and fluctuations in the finite-temperature Bose-Hubbard model. *Phys. Rev. A*, 70(1):013611, Jul 2004.

[24] D. van Oosten, P. van der Straten, and H. T. C. Stoof. Quantum phases in an optical lattice. *Phys. Rev. A*, 63(053601), 2001.

[25] C. N. Yang and C. P. Yang. One-dimensional chain of anisotropic spin-spin interactions. i. proof of bethe's hypothesis for ground state in a finite system. *Phys. Rev.*, 150(1):321–327, Oct 1966.

[26] C. N. Yang and C. P. Yang. One-dimensional chain of anisotropic spin-spin interactions. ii. properties of the ground-state energy per lattice site for an infinite system. *Phys. Rev.*, 150(1):327–339, Oct 1966.

[27] J. Hubbard. Calculation of partition functions. *Phys. Rev. Lett.*, 3(2):77–78, Jul 1959.

[28] Felix Bloch. Über die Quantenmechanik der Elektronen in Kristallgittern. *Zeitschrift für Physik A Hadrons and Nuclei*, 52(7):555–600, 1929.

[29] Gregory H. Wannier. The structure of electronic excitation levels in insulating crystals. *Phys. Rev.*, 52(3):191–197, Aug 1937.

[30] W. Kohn. Analytic properties of bloch waves and wannier functions. *Phys. Rev.*, 115(4):809–821, 1959.

[31] Dieter Jaksch. *Bose-Einstein Condensation and Applications*. Dissertation, Naturwissenschaftliche Fakultät der Leopold-Franzens-Universität Innsbruck, 1999.

[32] A. Albus, F. Illuminati, and J. Eisert. Mixtures of bosonic and fermionic atoms in optical lattices. *Phys. Rev. A*, 68(023606), 2003.

[33] M. Abramowitz and I. A. Stegun. *Handbook of Mathematical Functions with Formulas, Graphs, and Mathematical Tables*. Dover, New York, ninth dover printing, tenth gpo printing edition, 1964.

[34] Belen Paredes, Artur Widera, Valentin Murg, Olaf Mandel, Simon Fölling, Ignacio Cirac, Gora V. Shlyapnikov, Theodor W. Hänsch, and Immanuel Bloch. Tonks-girardeau gas of utracold atoms in an optical lattice. *Nature*, 429:277–281, 2004.

[35] M. A. Cazalilla. Differences between the tonks regimes in the continuum and on the lattice. *Phys. Rev. A*, 70(4):041604, Oct 2004.

[36] K. B. Efetov and A. I. Larkin. Correlation functions in one-dimensional systems with a strong interaction. *Sov. Phys.-JETP*, 42(2):390, 1975.

[37] U. Schollwöck. The density-matrix renormalization group. *Reviews of Modern Physics*, 77(1):259, 2005.

[38] C. Kollath, U. Schollwöck, J. von Delft, and W. Zwerger. Spatial correlations of trapped one-dimensional bosons in an optical lattice. *Phys. Rev. A*, 69(3):031601, Mar 2004.

[39] B. Laburthe Tolra, K. M. O'Hara, J. H. Huckans, W. D. Phillips, S. L. Rolston, and J. V. Porto. Observation of reduced three-body recombination in a correlated 1d degenerate bose gas. *Phys. Rev. Lett.*, 92(19):190401, May 2004.

[40] Vadim V. Cheianov, H. Smith, and M. B. Zvonarev. Exact results for three-body correlations in a degenerate one-dimensional bose gas. *Physical Review A (Atomic, Molecular, and Optical Physics)*, 73(5):051604, 2006.

[41] Kenneth Günter, Thilo Stöferle, Henning Moritz, Michael Köhl, and Tilman Esslinger. p-wave interactions in low-dimensional fermionic gases. *Physical Review Letters*, 95(23):230401, 2005.

[42] Taksu Cheon and T. Shigehara. Fermion-boson duality of one-dimensional quantum particles with generalized contact interactions. *Phys. Rev. Lett.*, 82(12):2536–2539, Mar 1999.

[43] M. D. Girardeau and M. Olshanii. Theory of spinor fermi and bose gases in tight atom waveguides. *Phys. Rev. A*, 70(2):023608, Aug 2004.

[44] Scott A. Bender, Kevin D. Erker, and Brian E. Granger. Exponentially decaying correlations in a gas of strongly interacting spin-polarized 1d fermions with zero-range interactions. *Physical Review Letters*, 95(23):230404, 2005.

[45] A. Minguzzi and M. D. Girardeau. Pairing of a harmonically trapped fermionic tonks-girardeau gas. *Physical Review A (Atomic, Molecular, and Optical Physics)*, 73(6):063614, 2006.

[46] K. Winkler, G. Thalhammer, F. Lang, R. Grimm, J. Hecker Denschlag, A. J. Daley, A. Kantian, H. P. Büchler, and P. Zoller. Repulsively bound atom pairs in an optical lattice. *Nature*, 441:853–856, 2006.

[47] G. N. Nikolopoulos, D. Petrosyan, and P. Lambropoulos. Electron wavepacket propagation in a chain of coupled quantum dots. *J. Phys.: Condens. Matter*, 16:4991–5002, 2004.

[48] M. Lewenstein, L. Santos, M. A. Baranov, and H. Fehrmann. Atomic bose-fermi mixtures in an optical lattice. *Phys. Rev. Lett.*, 92(050401), 2004.

[49] Z. Cheng and G. Kurizki. Theory of one-dimensional quantum gap solitons. *Phys. Rev. A*, 54:3576–3591, 1996.

[50] B. W. Shore. *The Theory of Coherent Atomic Excitation*. Wiley, New York, 1990.

[51] P. Lambropoulos and D. Petrosyan. *Fundamentals of Quantum Optics and Quantum Information*. Springer, Berlin, 2006.

[52] Rune Piil and Klaus Molmer. Tunnelling couplings in discrete lattices, single particle band structure and eigenstates of interacting atom pairs. *Physical Review A*, 76:023607, 2007.

[53] M.P.A. Fisher, P.B. Weichman, G. Grinstein, and D.S. Fisher. Boson localization and the superfluid-insulator transition. *Phys. Rev. B*, 40:546–570, 1989.

[54] Herman Feshbach. A unified theory of nuclear reactions. ii. *Annals of Physics*, 19(2):287–313, Aug 1962.

[55] S. Sadchev. *Quantum Phase Transitions*. Cambridge University Press, Cambridge, 1999.

[56] M. Takahashi. Correlation length and free energy of the s=1/2 xxz chain in a magnetic field. *Phys. Rev. B*, 44:12382–12394, 1991.

[57] B. McCoy and T. T. Wu. *The Two-Dimensional Ising Model*. Harvard University Press, Cambridge, MA, 1973.

[58] G. K. Campbell, J. Mun, M. Boyd, P. Medley, A. E. Leanhardt, L. G. Marcassa, D. E. Pritchard, and W. Ketterle. Imaging the mott insulator shells by using atomic clock shifts. *Science*, 313:649–652, 2006.

[59] David Petrosyan, Bernd Schmidt, James R. Anglin, and Michael Fleischhauer. Quantum liquid of repulsively bound pairs of particles in a lattice. *Physical Review A (Atomic, Molecular, and Optical Physics)*, 76(3):033606, 2007.

[60] Manuel Valiente and David Petrosyan. Two-particle states in the hubbard model. *At. Mol. Opt. Phys.*, 41:161002, 2008.

[61] F. D. M. Haldane. General relation of correlation exponents and spectral properties of one-dimensional fermi systems: Application to the anisotropic $s = 12$ heisenberg chain. *Phys. Rev. Lett.*, 45(16):1358–1362, Oct 1980.

[62] N. M. Bogoliubov, A. G. Izergin, and V. E. Korepin. Critical exponents for integrable models. *Nuclear Physics B*, 275(4):687 – 705, 1986.

[63] S. Eggert. *Lecture Note: Theoretical Survey of one dimensional wire systems.* Proceedings of 2006 A3 Summer school on physics and chemistry, 2006.

[64] Sebastian Eggert and Ian Affleck. Magnetic impurities in half-integer-spin heisenberg antiferromagnetic chains. *Phys. Rev. B*, 46(17):10866–10883, Nov 1992.

[65] Stefan A. Soeffing, Michael Bortz, and Sebastian Eggert. Wigner crystal vs. friedel oscillations in a finite quantum wire, 2008.

[66] J. K. Freericks and H. Monien. Strong-coupling expansions for the pure and disordered Bose-Hubbard model. *Phys. Rev. B*, 53(5):2691–2700, Feb 1996.

[67] Daniel Kleppner. Professor feshbach and his resonance. *Physics Today*, 57(8):12–13, 2004.

[68] Roahn Wynar, R. S. Freeland, D. J. Han, C. Ryu, and D. J. Heinzen. Molecules in a Bose-Einstein Condensate. *Science*, 287(5455):1016–1019, 2000.

[69] Bruno Laburthe Tolra, Cyril Drag, and Pierre Pillet. Observation of cold state-selected cesium molecules formed by stimulated raman photoassociation. *Phys. Rev. A*, 64(6):061401, Nov 2001.

[70] E. Braaten and H.-W. Hammer. Universality in few-body systems with large scattering length. *arXiv:cond-mat/0409292*, 2004.

Curriculum vitae

Curriculum vitae removed from online version.
Lebenslauf aus Online-Version entfernt.

Acknowledgement

A work as the present thesis is not possible without the preliminary work of many geniuses whose names can be found in the bibliography. Having the right idea for something is often more worth and difficult than exploring the consequences and possibilities of that idea. I, therefore, owe much to the people who gave the major ideas and input to my work. In particular I want to thank

Michael Fleischhauer
for supervising my work, for finding most of the interesting physical problems in this thesis and all the guidance and help

Lev Plimak
for introducing me in the world of stochastic simulation and DMRG and for all the support at the beginning of my work

David Petrosyan
for finding the effective Hamiltonian of the repulsively bound pairs of particles

Michael Bortz
for his help on the Luttinger liquid theory

Anna Minguzzi
for making me to look into the problem of correctly discretizing the p-wave interacting fermions

James Anglin
for his contribution to the “repulsively bound pairs of particles”- paper

Sebastian Eggert
for his contribution to the “attractively bound pairs of particles”- paper (to be published)

Further thanks go to:

all members and former members of the AG Fleischhauer

and

my parents